



**UNIVERSITAT POLITÈCNICA DE CATALUNYA
BARCELONATECH**

**Escola Tècnica Superior d'Enginyeria
de Telecomunicació de Barcelona**

**5G NETWORK PLANNING AND OPTIMIZATION USING
ATOLL**

A Master's Thesis

**Submitted to the Faculty of the
Escola Tècnica d'Enginyeria de Telecomunicació de
Barcelona**

Universitat Politècnica de Catalunya

by

Riviel Ernesto Rios

**In partial fulfilment
of the requirements for the degree of
MASTER IN TELECOMMUNICATIONS ENGINEERING**

Advisor: Anna UMBER, PhD; Ramon Ferrús, PhD

Barcelona, July 2019



UNIVERSITAT POLITÈCNICA
DE CATALUNYA
BARCELONATECH



Title of the thesis: 5G Network Planning and Optimization Using Atoll

Author: Riviell Ernesto Ríos

Advisor: Anna Umbert, PhD; Ramon Ferrús, PhD

Abstract

This thesis consists on the study of some 5G NR key features such as massive MIMO and beamforming and how they are modelled by Atoll, a network design and planning software. For this, a single cell was deployed on a sample area of Barcelona and different coverage, signal quality, capacity predictions and simulations were carried out. Some parameters such as the receiver height, the transmitter height, the number of antennas used in transmission and reception, the number of beams used by the beam-based antennas, the number of users and the different MIMO techniques, were tested and varied in order to understand their impact in area the cell can cover, its capacity, the traffic loads that can be handled and the data rates experienced by the users.

From the different studies performed, it was demonstrated how beamforming improved the signal quality and the network capacity thanks the high gain beams pointed toward users. Also, it was shown how the different MIMO techniques made use of diversity and capacity gains to improve the $C/(I+N)$ level at the receiver and the user throughput.

Resumen

Esta tesis consiste en el estudio de algunas de las características principales de 5G NR como lo son massive MIMO y beamforming y cómo son modeladas por Atoll, un software de diseño y planificación de redes. Para ello, una sola celda fue desplegada en un área de muestra de Barcelona y diferentes predicciones de cobertura, calidad de señal, capacidad y simulaciones fueron llevadas a cabo. Algunos parámetros, como la altura del receptor, la altura del transmisor, el número de antenas usado en transmisión y recepción, el número de beams utilizado por las antenas con capacidades de beamforming, el número de usuarios y las diferentes técnicas de MIMO fueron probadas y variadas con el fin de entender su impacto en el área que una celda puede cubrir, su capacidad, las cargas de tráfico que pueden ser manejadas y la velocidad de datos experimentada por los usuarios.

De los diferentes estudios realizados, pudo ser demostrado cómo beamforming mejoró la calidad de la señal y la capacidad de la red gracias a los beams con alta ganancia apuntados hacia los diferentes usuarios. También, fue mostrado cómo las diferentes técnicas de MIMO hicieron uso de las ganancias de diversidad y de capacidad para mejorar el nivel de $C/(I+N)$ en el receptor y las velocidades en el usuario.

Resum

Aquesta tesi consisteix en l'estudi d'algunes de les característiques principals del 5G NR com són massive MIMO i beamforming, i com són modelades per Atoll, un programari de disseny i planificació de xarxes. Per a això, es va desplegar una sola cel·la en una àrea de mostra de Barcelona i s'han dut a terme diferents prediccions de cobertura, qualitat de senyal, capacitat i simulacions. Alguns paràmetres s'han provat i modificat com l'altura del receptor, l'altura del transmissor, el nombre d'antenes usat en transmissió i recepció, el nombre de beams utilitzat per les antenes amb capacitats de beamforming, el nombre d'usuaris i les diferents tècniques de MIMO, per tal d'entendre el seu impacte en l'àrea que una cel·la pot cobrir, la seva capacitat, les càrregues de trànsit que poden ser manejades i les velocitats de dades experimentades pels usuaris.

Dels diferents estudis realitzats, s'ha demostrat com el beamforming millora la qualitat del senyal i la capacitat de la xarxa gràcies als beams amb alt guany apuntant cap als diferents usuaris. També, s'ha mostrat com les diferents tècniques de MIMO fan ús dels guanys de diversitat i de capacitat per millorar el nivell de $C/(I+N)$ en el receptor i les velocitats en l'usuari.

Dedication: This thesis is dedicated to my beloved family, who despite the distance, always supported me and encouraged me to continue in times when things seemed to be impossible to achieve.

Acknowledgements

I would like to thank my supervisors, Anna Umbert and Ramon Ferrús, who gave me the opportunity to work in this thesis, for their guidance and time dedicated. Also, I would like to thank Sergio Garcia, from the technical staff, who always helped me when needed.

Revision history and approval record

Revision	Date	Purpose
0	06/06/2019	Document creation
1	14/07/2019	Document revision
2	15/07/2019	Document correction
3	16/07/2019	Document revision

Written by:		Reviewed and approved by:	
Date	13/07/2019	Date	16/07/2019
Name	Riviel Ernesto Ríos	Name	Anna Umbert / Ramon Ferrús
Position	Project Author	Position	Project Supervisor

Table of contents

Abstract	1
Resumen	1
Resum	2
Acknowledgements	4
Revision history and approval record	5
Table of contents	6
List of Figures	8
List of Tables	11
1. Introduction	12
1.1. Context and motivation.....	12
1.2. Objectives.....	12
1.3. Document structure.....	13
2. 5G radio technology fundamentals	14
2.1. 5G New Radio (NR).....	14
2.1.1. 5G NR use cases.....	14
2.1.2. Technical requirements and frequency bands.....	15
2.1.3. Waveform, numerology and frame structure.....	17
2.1.4. Duplex schemes.....	18
2.1.5. NR physical layer.....	19
2.2. Multi-antenna transmission.....	21
2.3. Millimeter wave communications.....	23
3. Atoll planning tool for 5G NR networks	25
3.1. General parameters for network configuration.....	25
3.2. Traffic parameters.....	30
3.3. Beamforming features.....	31
3.4. MIMO features.....	34
3.5. Propagation models.....	38
3.6. Predictions and simulations.....	39
4. Deployment area and radio propagation modelling	41
4.1. Geographical area of study and data.....	42
4.1.1. Digital Terrain Model (DTM).....	42
4.1.2. Clutter classes.....	43
4.1.3. Clutter heights.....	45
4.1.4. Vector layers.....	47
4.2. Radio propagation modelling.....	48
4.2.1. Use of clutter information.....	48
4.2.2. Impact of the receiver height.....	51
4.2.3. Ray tracing on microcells and macrocells.....	56
4.2.4. Impact of the transmitter height.....	59
5. Beamforming features on 5G radio planning	62
5.1. Beamforming gain.....	62
5.2. Impact of the number of beams.....	69
5.3. Impact of the number of antennas elements.....	70
5.4. Impact of the receiver height.....	71
5.5. 3D simulation results.....	74
6. Massive MIMO features on 5G radio planning	77

6.1.	Transmit diversity	77
6.1.1.	Impact of transmission antennas on transmit diversity mode	77
6.1.2.	Impact of receiving antennas on transmit diversity mode	79
6.2.	Single-user MIMO	82
6.2.1.	Impact of transmission antennas on SU-MIMO	82
6.2.2.	Impact of receiving antennas on SU-MIMO	83
6.3.	Multi-user MIMO	86
6.3.1.	Impact of receiving antennas on MU-MIMO	86
6.3.2.	Impact of transmission antennas on MU-MIMO	89
6.3.3.	Impact of the number of users on MU-MIMO	92
6.3.4.	3D simulation results	94
7.	Conclusions and future development	96
	Bibliography	98
	Abbreviations and acronyms	99

List of Figures

Figure 1. 5G NR uses cases [1]	15
Figure 2. 5G NR frame structure [5]	18
Figure 3. 5G NR duplex schemes	18
Figure 4. NR user-plane protocol stack	19
Figure 5. Phased array antenna [10]	21
Figure 6. Antenna panel with 64 dual-polarized antenna elements	22
Figure 7. Massive MIMO scheme	23
Figure 8. Atoll working environment	25
Figure 9. Bearer selection threshold according to the $C/(I+N)$	30
Figure 10. Physical parameters of beamforming antennas	32
Figure 11. Beamforming pattern parameters	33
Figure 12. Beam patterns	33
Figure 13. SU-MIMO 16x8 capacity gains depending on the $C/(I+N)$ level	34
Figure 14. MU-MIMO 16x8 capacity gains	36
Figure 15. Multi-user diversity gain	37
Figure 16. Vertical and horizontal components in the Aster Propagation Model	38
Figure 17. Barcelona sample area coordinates	42
Figure 18. Digital Terrain Model data	43
Figure 19. Clutter classes	44
Figure 20. Clutter height	46
Figure 21. Vector layers	47
Figure 22. Path loss using the Aster Propagation Model (left) and the Standard Propagation Model (right)	49
Figure 23. Path loss distribution using the Aster Propagation Model and the Standard Propagation Model	50
Figure 24. Path loss using the Aster Propagation Model with 5 m receiver height	52
Figure 25. Path loss distribution using the Aster Propagation Model and receiver height at 1.5 m vs receiver height at 5 m (top left), 10 m (top right), 20 m (bottom left) and 30 m (bottom right)	53
Figure 26. Path loss using the Standard Propagation Model with 5 m receiver height	54
Figure 27. Path loss distribution for the receiver height at 1.5 m vs receiver height at 5 m (top left), 10 m (top right), 20 m (bottom left) and 30 m (bottom right) using the Standard Propagation Model	55
Figure 28. Path loss using the Aster Propagation Model and Standard Propagation Model with 10 m receiver height	56
Figure 29. Path loss using the Aster Propagation Model without ray tracing (left) and with ray tracing (right) for a micro cell	57
Figure 30. Path loss distribution using the Aster Propagation Model with and without ray tracing for a micro cell	58
Figure 31. Path loss distribution using the Aster Propagation Model with and without ray tracing for a macro cell	59
Figure 32. Path loss distribution for the transmitter height at 30 m vs transmitter height at 15 m (left) and at 45 m (right) using the Aster Propagation Model	60
Figure 33. Path loss distribution for the transmitter height at 30 m vs transmitter height at 15 m (left) and at 45 m (right) using the Standard Propagation Model	61

Figure 34. SS-RSRP level with beamforming antenna (left) and without beamforming (right).....63

Figure 35. SS-RSRP level distribution with beamforming antenna and without beamforming antenna.....63

Figure 36. PDSCH level with beamforming antenna (left) and without beamforming (right)64

Figure 37. PDSCH level distribution with beamforming antenna and without beamforming antenna65

Figure 38. PDSCH CINR distribution with beamforming antenna and without beamforming antenna66

Figure 39. Modulation with beamforming antenna (left) and without beamforming (right)67

Figure 40. Modulation distribution with beamforming antenna and without beamforming antenna67

Figure 41. Peak RLC allocated bandwidth throughput with beamforming antenna (left) and without beamforming (right)68

Figure 42. Throughput distribution with beamforming antenna and without beamforming antenna69

Figure 43. Throughput distribution of beamformer 2 and default beamformer70

Figure 44. Throughput distribution of beamformer 3 and default beamformer71

Figure 45. PDSCH signal level distribution for receiver heights at 10 m (top left), 20 m (top right), 40 m (bottom left) and 50 m (bottom right) using beamforming 2 and the 70deg 17dBi 3Tilt antenna.....72

Figure 46. Throughput distribution for receiver heights at 10 m (top left), 20 m (top right), 40 m (bottom left) and 50 m (bottom right) using beamforming 2 and the 70deg 17dBi 3Tilt antenna74

Figure 47. User connection distribution using beamformer 2 (left) and using the 70deg 17dBi 3Tilt antenna (right)76

Figure 48. PDSCH C/(I+N) for SISO vs diversity 4x1 (top left), 16x1 (top right), 64x1 (bottom left) and 128x1 (bottom right).....78

Figure 49. Throughput for SISO vs diversity 4x1 (top left), 16x1 (top right), 64x1 (bottom left) and 128x1 (bottom right).....79

Figure 50. PDSCH C/(I+N) for SISO vs diversity 64x1 (top left), 64x2 (top right), 64x4 (bottom left) and 64x8 (bottom right).....80

Figure 51. Throughput for SISO vs diversity 64x1 (top left), 64x2 (top right), 64x4 (bottom left) and 64x8 (bottom right).....81

Figure 52. Throughput for SISO vs SU-MIMO 4x4, 16x4, 64x4, 128x482

Figure 53. PDSCH C/(I+N) for SISO vs SU-MIMO 64x1 (top left), 64x2 (top right), 64x4 (bottom left) and 64x8 (bottom right).....84

Figure 54. Throughput for SISO vs SU-MIMO 64x1 (top left), 64x2 (top right), 64x4 (bottom left) and 64x8 (bottom right).....85

Figure 55. PDSCH C/(I+N) for SISO vs MU-MIMO 64x1 (top left), 64x2 (top right), 64x4 (bottom left) and 64x8 (bottom right).....87

Figure 56. Throughput for SISO vs MU-MIMO 64x1 (top left), 64x2 (top right), 64x4 (bottom left) and 64x8 (bottom right).....88

Figure 57. PDSCH C/(I+N) for SISO vs MU-MIMO 4x4 (top left), 16x4 (top right), 64x4 (bottom left) and 128x4 (bottom right).....90

Figure 58. Throughput for SISO vs MU-MIMO 4x4 (top left), 16x4 (top right), 64x4 (bottom left) and 128x4 (bottom right).....91

Figure 59. Throughput for SISO vs MU-MIMO 64x1 for 10 users (top left), 20 users (top right), 30 users (bottom left) and 40 users (bottom right)93

Figure 60. User connection distribution using beamformer 2 together with MIMO95

List of Tables

Table 1. Minimum Technical Performance Requirements for IMT-2020 [2]	15
Table 2. NR Operating Bands [3].....	16
Table 3. Base Station Subsystem Equipment.....	26
Table 4. Transmitter Total Loses	26
Table 5. 5G NR Cell Parameters	28
Table 6. Radio Bearer for 5G NR Radio Equipment	28
Table 7. Broadband Service Characteristics.....	30
Table 8. Business User Profile Characteristics	31
Table 9. MU-MIMO Diversity Gain.....	35
Table 10. Transmit and Receive Diversity Gains	37
Table 11. Propagation Models Characteristics	38
Table 12. Coverage Prediction in Atoll	39
Table 13. 3.5 GHz Frequency Band Characteristics	41
Table 14. DTM Parameters of Accuracy.....	43
Table 15. Clutter Classes Parameters of Accuracy	43
Table 16. Clutter Classes	44
Table 17. Clutter Height File Parameters of Accuracy	46
Table 18. Vector Layers	47
Table 19. Losses per Clutter Class for SPM.....	48
Table 20. Beamforming Antenna Parameters.....	62
Table 21. Average Results for 3D Simulations Using Beamforming	75
Table 22. Diversity Gains and Covered Area for Transmit Diversity	80
Table 23. Capacity Gain and Maximum Throughput for SU-MIMO with Different Number of Transmission Antennas	83
Table 24. Maximum Capacity Gains and Maximum Throughputs for SU-MIMO with Different Number of Receiving Antennas	86
Table 25. Minimum Gain, Maximum Gain and Maximum Throughput for MU-MIMO with Different Number of Receiving Antennas.....	89
Table 26. Total Gains and Maximum Throughputs for MU-MIMO with Different Number of Transmission Antennas	92
Table 27. Maximum Gain and Maximum Throughput for Different MU-MIMO Users	93
Table 28. Average Results for 3D Simulations Using Beamforming and MIMO	94

1. Introduction

1.1. Context and motivation

Over the past decades, mobile communication technology has been developing as the users' demands keeps growing and new usage scenarios are discovered. The evolution of mobile communications has gone from analog voice in the 80's with the first generation of mobile communications (1G), to digital voice in the 90's with 2G, to mobile broadband in the beginning of the 2000 with 3G, which enabled fast wireless internet access and left behind the voice as the main focus, to opening the way to further enhanced mobile broadband with 4G and LTE as the main technology around 2010.

Now, as we face the beginning of a new decade, the fifth generation of mobile communication (5G) promises to address not only the insatiable demand for mobile broadband with multi-Gbps data rates, but also to enable new use cases, such as massive scale communications connecting thousands of devices, sensors, cameras, providing new solutions in areas like industry, transport and logistics, agriculture and also guaranteeing ultra-reliable and low latency services with applications in the public safety area, remote surgery, communication between vehicles, etc.

In order to be able to support all these use scenarios the 5G technology has some key features such as beamforming, massive MIMO and the use of millimeter wave that improve the coverage and the capacity, the robustness and reliability of the communications.

But before the commercial deployment of any new technology, there is a phase of planning, where the radio engineering aspects such as determining the location of the base stations, estimating the capacity and size of the cells in terms of coverage and capacity, assigning the frequencies and studying the radio propagation and interference on the environment are studied and simulated.

To do this type of planning, operators use tools such as Atoll. Atoll is a platform from the company Forsk, for wireless network design and optimization that supports a wide range of radio access technologies.

1.2. Objectives

This thesis aims to make use of Atoll to test the capabilities and key features of the 5G radio access technology. For this, the following objectives were defined:

- Identify the different parameters that Atoll allows to configure for modelling a 5G network.
- Understand how Atoll makes use of different geographic data to model the terrain characteristics.
- Identify the differences on the path loss calculations carried out by Atoll between a transmitter and a receiver using different propagation models.
- Determine how coverage, signal quality and user throughput can be improved by using beamforming-capable antennas.
- Determine how coverage, signal quality and user throughput can be improved by using different MIMO configurations.

1.3. Document structure

This thesis is divided into 7 chapters.

The first chapter consists on an introduction of the 5G technology and the objectives of the thesis.

The second chapter explains the fundamental concepts and key features of 5G, as a preparation chapter to understand and give a context to the upcoming chapters.

The third chapter presents the capabilities of Atoll and the different parameters related to the radio calculation, propagation models, beamforming features and MIMO features included in the software.

The fourth chapter describes the geographical area where the study takes place, the geographic data used in Atoll necessary for the different calculations, and a comparative between different propagation models to see their path loss response depending on the type of data used the type of cell, the receiver height and the transmitter height.

The fifth chapter consists on the analysis of coverage predictions in the downlink and simulations to determine how beamforming changes the performance of a network.

The sixth chapter consists on how Atoll models the massive MIMO capabilities of 5G NR the analysis of MIMO performance in terms of signal quality and throughput.

Finally, the seventh chapter presents the final conclusions of the thesis and the future work to could be carry out continue the analysis of the 5G network planning and optimization.

2. 5G radio technology fundamentals

In this chapter, the fundamental concepts and the key features of 5G NR are presented. The first section of this chapter provides a brief introduction of 5G NR, its use cases and important concepts on its design. The second section outlines the physical channels defined for NR. The third section talks the multi-antenna transmission where concepts as beamforming and massive MIMO are discussed. Finally, section four talks about the 5G millimeter waves communications.

2.1. 5G New Radio (NR)

The fifth generation of the wireless access technology is known as 5G New Radio (5G NR) and it has been developed by the Third-Generation Partnership Project (3GPP) over the past years with the goal to address a variety of scenarios to be enabled by future enhanced mobile technologies.

Compared to LTE, the previous 4G radio access technology, 5G NR presents many benefits, such as:

- Exploitation of higher frequency bands in order to support very wide transmission bandwidths and very high data rates.
- Ultra-lean design to enhance network energy performance and reduce interference, avoiding the always-on transmissions.
- Support of multiple subcarriers spacing
- Forward compatibility for the future, enabling new services yet unknown.
- Low latency to improve performance.
- Beam-centric design enabling extensive usage of beamforming and massive number of antenna elements not only for data transmission but also for control-plane procedures.

This section covers fundamental concepts and terminologies related to the 5G NR technology.

2.1.1. 5G NR use cases

5G has been thought to cover three major use cases:

- **Enhanced mobile broadband (eMBB):** services that demand high data rates, high traffic volumes and wide-area coverage. The eMBB address human-centric communications.
- **Massive machine-type communication (mMTC):** services characterized by a massive number of devices, such as sensors, wearable, IoT devices, etc., that do not require high energy consumption and at a low cost. These devices consume and generate small amount of data, hence, support of high data rates is not important. This is machine-centric use case.
- **Ultra-reliable and low-latency communication (URLLC):** services that require very low latency and very high reliability and availability. Some examples are traffic safety, factory automation, e-health services, self-driving car, etc. It covers human- and machine-centric communications.

Even though these are the three distinctive use cases, there are scenarios where use cases may be combined, due to the wide range of possibilities for specific services that this technology brings.

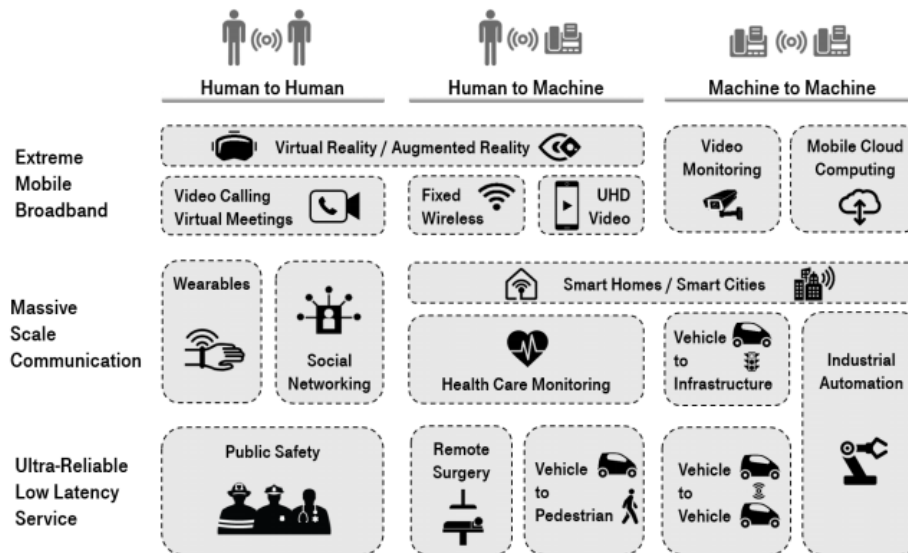


Figure 1. 5G NR uses cases [1]

2.1.2. Technical requirements and frequency bands

As part of the standardization process of 5G, the ITU-R, the radio communication sector of the International Telecommunication Union (ITU), responsible for ensuring efficient use of the RF spectrum, issued the International Mobile Telecommunications-2020 (IMT-2020), a series of requirements for the 5G networks.

The following table summarizes the minimum requirements related to technical performance for IMT-2020 radio interfaces, which are based on a set of capabilities needed to support the 5G use cases and usages scenarios.

Table 1. Minimum Technical Performance Requirements for IMT-2020 [2]

Parameter	Minimum Technical Performance Requirement
Peak data rate	Downlink: 20 Gbps Uplink: 10 Gbps
Peak spectral efficiency	Downlink: 30 bit/s/Hz Uplink: 15 bit/s/Hz
User-experienced data rate	Downlink: 100 Mbps Uplink: 50 Mbps
Area traffic capacity	10 Mbps/m ² (indoor hotspot for eMBB)
User plane latency	4 ms for eMBB 1 ms for URLLC
Control plane latency	20 ms
Connection density	1,000,000 devices per km ²
Energy efficiency	Efficient data transmission in a loaded case

	Low energy consumption when there is no data High sleep ratio Long sleep duration
Reliability	1-10 ⁻⁵ success probability of transmitting a layer 2 PDU of 32 bytes within 1 ms, at coverage edge in Urban Macro for URLLC
Mobility	1.5 bit/s/Hz at 10 km/h for indoor hotspot eMBB 1.12 bit/s/Hz at 30 km/h for dense urban eMBB 0.8 bit/s/Hz at 120 km/h for rural eMBB 0.45 bit/s/Hz at 500 km/h for rural eMBB
Mobility interruption time	0 ms
Bandwidth	At least 100 MHz and up to 1 GHz in higher frequency bands. Scalable bandwidth shall be supported

NR can be deployed in different frequency bands, which were defined by 3GPP on the Release 15 work. Because of different RF requirements (e.g. maximum transmission power), these bands were divided into two frequency ranges:

- **Frequency range 1 (FR1)** that includes all existing and new bands below 6 GHz.
- **Frequency range 2 (FR2)** that includes new bands in the range of 24.25 – 52.6 GHz.

At the same time, 3GPP defined the operating bands, corresponding to different frequency ranges for downlink and uplink.

Table 2. NR Operating Bands [3]

NR Operating Band	Uplink Range (MHz)	Downlink Range (MHz)	Duplex Mode
Frequency Range 1 (FR1)			
n1	1920 – 1980	2110 – 2170	FDD
n2	1850 – 1910	1930 – 1990	FDD
n3	1710 – 1785	1805 – 1880	FDD
n5	824 – 849	869 – 894	FDD
n7	2500 – 2570	2620 – 2690	FDD
n8	880 – 915	925 – 960	FDD
n12	699 – 716	729 – 746	FDD
n20	832 – 862	791 – 821	FDD
n25	1850 – 1915	1930 – 1995	FDD
n28	703 – 748	758 – 803	FDD
n34	2010 – 2025	2010 – 2025	TDD
n38	2570 – 2620	2570 – 2620	TDD
n39	1880 – 1920	1880 – 1920	TDD
n40	2300 – 2400	2300 – 2400	TDD
n41	2496 – 2690	2496 – 2690	TDD
n50	1432 – 1517	1432 – 1517	TDD
n51	1427 – 1432	1427 – 1432	TDD
n66	1710 – 1780	2110 – 2200	FDD
n70	1695 – 1710	1995 – 2020	FDD
n71	663 – 698	617 – 652	FDD

n74	1427 – 1470	1475 – 1518	FDD
n75	N/A	1432 – 1517	SDL
n76	N/A	1427 – 1432	SDL
n77	3300 – 4200	3300 – 4200	TDD
n78	3300 – 3800	3300 – 3800	TDD
n79	4400 – 5000	4400 – 5000	TDD
n80	1710 – 1785	N/A	SUL
n81	880 – 915	N/A	SUL
n82	832 – 862	N/A	SUL
n83	703 – 748	N/A	SUL
n84	1920 – 1980	N/A	SUL
n86	1710 – 1780	N/A	SUL
Frequency Range 2 (FR2)			
n257	26500 – 29500	26500 – 29500	TDD
n258	24250 – 27500	24250 – 27500	TDD
n260	37000 – 40000	37000 – 40000	TDD
n261	27500 – 28350	27500 – 28350	TDD

2.1.3. Waveform, numerology and frame structure

5G NR uses orthogonal frequency division multiplexing (OFDM) with cyclic prefix (CP) for both downlink and uplink.

One of the key features of 5G NR is its scalable OFDM numerology ($\mu=0,1,2,3,4$), which adopts flexible subcarrier spacing of $2^\mu \cdot 15$ kHz (from 15 kHz up to 240 kHz). Accordingly, the CP is also proportionally scalable. This allows a wide range of deployment scenarios, from frequency bands below 1 GHz up to millimeter wave bands. [4]

The NR time-domain structure consists on a 10 ms frame divided into ten 1 ms subframes. In turn, a subframe is divided into slots of 14 OFDM symbols each, and its duration in milliseconds depends on the numerology.

On the frequency domain, the resource block (RB) consists of 12 consecutive subcarriers. A NR radio carrier is limited to 3300 active subcarriers (275 RB) which results in carrier bandwidths of 50, 100, 200 and 400 MHz for subcarrier spacing of 15, 30, 60 and 120 kHz, respectively. If even larger bandwidths are to be supported, carrier aggregation can be used, where multiple NR carriers can be aggregated and transmitted in parallel to or from the same device. Up to 16 carriers, can be aggregated allowing bandwidths up to 6.4 GHz.

Figure 2 shows the frame structure previously discussed.

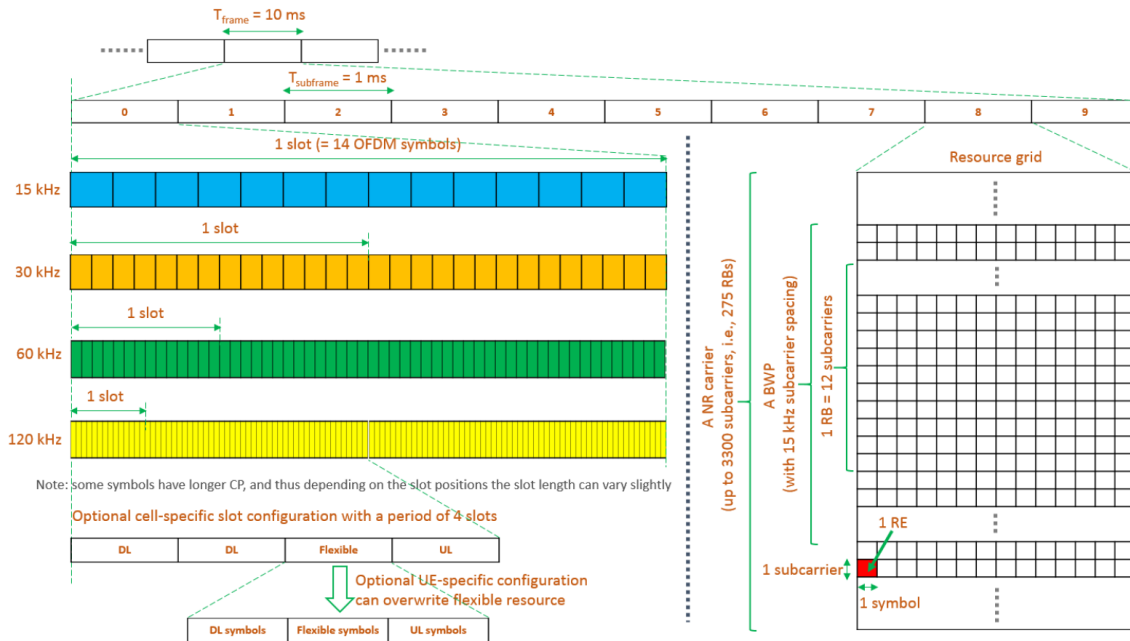


Figure 2. 5G NR frame structure [5]

2.1.4. Duplex schemes

5G NR supports both frequency-division duplex (FDD) for lower frequency bands and time-division duplex (TDD) for higher frequency bands, subject to either half-duplex or full duplex.

In the case of TDD operation, a single carrier frequency is used for separated downlink and uplink transmissions. NR uses dynamic TDD where a slot can be dynamically allocated to either uplink or downlink as part of the scheduler decision. TDD systems provide a large guard time where neither downlink nor uplink transmissions occur, which allows switching the transmission direction and to avoid interference at the base station. [6]

On the other hand, for FDD operation, uplink and downlink transmissions occur simultaneously but use different carrier frequencies. There is also possible a half-duplex mode, where transmissions are separated in frequency and in time.

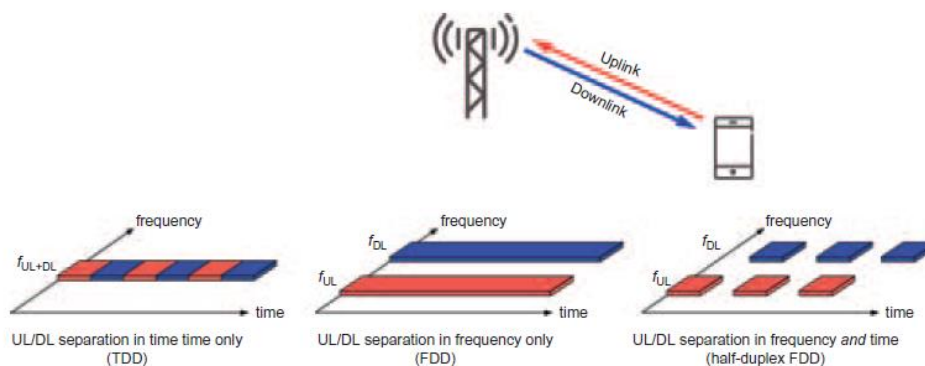


Figure 3. 5G NR duplex schemes

2.1.5. NR physical layer

5G NR protocol architecture is separated into control-plane and data-plane. The user plane is in charge of user data and the control plane is responsible for connection setup, mobility and security.

The user-plane protocol stack is split into the following layers: physical layer (PHY), medium access control layer (MAC), radio link control layer (RLC), packet data convergence protocol layer (PDCP) and service data adaptation protocol (SDAP) layer. The functionalities of these layers. In particular, the PHY layer handles coding/decoding, modulation/demodulation, multi-antenna processing and mapping of signals to physical time-frequency resources.

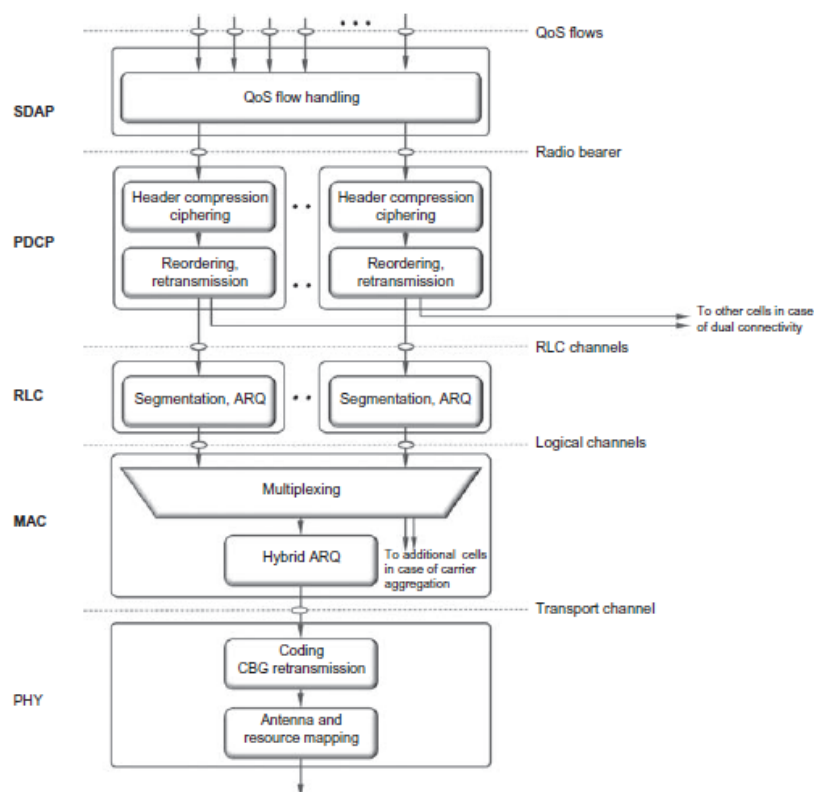


Figure 4. NR user-plane protocol stack

The time-frequency resources carrying information from higher layers (above PHY) are termed physical channels. [7]

The physical channels defined for NR are the following:

- **Physical Downlink Shared Channel (PDSCH):** main physical channel used for unicast data transmission. It also used for transmission of paging information and delivery of part of the system information.
- **Physical Broadcast Channel (PBCH):** carries part of the system information, required by the device to access the network.

- **Physical Downlink Control Channel (PDCCH):** used for downlink control information, mainly scheduling decisions, required for reception of PDSCH and for scheduling grants enabling transmission on the PUSCH.
- **Physical Uplink Shared Channel (PUSCH):** is the uplink counterpart to the PDSCH.
- **Physical Uplink Control Channel (PUCCH):** used by the device to send hybrid-ARQ acknowledgements, to send channel-state reports and for requesting resources to transmit uplink data upon.
- **Physical Random-Access Channel (PRACH):** used by the UE to request connection setup referred to as random access.

The downlink and uplink transmission between gNB (the radio access network node) and the UE work as follows. [8]

In the downlink, the UE monitors the PDCCH, typically once per slot. After detecting a valid PDCCH, the UE receives one unit of data (transport block) on the PDSCH following the scheduling decision of the gNB. Afterwards, the UE responds with a hybrid ARQ acknowledgment indicating if data was successfully decoded or not.

In the uplink, the UE requests the gNB for physical time-frequency resources to transmit data (scheduling request) and this request is sent over the PUCCH. In response, the gNB sends a scheduling grant over the PDCCH, which gives permission to a UE to use certain resources for transmission. Following the scheduling grant, the UE schedules its data transmission over the PUSCH, data that is received by the gNB and sends hybrid ARQ acknowledgement indicating if the data was decoded correctly or not.

On the other hand, the physical signals correspond to a set of time-frequency resources used by the PHY layer but do not carry information originating from higher layers. These signals are reference signals used for purposes such as demodulation, channel estimation, synchronization and channel-state information.

The downlink physical signals are:

- Demodulation Reference Signal (DM-RS)
- Phase Tracking Reference Signal (PT-RS)
- Channel State Information Reference Signal (CSI-RS)
- Primary Synchronization Signal (PSS)
- Secondary Synchronization Signal (SSS)

Furthermore, the uplink physical signals are:

- Demodulation Reference Signal (DM-RS)
- Phase Tracking Reference Signal (PT-RS)
- Sounding Reference Signal (SRS)

In particular, the PSS and the SSS are signals used in the cell search process, used by UE to find a new cell. The PSS is the first signal that the UE search for and the SSS is a signal transmitted to enable detection of the physical cell ID, an identifier of a cell at physical layer.

Also, 3GPP define some physical layer measurements. One of these measurements is the SS reference signal received power (SS-RSRP), which is defined as the linear average over the power contributions (in Watts) of the resource elements that carry secondary synchronization signals (SSS). [9] This measurement is relevant in the next chapters for understanding the performance of the cell.

2.2. Multi-antenna transmission

Multi-antenna transmission, through the use of massive Multiple Input Multiple Output (MIMO) and beamforming, is a key feature of 5G NR and its use can improve the mobile communication system performance.

It is possible to use multiple antennas on the transmitter to provide diversity against fading by utilizing the fact that different antennas may be at least partly uncorrelated, due to the inter-antenna spacing or due to different polarization between antennas.

Moreover, by adjusting the phase of each antenna element, multiple antennas on the transmitter can be used to provide directivity, that is, to focus the transmitted power in a certain direction [6]. This corresponds to the concept of beamforming, which actually it is just a special implementation of MIMO. This directivity can increase the data rate and range due to higher power reaching a specific location in space, and also reduces interference, which improves the spectrum efficiency.

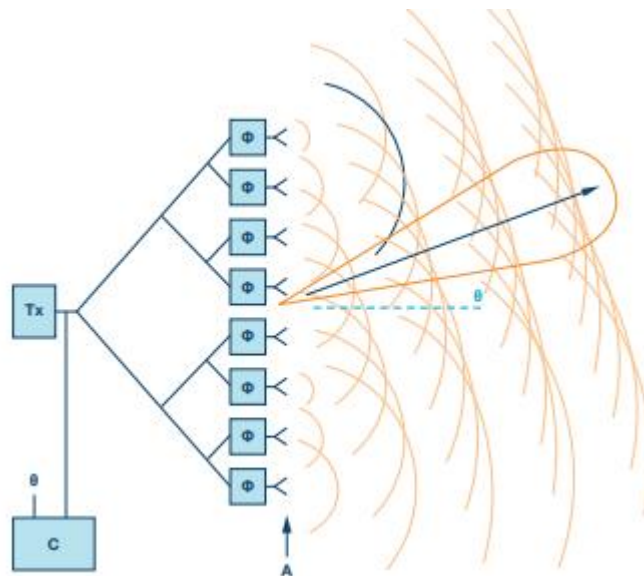


Figure 5. Phased array antenna [10]

Similarly, multiple antennas on the receiver can provide diversity, limiting the reception only in the direction of a target signal, while suppressing interference arriving from other directions.

Multiple antennas can be both used at the transmitter and the receiver, with which spatial multiplexing is achieved. This corresponds to the transmission of multiple layers of information in parallel using the same time and frequency resources.

Antenna panels, such as the one illustrated on Figure 5, consisting on a large number of small antennas can be used to change the beam direction by adjusting individually the phase of the signals applied to each antenna element. This can be done both in the transmitter side and in the receiver side. The use of focused beams maximizes the user equipment (UE) SNR, consequently improving the communication link for higher modulation and coding schemes. [11]

Since the antenna elements separation is proportional to the wavelength, these antenna panels can have a very reduced size at high frequencies. The antenna panel shown on Figure 5 consists of 64 dual-polarized antenna elements, targeting the 28 GHz band. In order to have a reference of the size of the antenna panel, a AAA battery was placed next to it.

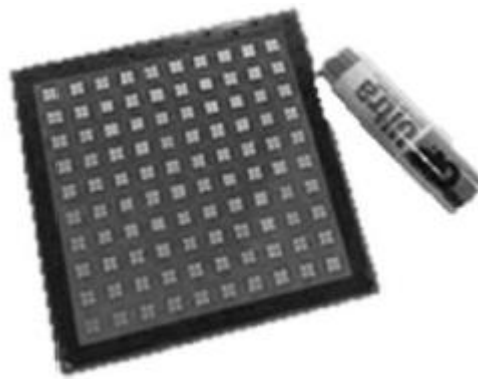


Figure 6. Antenna panel with 64 dual-polarized antenna elements

On the other hand, depending on the number of users, different multi-antenna schemes can be considered: single-user MIMO (SU-MIMO) or spatial multiplexing and multi-user MIMO (MU-MIMO).

In SU-MIMO, a single user is scheduled within a given time/frequency resource with transmission of a large number of layers in parallel (up to 8 layers). In other words, a UE can receive at most 8 different streams from the base station in the downlink. This scheme is mainly targeted at cell centered users with sufficient carrier-to-interference-and-noise $C(I+N)$ conditions, in order to improve the data rate. [12]

In MU-MIMO, multiple users are scheduled simultaneously within the same time/frequency resource but with a limited number of spatial layers per scheduled device, in this case, a maximum of 4 layers. In contrast with SU-MIMO, where the spatial multiplexing gain is confined to a single user, MU-MIMO allows multiple co-scheduled users to exploit this gain among two or more UE.

One important benefit of using MU-MIMO, is the possibility of reducing the circuitry complexity on the UEs, since UEs would only require a single antenna to benefit from the gains. This is contrary to SU-MIMO which only provides considerable gains with more than one antenna at the user equipment.

In 5G NR, all these the benefits of the MIMO schemes can be taken to a larger scale with the use of hundreds to thousands of antennas at the base station. This is referred as Massive MIMO, as seen on Figure 6. A larger number of antennas provides the advantages of increased gain, signal to noise ratio, coverage, capacity, data rates and decreased latency, compared to the conventional MIMO systems with fewer antennas. [13]

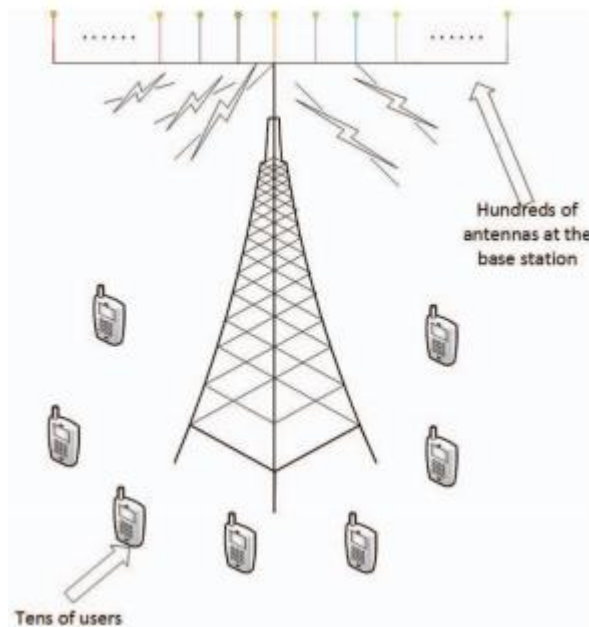


Figure 7. Massive MIMO scheme

2.3. Millimeter wave communications

NR can operate in frequencies above 24.25 GHz, corresponding to the frequency range 2 (FR2). This range of frequencies is also known as millimeter wave (mmWave) frequencies.

The main reason of interest behind the use of mmWave is the huge amount of spectrum available in these higher bands. While bands below 6 GHz offer channel bandwidths of up to 100 MHz, the mmWave band offers much larger bandwidths of 500 MHz or even 1 GHz. [14]

These frequencies are expected to support data rates in the order of the Gbps, however, due to high frequencies, mmWave presents major impediments, such as high path loss, increased effect of blockage as a result of weaker non-line-of-sight paths and attenuation due to rain and atmospheric absorption.

It is known that the free space path loss is dependent on the squared of the carrier frequency f_c^2 and therefore, for example, increasing the frequency from 3 GHz to 30 GHz, will add a power loss of 20 dB, regardless the distance between the transmitter and the receiver. [15]

With the small wavelengths, mmWave band is sensitive to blockage by obstacles with a significantly larger size than the wavelength (e.g human body). Studies has shown that human body can attenuate mmWave signals up to 35 dB. [16]

Also, mmWaves signals are affected by many atmospheric factors such as precipitation due to rain, since raindrops are approximately of the same size as the wavelengths; interaction with gas molecules like oxygen, nitrogen dioxide and water vapor present in the atmosphere; and power loss due to foliage obstruction caused by vegetation and the effects of multipath dispersion, diffraction and reflection. [17]

Nevertheless, technologies such as massive MIMO and beamforming that make use of hundreds of antenna elements, consequently, offering high gains help overcome the high path losses and blockages. [18]

3. Atoll planning tool for 5G NR networks

Atoll is a platform from the company Forsk, for wireless network design and optimization that supports a wide range of radio access technologies such as 5G NR, LTE, NB-IoT, UMTS, GSM, CDMA and with the latest technology advances such as MIMO, 3D Beamforming and mmWave propagation. This platform can provide a framework to operators and vendors for designing, optimizing and planning their networks, as technology keeps evolving and users are demanding more and better services.

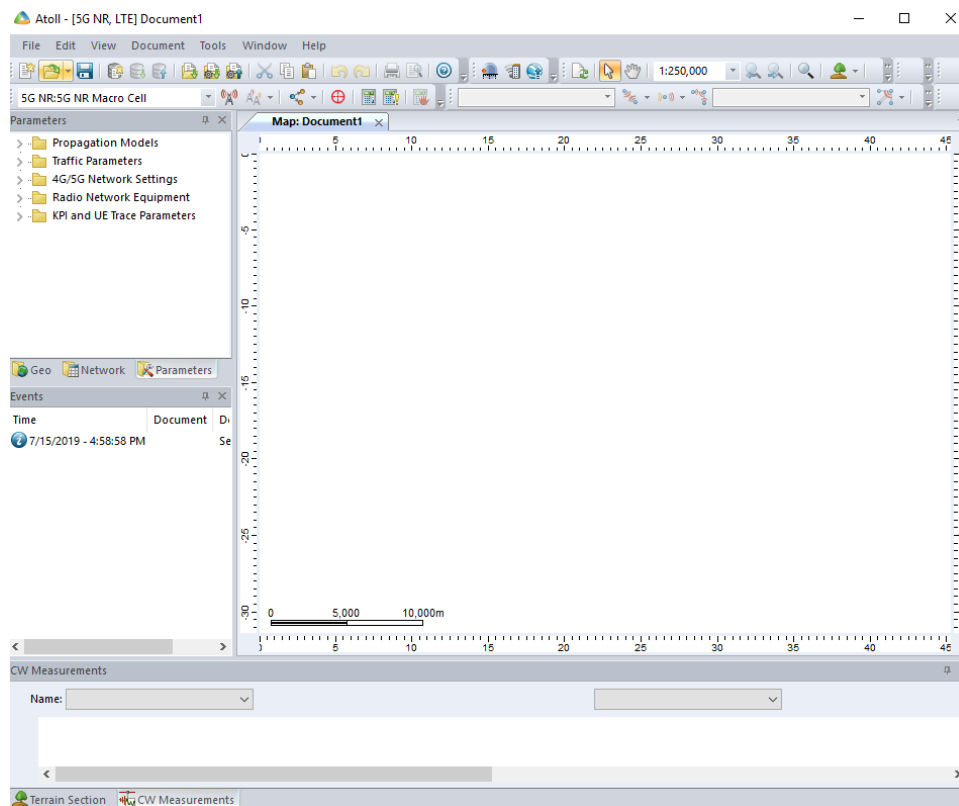


Figure 8. Atoll working environment

In this chapter, some of the key features of Atoll and parameters configured related to the radio calculation, propagation models, the traffic and capacity planning for 5G NR networks are presented. The configurations mentioned in this chapter are used for the studies carried out on the upcoming chapters, so they should be considered all the time, unless specified differently.

It is important to clarify that most of the information presented in this chapter was obtained from the Atoll User Manual [19], the Atoll Technical Reference Guide [20], the Aster User Manual [21] and the Aster Technical Reference Guide [22].

3.1. General parameters for network configuration

Atoll allows to model the different equipment and parameters necessary to design a network, which include the base station, the transmitter equipment and the cell parameters.

The site is defined as the geographical point where the base station and its transmitters are located. Transmitters consist of all the all the equipment used to generate the radio waves in order to transmit or receive data with the use of an antenna. Finally, a cell is the RF channel configured on a transmitter.

The base station subsystem consists of three elements and their properties are taken into account to calculate the downlink and uplink losses:

- **Tower-mounted amplifier (TMA):** are used to reduce the composite noise figure of the base station.
- **Feeder cables:** connect the TMA with the antenna.
- **Transmitter equipment.**

The following table shows the parameters configured for the base station subsystem.

Table 3. Base Station Subsystem Equipment

TMA	Default TMA Equipment
Feeder	Default 1/2" Feeder
Transmitter	Default eNode-B Equipment
Feeder length	5 m (tx) / 5 m (rx)

Due to the use of these predefined equipment, the total transmission and reception losses were:

Table 4. Transmitter Total Loses

	Transmission	Reception
Total losses (dB)	1.51	-2.09

Parameters such as the antenna model, the mechanical azimuth, mechanical downtilt and the number of antennas for transmission and reception can also be defined. Mechanical azimuth was set to 240° and mechanical downtilt was set to 0°. The antenna model and the number of transmission antennas are not mentioned in this chapter, since they are configured specifically for the studies on the other chapters.

The cell parameters that Atoll allows to configure are the following:

- **Carrier:** The carrier of the cell in the frequency band. Indicated the carrier bandwidth.
- **Max power (dBm):** The cell's maximum transmission power.
- **SSS EPRE (dBm):** The SSS energy per resource element. This value is used to calculate the transmission power corresponding to the secondary synchronization signal (SSS).
- **PSS EPRE offset / SSS (dB):** The difference in the energy of a resource element belonging to the PSS with respect to the energy of an SSS resource element. This value is used to calculate the transmission power corresponding to the primary synchronization signal (PSS).

- **Layer:** The network layer to which the cell belongs. It can be either macro layer (for macro cells) or small layer (for small/micro cells).
- **Cell type:** This indicates whether the cell is configured as primary PCell, a secondary SCell (UL), or a secondary SCell (DL).
- **Min SS-RSRP (dBm):** The minimum SS-RSRP required for a user to be connected to the cell. The SS-RSRP is compared with this threshold to determine whether or not a user is within the cell's coverage or not.
- **SS/PBCH numerology:** The numerology used by the cell for SS/PBCH.
- **SS/PBCH periodicity:** The periodicity of the SS/PBCH bursts.
- **SS/PBCH OFDM symbols:** The OFDM symbols at which the SS/PBCH blocks start and the number of SS/PBCH blocks per SS/PBCH burst.
- **PDCCH overhead (OFDM symbols):** The number of OFDM symbols per subframe assigned to the physical downlink control channel (PDCCH).
- **Traffic numerology:** The numerology used by the cell for traffic channels (PDCCH, PDSCH and PUSCH).
- **TDD DL OFDM symbols (%):** The percentage of downlink OFDM symbols out of the total number of OFDM symbols per frame.
- **Radio equipment:** cell's radio equipment.
- **Scheduler:** The scheduler used by the cell for bearer selection and resource allocation.
- **Diversity support (DL):** The type of antenna diversity technique supported by the cell in downlink.
- **Diversity support (UL):** The type of antenna diversity technique supported by the cell in uplink.
- **Number of MU-MIMO users (DL):** The average number of MU-MIMO users that share the same resources on the downlink.
- **Number of MU-MIMO users (UL):** The average number of MU-MIMO users that share the same resources on the uplink.
- **Traffic load (DL) (%):** The downlink traffic load percentage.
- **Traffic load (UL) (%):** The uplink traffic load percentage.
- **Max traffic load (DL) (%):** The downlink traffic load not to be exceeded.
- **Max traffic load (UL) (%):** The uplink traffic load not to be exceeded.
- **UL noise rise (dB):** The uplink noise rise in dB.
- **Fractional power control factor:** This factor is used for path loss compensation when performing fractional power control on the uplink. For example, if this factor is set to 0.8, only 80% of the actual path loss will be considered when estimating the received power.
- **Number of required PRACH RSI:** The number of required PRACH RSIs for this cell. The number of PRACH RSIs needed for any cell depends on the used PRACH preamble format and the cell size.
- **Max number of 4G/5G neighbors:** The maximum number of 5G NR neighbors that the cell can have.
- **Max number of inter-technology neighbors:** The maximum number of other technology neighbors that the cell can have.

Atoll have predefined station templates, where all these parameters are set by default. To create the network, one of these templates was used but changes on the frequency

band and the carrier used were applied. The following table shows the final cell configuration:

Table 5. 5G NR Cell Parameters

Frequency band	n78 (3.5 GHz)
Carrier	50 MHz - NR-ARFCN 625000
Max power (dBm)	50
SSS EPRE (dBm)	15
PSS EPRE offset / SSS (dB)	3
Layer	Macro Layer
Cell type	PCell
Min SS-RSRP (dBm)	-140
SS/PBCH numerology	0 (15 kHz)
SS/PBCH periodicity	10 ms
SS/PBCH OFDM symbols	{4,8,16,20}+28n [Lmax=4]
PDCCH overhead (OFDM symbols)	1
Traffic numerology	2 (60 kHz Normal CP)
TDD DL OFDM symbols (%)	50
Radio equipment	5G NR Radio Equipment
Scheduler	Proportional Fair
Diversity support (DL)	Transmit Diversity; SU-MIMO; MU-MIMO
Diversity support (UL)	Receive Diversity; SU-MIMO; MU-MIMO
Number of MU-MIMO users (DL)	1
Number of MU-MIMO users (UL)	1
Number of users (DL)	1
Number of users (UL)	1
Traffic load (DL) (%)	100
Traffic load (UL) (%)	100
Max traffic load (DL) (%)	100
Max Traffic Load (UL) (%)	50
UL noise rise (dB)	3
Fractional power control factor	1
Number of required PRACH RSI	10
Max number of 4G/5G neighbors	16
Max number of inter-technology neighbors	16

The 5G NR Radio Equipment defines the radio bearers and bearer selection threshold for the transmitter and the user equipment.

Table 6. Radio Bearer for 5G NR Radio Equipment

Radio Bearer Index	Modulation	Channel Coding Rate	Bearer Efficiency (bits/symbol)
19	QPSK	0.117188	0.2344

20	QPSK	0.188477	0.377
21	QPSK	0.300781	0.6016
22	QPSK	0.438477	0.877
23	QPSK	0.587891	1.1758
24	16QAM	0.369141	1.4766
25	16QAM	0.423828	1.6953
26	16QAM	0.478516	1.9141
27	16QAM	0.540039	2.1602
28	16QAM	0.601563	2.4063
29	16QAM	0.642578	2.5703
30	64QAM	0.455078	2.7305
31	64QAM	0.504883	3.0293
32	64QAM	0.553711	3.3223
33	64QAM	0.601563	3.6094
34	64QAM	0.650391	3.9023
35	64QAM	0.702148	4.2129
36	64QAM	0.753906	4.5234
37	64QAM	0.802734	4.8164
38	64QAM	0.852539	5.1152
39	256QAM	0.666504	5.332
40	256QAM	0.694336	5.5547
41	256QAM	0.736328	5.8906
42	256QAM	0.77832	6.2266
43	256QAM	0.821289	6.5703
44	256QAM	0.864258	6.9141
45	256QAM	0.89502	7.1602
46	256QAM	0.925781	7.4063

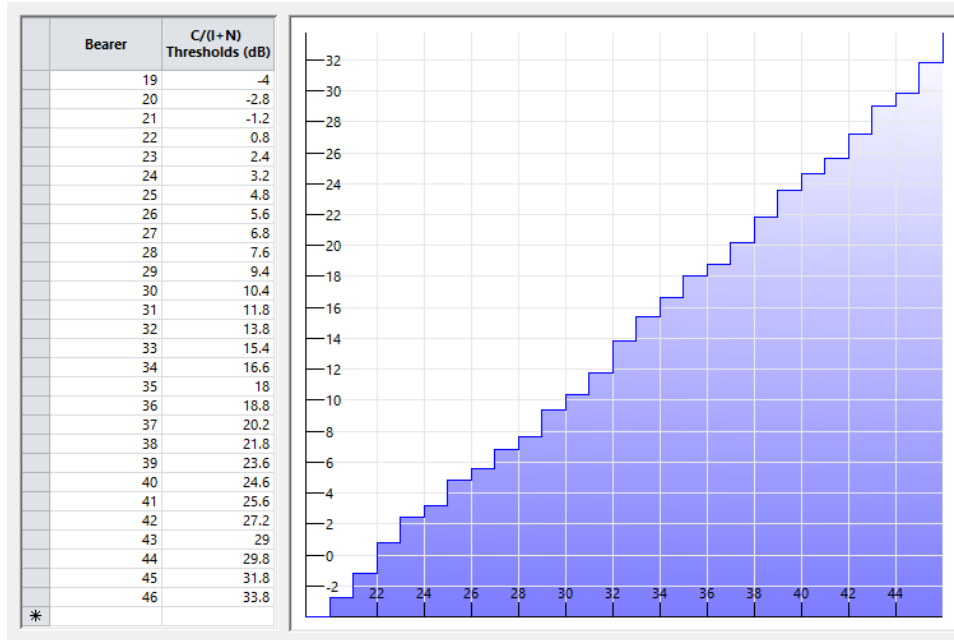


Figure 9. Bearer selection threshold according to the C/(I+N)

3.2. Traffic parameters

In Atoll the traffic parameters are common for all the radio access technology and define the services demanded by the users, their mobility, the terminals they use, the user profile and the environment where they are located according to the user density.

Services such as voice, internet, broadband, etc., are available to subscribers in Atoll. However, the type of service used for 5G NR subscribers was the broadband service, since future 5G networks will handle huge amount of wide bandwidth data.

This service has the following characteristics:

Table 7. Broadband Service Characteristics

Parameter	Uplink	Downlink
Highest modulation	64QAM	64QAM
Lowest modulation	BPSK	BPSK
Highest coding rate	0,95	0,95
Lowest coding rate	0,3	0,3
Max throughput demand	5,000 kbps	20,000 kbps
Min throughput demand	500 kbps	1,000 kbps

The mobility type defines the average user speed to simulate the user behavior. In 5G NR, the information about the receiver mobility is required for determining which bearer threshold to use.

The mobility type used for 5G NR subscribers was the pedestrian type, which corresponds to a speed of 3 km/h.

The terminal is the user equipment used in the network, in this case the mobile phone.

The terminal used was a 5G Smartphone with the following defined parameters:

- **Min power:** -40 dBm
- **Max power:** 23 dBm
- **Noise figure:** 8 dB
- **Losses:** 0 dB
- **Frequency band:** n78
- **Radio equipment:** 5G NR Radio Equipment
- **MIMO Support:** yes
- **Antenna gain:** 0 dB
- **Number of transmission antennas:** 4
- **Number of reception antennas:** 4
- **Highest supported modulation:** 256 QAM

The user profile considered was the business user with the following characteristics:

Table 8. Business User Profile Characteristics

User Profile	Service	Terminal	Calls/hours	Duration (sec)	UL Volume (Kbytes)	DL Volume (Kbytes)
Business User	Broadband	5G Smartphone	0.05	65	10000	50000

Finally, the environment class describes the areas in terms of user profiles, mobility type and density. The environment was configured to be dense urban with 8000 business user pedestrian subscribers per km².

3.3. Beamforming features

3D beamforming is one of the key features of Atoll, which enables beamforming in both horizontal and vertical planes.

In Atoll, 3D beamforming represents uniform planar array antennas with antenna elements aligned horizontally and vertically across a two-dimensional plane. Each 3D beamforming antenna is defined by its operating frequency range, the number of antenna elements, inter-element spacing, number of ports, polarization and the radiation patterns of all the beams the antenna forms.

Atoll models 3D beamforming by distinguishing between the antenna model and the beam pattern:

- The 3D beamforming models represent the physical beamforming antenna equipment, which produces multiple antenna patterns.
- The 3D beamforming patterns represent the beam patterns that are produced by the beamforming model.

The parameters that can be configured that describe the physical characteristics of the 3D beamforming antenna panel are:

- **Frequency range:** the range of frequencies in MHz within which the 3D beamforming antenna is designed to operate.

- **Vertical spacing:** the distance between two vertical antenna elements in multiples of the wavelength.
- **Horizontal spacing:** the distance between two horizontal antenna elements in multiples of the wavelength.
- **Columns (N):** the number of columns of the antenna elements within the panel.
- **Rows (M):** the number of rows of the antenna elements within the panel.
- **Transmission ports:** the number of ports used in transmission.
- **Reception ports:** the number of ports used in reception.

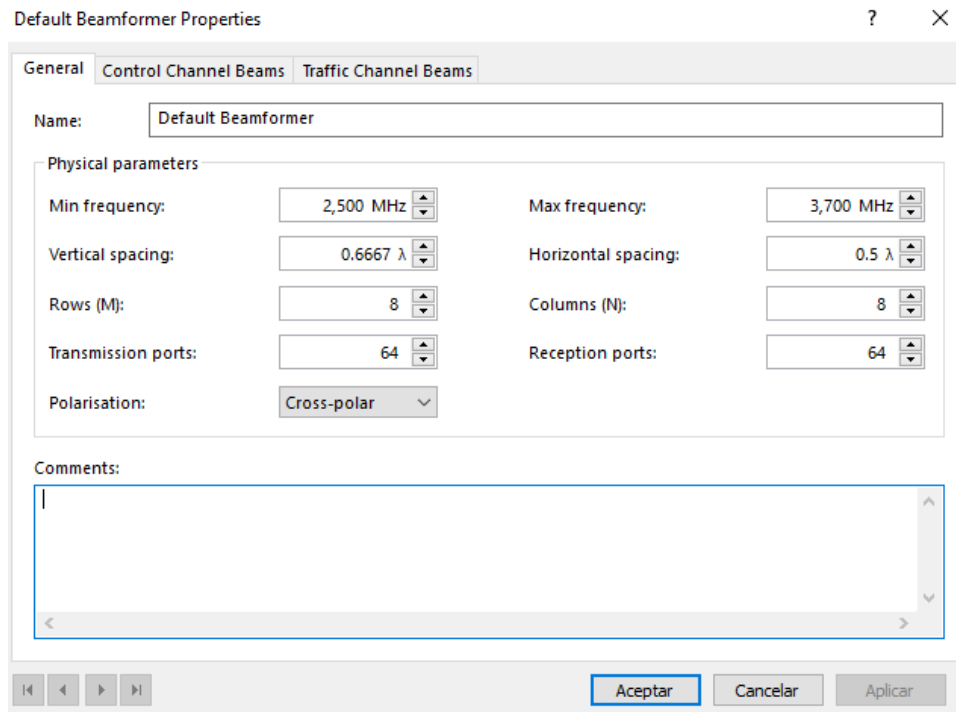


Figure 10. Physical parameters of beamforming antennas

On the other hand, each 3D beamforming pattern is represented for the following parameters:

- **Beam type:** specifies whether the beam is a control channel beam, a traffic channel beam or both. Control channel beams are used for the SS/PBCH block in 5G NR, while traffic channel beams are used for the PDCCH and PDSCH.
- **Beam index:** specifies the unique index of the beam pattern within the 3D beamforming model.
- **Electrical azimuth (°):** the azimuth towards which the beam pattern points.
- **Electrical tilt (°):** the tilt towards which the beam pattern points.
- **Horizontal elements (m):** specifies the number of horizontal antenna elements used to form the beam pattern.
- **Vertical elements (n):** specifies the number of vertical antenna elements used to form the beam pattern.
- **Boresight gain (dB):** specifies the gain of the beam in the direction define by its azimuth and tilt.
- **Half-power beamwidth (°):** displays the aperture of its horizontal pattern corresponding to the pattern attenuation of 3 dB.

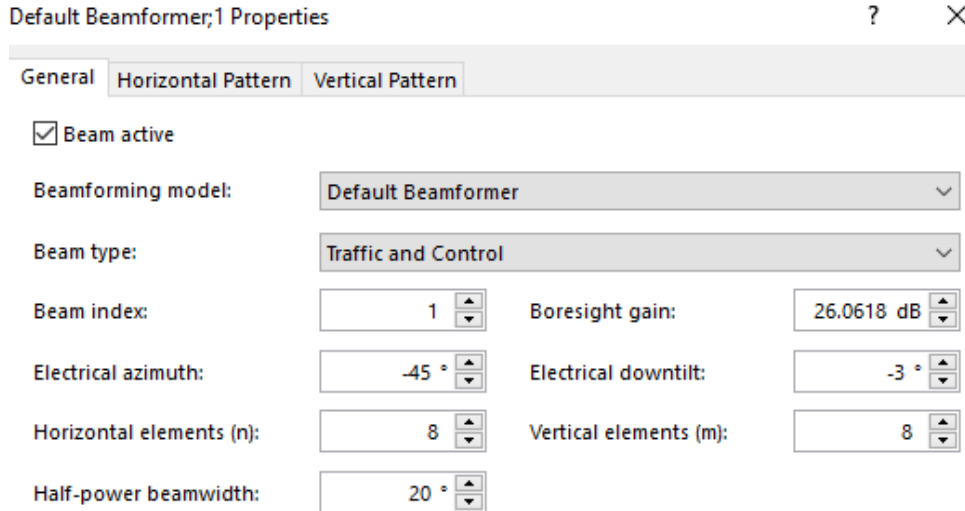


Figure 11. Beamforming pattern parameters

Atoll, as shown in Figure 12, allows to graphically see the different beam patterns corresponding to each of the beam indexes generated by the antennas.

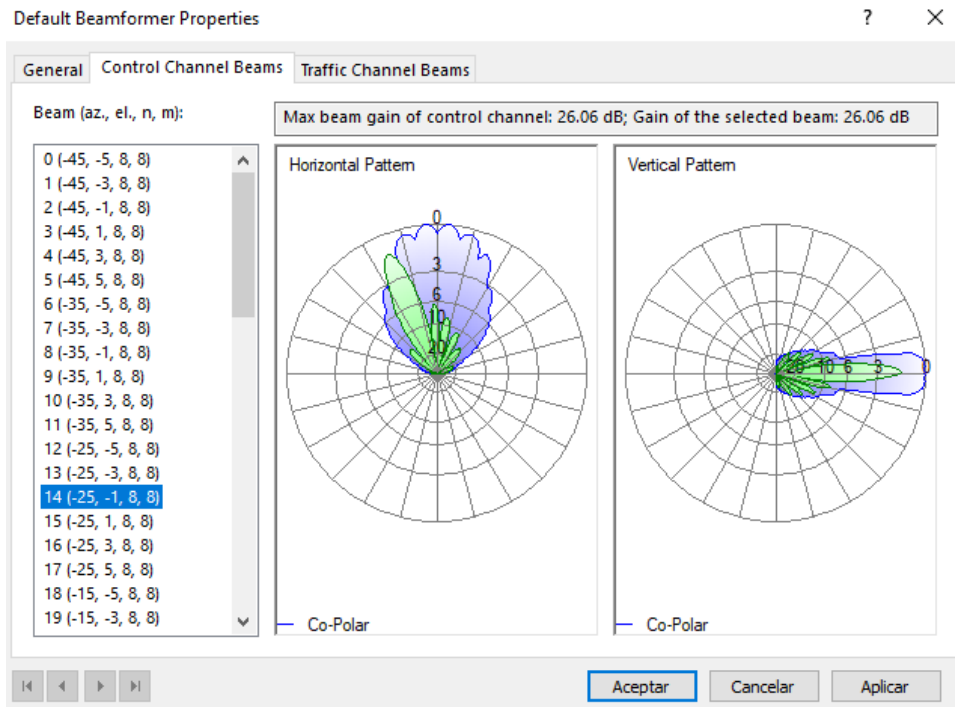


Figure 12. Beam patterns

3.4. MIMO features

Atoll supports different MIMO configurations: transmit and receive diversity, single-user MIMO (SU-MIMO) or spatial multiplexing and multi-user MIMO (MU-MIMO) or collaborative MIMO.

During calculations, a user terminal with MIMO capabilities, connected to a cell that supports SU-MIMO or MU-MIMO, will benefit from the MIMO gain or not depending if the PDSCH or PUSCH $C/(I+N)$ on the point where the user is located is higher or equal than the threshold defined in the 5G NR radio equipment. This threshold is defined by default by Atoll to be 14 dB. It means that only above this value, SU-MIMO and MU-MIMO can be used.

The SU-MIMO gain, which is a capacity gain defined in the radio equipment properties to improve the throughput, varies according number of transmission and reception antennas and the $C/(I+N)$ level. For example, figure X shows the SU-MIMO gains for a transmitter with 16 antennas and a receiver with 8 antennas.

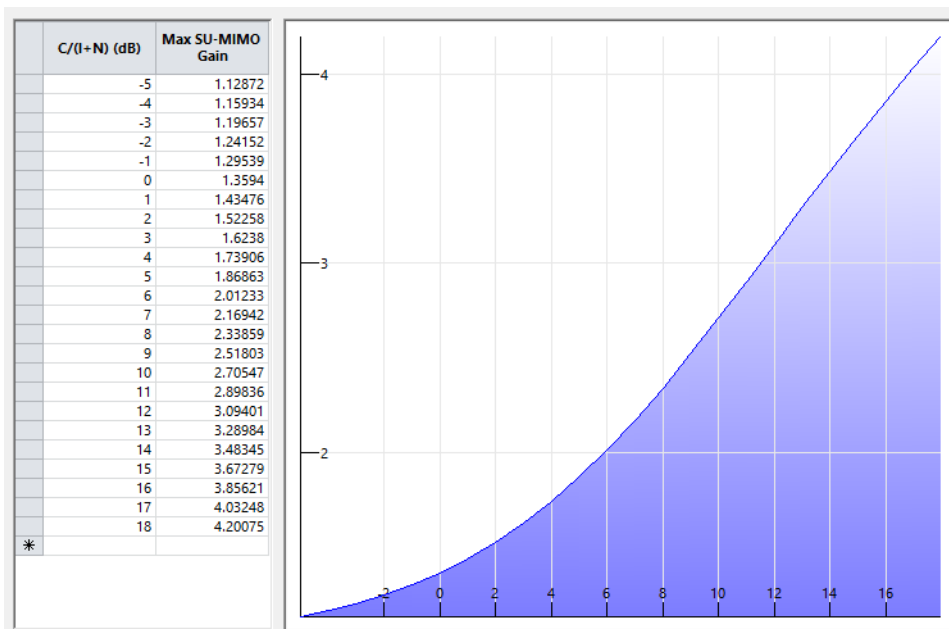


Figure 13. SU-MIMO 16x8 capacity gains depending on the $C/(I+N)$ level

In the case of the MU-MIMO, there are two types of gains defined on the radio equipment properties, the MU-MIMO diversity gain applied to the $C/(I+N)$ level and the MU-MIMO capacity gain. The first one improves the $C/(I+N)$ level depending on number of antennas. On the other hand, the capacity gain depends not only on the number of antennas but also on the average number of MU-MIMO users that share the same resources on the downlink or uplink. The diversity gains and the capacity gains defined by Atoll for a transmitter with 16 antennas and a receiver with 8 antennas are in Table X and Figure X, respectively.

Table 9. MU-MIMO Diversity Gain

Transmission Antennas	Reception Antennas	Diversity Gain (dB)	Transmission Antennas	Reception Antennas	Diversity Gain (dB)
128	1	9.0309	1	32	9.0309
128	2	6.0206	2	32	6.0206
128	4	3.0103	4	32	3.0103
128	8	0	8	32	0
64	1	9.0309	1	16	9.0309
64	2	6.0206	2	16	6.0206
64	4	3.0103	4	16	3.0103
64	8	0	8	16	0
32	1	9.0309	2	1	3.0103
32	2	6.0206	4	1	6.0206
32	4	3.0103	8	1	9.0309
32	8	0	1	2	3.0103
16	1	9.0309	2	2	0
16	2	6.0206	4	2	3.0103
16	4	3.0103	8	2	6.0206
16	8	0	1	4	9.0309
1	128	9.0309	2	4	3.0103
2	128	6.0206	4	4	0
4	128	3.0103	8	4	3.0103
8	128	0	1	8	6.0206
1	64	9.0309	2	8	9.0309
2	64	6.0206	4	8	3.0103
4	64	3.0103	8	8	0
8	64	0			

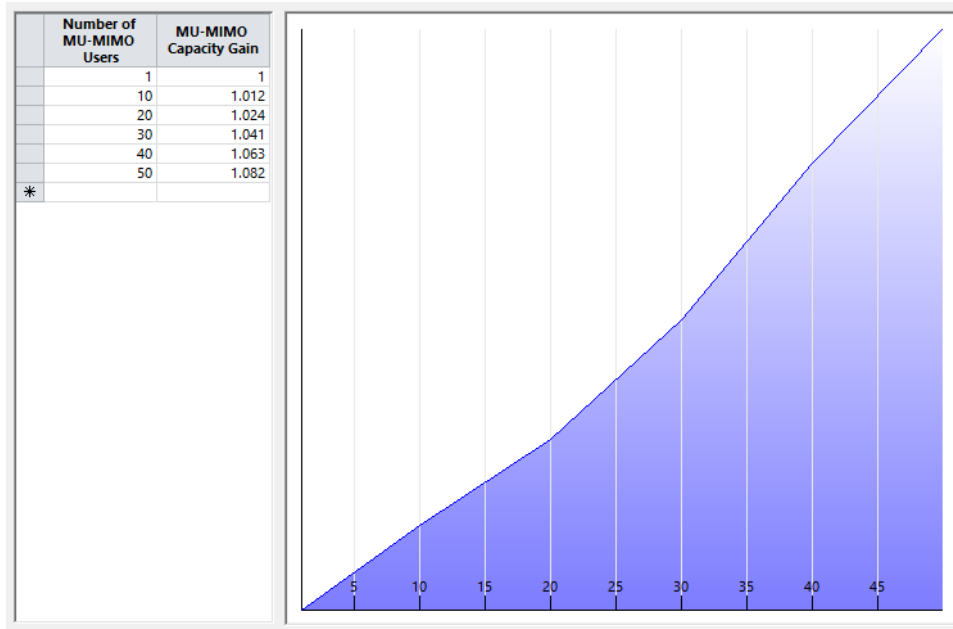


Figure 14. MU-MIMO 16x8 capacity gains

On the other hand, if the cell uses a proportional fair scheduler, there is a third gain applied for MU-MIMO cases, which is called multi-user diversity gain (not confuse with the MU-MIMO diversity gain defined in the radio equipment properties).

This gain depends on the number of users simultaneously connected to the cell, in downlink or uplink, and it is only applied to the throughput if the PDSCH or PUSCH $C/(I+N)$ is lower than a predefined value used by Atoll. For section 6.3 this value was set to 30 dB.

In other words, if the PDSCH or PUSCH $C/(I+N)$ is between 14 dB and 30 dB, three gains are applied: the MU-MIMO diversity gain, the MU-MIMO capacity gain and the multi-user diversity gain. Above 30 dB, the multi-user diversity gain is no longer applied.

In the case of transmit and receive diversity, a terminal with MIMO capabilities connected to a cell that supports diversity, will benefit from diversity gain if the PDSCH or PUSCH $C/(I+N)$ is below the 14 dB threshold.

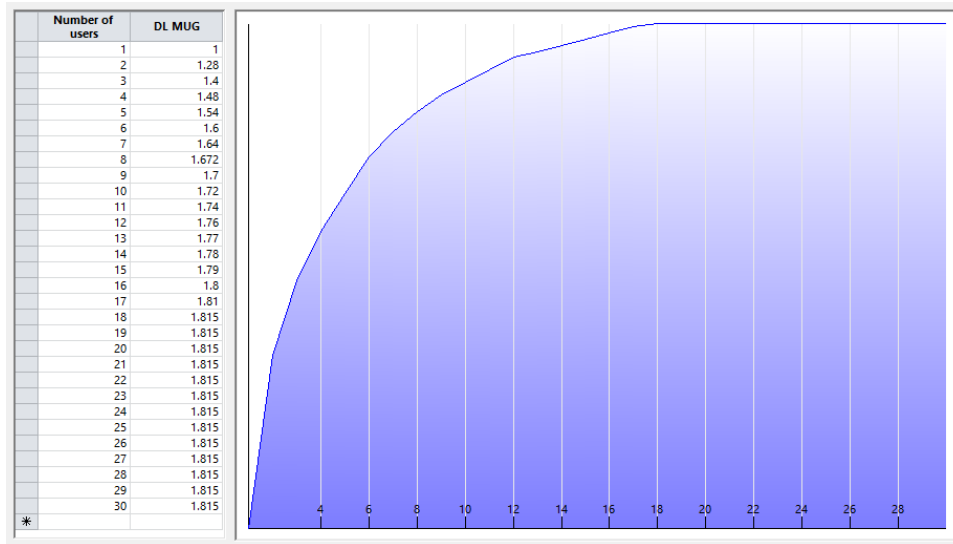


Figure 15. Multi-user diversity gain

The following table shows the transmit and receive diversity gains defined by Atoll.

Table 10. Transmit and Receive Diversity Gains

Transmission Antennas	Reception Antennas	Diversity Gain (dB)	Transmission Antennas	Reception Antennas	Diversity Gain (dB)
128	1	9.0309	1	32	9.0309
128	2	12.0412	2	32	12.0412
128	4	15.0515	4	32	15.0515
128	8	18.0618	8	32	18.0618
64	1	9.0309	1	16	9.0309
64	2	12.0412	2	16	12.0412
64	4	15.0515	4	16	15.0515
64	8	18.0618	8	16	18.0618
32	1	9.0309	2	1	3.0103
32	2	12.0412	4	1	6.0206
32	4	15.0515	8	1	9.0309
32	8	18.0618	1	2	3.0103
16	1	9.0309	2	2	6.0206
16	2	12.0412	4	2	9.0309
16	4	15.0515	8	2	12.0412
16	8	18.0618	1	4	6.0206
1	128	9.0309	2	4	9.0309
2	128	12.0412	4	4	12.0412
4	128	15.0515	8	4	15.0515
8	128	18.0618	1	8	9.0309
1	64	9.0309	2	8	12.0412
2	64	12.0412	4	8	15.0515
4	64	15.0515	8	8	18.0618
8	64	18.0618			

3.5. Propagation models

Different propagation models, suited for certain conditions, frequencies and radio technologies are available in Atoll for path loss calculations.

Particularly, the Standard Propagation Model (SPM) and the Aster Propagation Model are the models studied for the following chapter.

The following table summarizes the frequency range, the necessary geographic data and the recommended use for these propagation models.

Table 11. Propagation Models Characteristics

Propagation Model	Frequency Range (GHz)	Geo Data Taken into Account	Recommended Use
Standard Propagation Model	0.15 – 3.5	Terrain profile Statistical clutter	$1 < d < 20$ km
Aster	0.15 – 60	Terrain profile Statistical or deterministic clutter 3D building and line vectors	All type of environments, particularly dense urban areas. Small, micro, and macro cells.

The Standard Propagation Model (SPM) is based on the Hata formulas and is suited for scenarios in the 150 to 3500 MHz band over long distances.

On the other hand, the Aster Propagation Model is a ray-tracing propagation model that supports all radio access technologies and it is suited for urban and dense urban environments. Its ray-tracing capability allows to add horizontal diffraction and reflection.

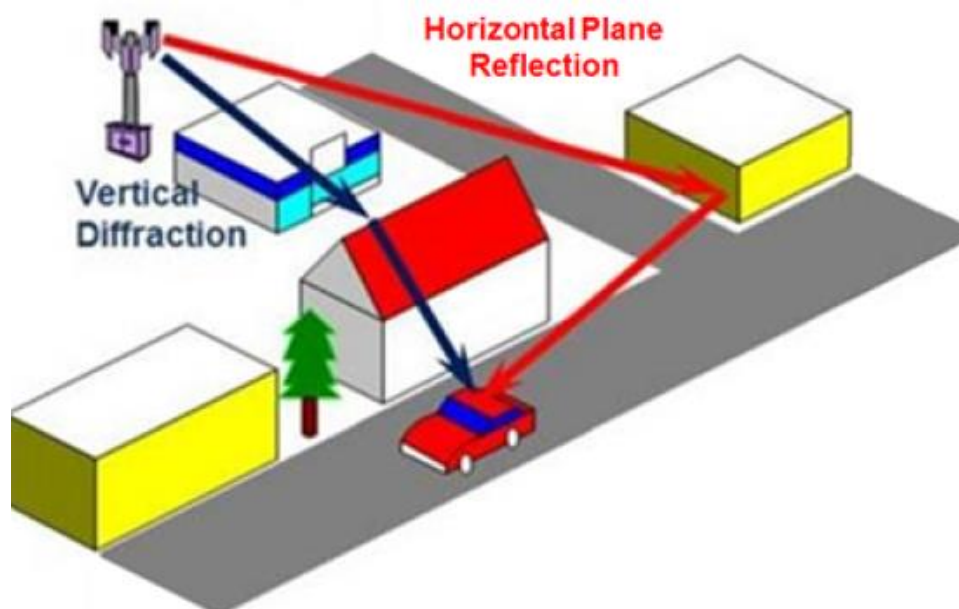


Figure 16. Vertical and horizontal components in the Aster Propagation Model

3.6. Predictions and simulations

5G NR coverage predictions in Atoll allows to analyze the effective signal levels, signal quality and throughput, where each pixel of the map is considered as a non-interfering user, with a defined service, mobility type and terminal.

The following table summarizes the different coverage predictions in Atoll.

Table 12. Coverage Prediction in Atoll

Coverage Prediction	Description
Network coverage	Predicts the effective signal levels of different type of 5G NR signals for the downlink and the uplink. This prediction includes SS-RSRP Level, PDSCH and PUSCH signal level, best control channel beam and best traffic channel beam.
Network quality	Predicts the interference levels. This prediction includes PDSCH and PUSCH C/(I+N) level and SS-SIRN level.
Service areas	Displays the 5G NR radio bearers based on the C/(I+N) level for each pixel for the downlink and the uplink. Also displays the modulation schemes used.
Network capacity	For 5G NR scenarios, it shows the peak RLC allocated bandwidth throughput for downlink and uplink.

On the other hand, Atoll is also capable of studying the network capacity using a realistic user distribution and traffic demands by means of simulations.

A simulation, different from a prediction, corresponds to a given distribution of 5G users. It is a snapshot of the 5G network, which its principal outputs are a geographic user distribution with a certain traffic demand, resources allocated to each user of the distribution and cell loads.

Atoll allows to define a 3D distribution of users by means of traffic maps, where user distribution can be defined in terms density of users, number of users distributed randomly on a certain area, or by entering the coordinates of fixed users. The vertical distribution of users (altitudes) can either be entered individually for each user on the traffic map parameters or as an average altitude defined as a parameter of the simulation.

The simulation process in 5G consists of the following steps:

- **Mobile generation and distribution:** Atoll generates user distribution for each simulation using a Monte Carlo algorithm basing on traffic maps and weighting it with a Poisson distribution.
- **Best server determination:** Atoll determines the best serving cell for each mobile, which is the transmitter from which the user receive the highest signal level.

- **Downlink calculations:** it includes calculation of $C/(I+N)$ for the various physical signals and channels, determination of the best available bearer, allocation of resources and calculation of user throughputs.
- **Uplink calculations:** it includes calculation of $C/(I+N)$ for the various physical channels, determination of the best available bearer, uplink power control and uplink bandwidth allocation, resource allocation, update of uplink noise rise values for cells, and calculation of user throughputs.

At the end of the simulations, active users can be connected if they have a best server assigned and a bearer corresponding to their activity status.

Users may also be rejected for no coverage if there is no server assigned, and for no service if there are no bearers assigned in the downlink or in the downlink.

Results from simulations can show the channel and user throughput, the connection success rate in downlink and uplink, the number of users rejected, the traffic load of the cell, etc.

Some of the throughputs obtained after a simulation are:

- **Peak RLC throughput:** corresponds to the maximum RLC layer throughput that can be achieved at a given location using the highest 5G NR bearer available. This is the raw throughput and doesn't consider the effects of retransmission due to errors or higher layer coding encryption.
- **Effective RLC throughput:** the net RLC layer throughput that can be achieved using the highest 5G NR bearer available computed taking into account the reduction of throughput due to retransmission errors.
- **Application throughput:** is the application layer throughput at a given location using the highest 5G NR bearer available computed taking into account the reduction of throughput due to PDU/SDU header information, padding, encryption, coding and other types of overhead.
- **Cumulated throughputs:** refers to the sum of user throughputs of all the users connected to the cell, both in downlink and uplink, respectively.

4. Deployment area and radio propagation modelling

In the first part of this chapter, the geographical area where the study takes place and the geographic data used in Atoll necessary for different calculations is described.

The second part of the chapter consists on a comparative between different propagation models to see their path loss response depending on the type of data used (statistical or deterministic), the type of cell (macro cells or micro cells), the receiver height and the transmitter height.

The table below shows the frequency band used for this study.

Table 13. 3.5 GHz Frequency Band Characteristics

Band	Duplex Mode	Frequency (GHz)	Uplink (GHz)	Downlink (GHz)	Duplex Spacing (MHz)	Channel Bandwidth (MHz)
n78	TDD	3.5	3.3-3.8	3.3-3.8	N/A	10, 20, 40, 50, 60, 80, 100

4.1. Geographical area of study and data

The study takes place in a 4 km² sample area of Ciutat Vella district, Barcelona (Spain).

The coordinate system used is WGS 84 / UTM zone 31 N and the coordinates of the bounding rectangle are:

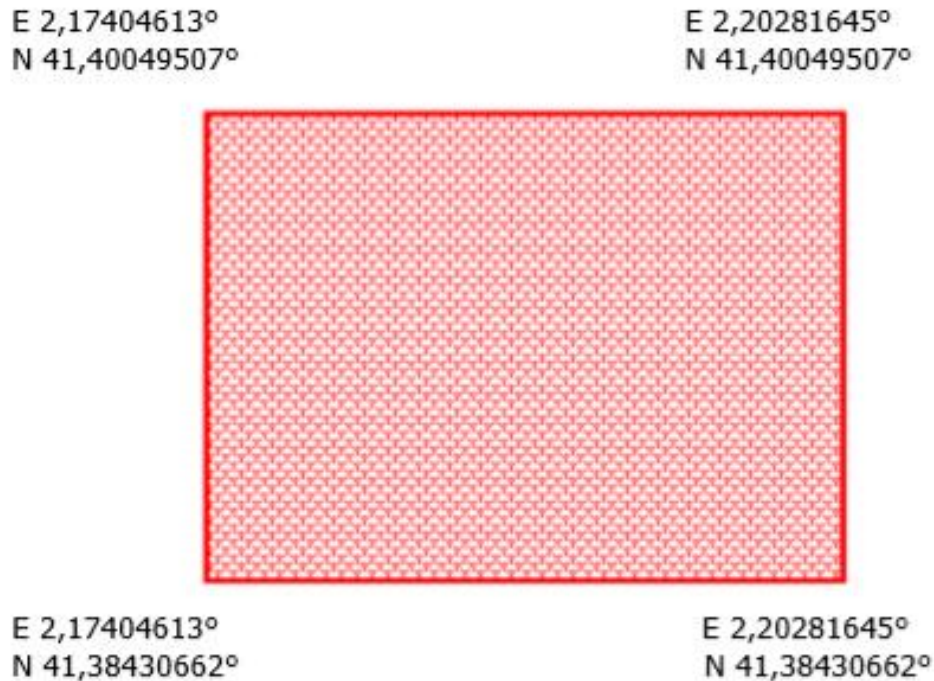


Figure 17. Barcelona sample area coordinates

In order to carry out the different calculations (path loss, coverage, signal level, etc), four geographic data types are imported to Atoll:

- Digital Terrain Model (DTM).
- Clutter Classes.
- Clutter Heights.
- Vector Layers.

It is important to clarify that the geographic data used for this study is available and was taken from the webpage of Visicom, a data provider of digital mapping products [23].

4.1.1. Digital Terrain Model (DTM)

The DTM describes the elevation of the ground over sea level. It is automatically taken into account by the propagation model during computations.

In the file used, each image pixel stores the value of the terrain elevation, with a range from 0 to 27 meters.

The following table shows the accuracy of the DTM file used.

Table 14. DTM Parameters of Accuracy

Parameters of Accuracy	Value
Resolution (cell size)	1 m
Absolute planimetric accuracy (x,y)	2-3 m
Absolute altimetric accuracy (z)	2-3 m

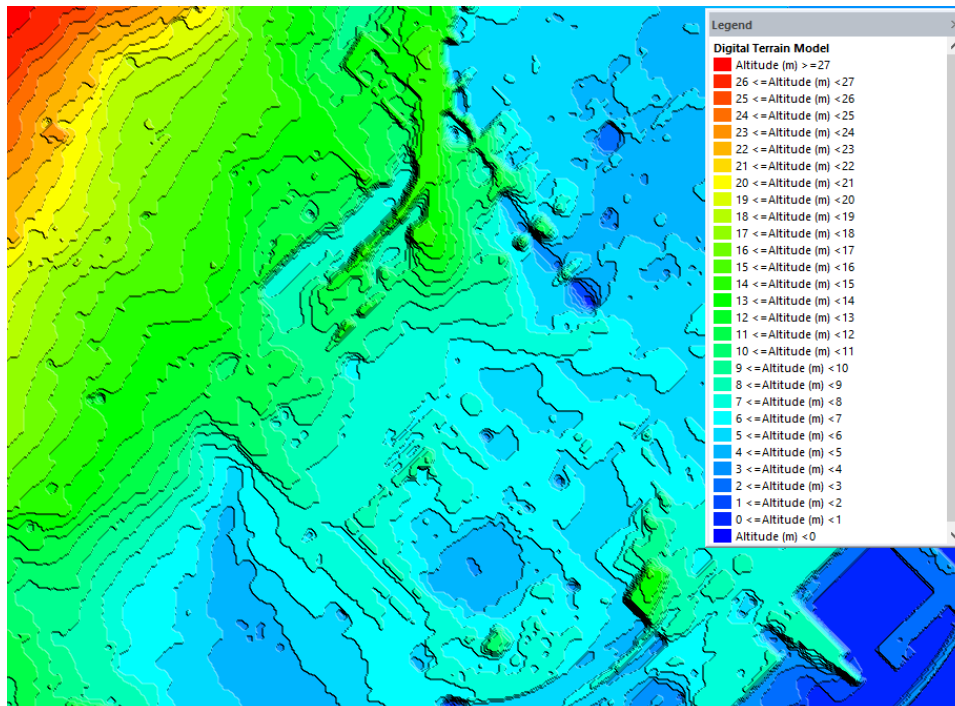


Figure 18. Digital Terrain Model data

4.1.2. Clutter classes

The clutter class data file describes the land covered or land used. Clutter classes are taken into account by the propagation model during computations.

Each pixel in the clutter class file contains a code (from a maximum of 256 possible classes) which corresponds to a clutter class or to a certain type of ground used or covered.

The height of the terrain is defined as an average height for each clutter class.

The following table shows the accuracy of the Clutter Classes file used.

Table 15. Clutter Classes Parameters of Accuracy

Parameters of Accuracy	Value
Resolution (cell size)	1 m
Absolute planimetric accuracy (x,y)	2-3 m

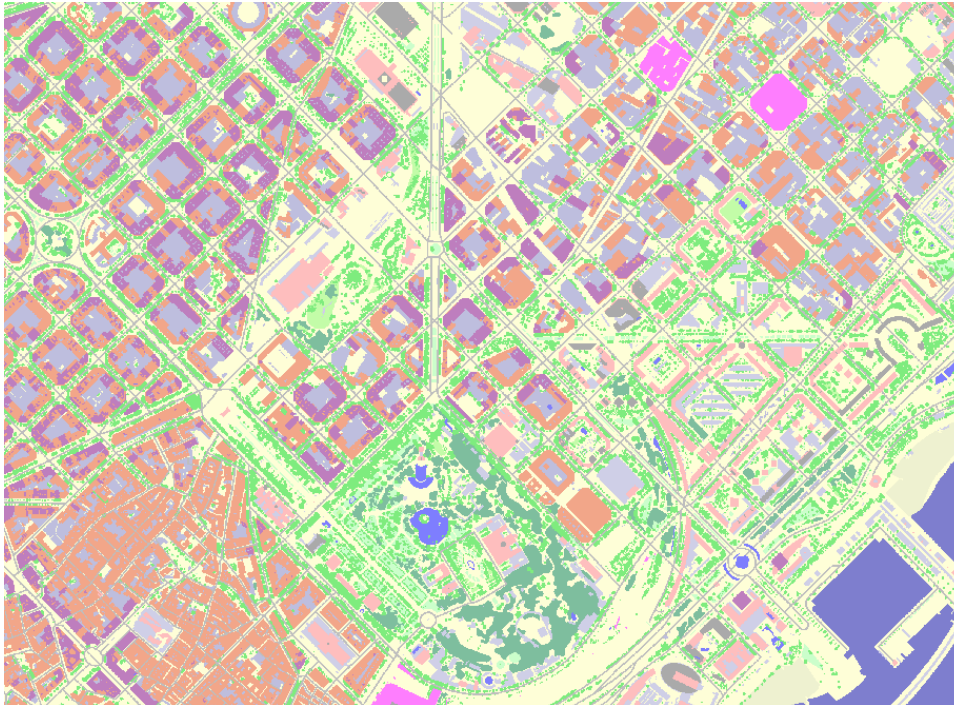


Figure 19. Clutter classes

A table of the correspondences between codes and clutter class names is presented below.

Table 16. Clutter Classes

	Code	Class Name	Class Description
	1	Open	Open space outside the town without vegetation.
	2	Forest	Forested lands with closed tree canopy. No distinction is made between deciduous and coniferous.
	3	Sea	Sea and ocean.
	4	Inland water	Rivers, canals of more than 10 m width, lakes, reservoirs.
	5	Residential	Houses in suburban environment. Suburban dwellings. Lots may be as small as 30m by 30m, but are usually larger and include vegetation cover. Individual houses are frequently visible. Average height is below 15m.
	6	Mean urban	Areas within urban perimeter. The mean urban should have mean street density with no pattern, the major streets are visible, the built-up features appear distinct from each other. Some small vegetation could be included. Height is 15-30m.
	7	Dense urban	Areas within urban perimeter. This includes dense urban areas with dense development where built-up features do not appear distinct

			from each other. It also includes built-up features of the downtown district with heights 15-30m .
	8	Block buildings	Groups of buildings, either parallel or not, that may be separated by large green space. Height is above 30 m..
	9	Industrial	Areas including buildings with large footprints separated by streets (factories, shopping malls, storehouses etc.).
	10	Villages	Small built-up area in rural surrounding.
	11	Open in urban	Open spaces inside the town: streets, avenues, vacant lots, squares.
	12	Parks in urban	Park of less than 20m height trees.
	13	Airport	Territory of airport without buildings and runways.
	14	Wetland	Swampland.
	15	Dense residential	Groups of houses or collective residential buildings in suburban environment. Suburban density typically involves laid out street patterns in which streets are visible. There is no open space between constructions. Average height is below 15m.
	16	Dense urban high	Financial District. Heights are over 40 m.
	17	Buildings	Isolated cluster of high towers or skyscrapers higher than 40 m.
	18	Sparse forest	Forested lands with a low density of trees and without canopy tree.
	19	Grass	The territory covered by low grass.
	20	Agricultural	Lands used for agriculture.
	21	Barren	Areas covered by sparse, stunted vegetation.

4.1.3. Clutter heights

Clutter height maps describe the altitude of a clutter over the DTM with one altitude defined by pixel.

This map can offer more precise information than defining an altitude per clutter class because, in a clutter height file, it is possible to have different heights within a single clutter class.

When the clutter altitude is defined in both clutter class map and clutter height map, the clutter altitude is taken from the clutter height map.

The map used for the study includes buildings and vegetated areas.

The parameters of accuracy are shown in the table below.

Table 17. Clutter Height File Parameters of Accuracy

Parameters of Accuracy	Value
Resolution (cell size)	1 m
Absolute planimetric accuracy	2-3 m
Accuracy of building heights	2-3 m
Minimal mapping unit for buildings	16 m ²
Minimal recognizable height for buildings	3 m
Accuracy of other obstacles heights	5 m
Minimal mapping unit for vegetation	50 m ²
Minimal recognizable height for vegetation	5 m

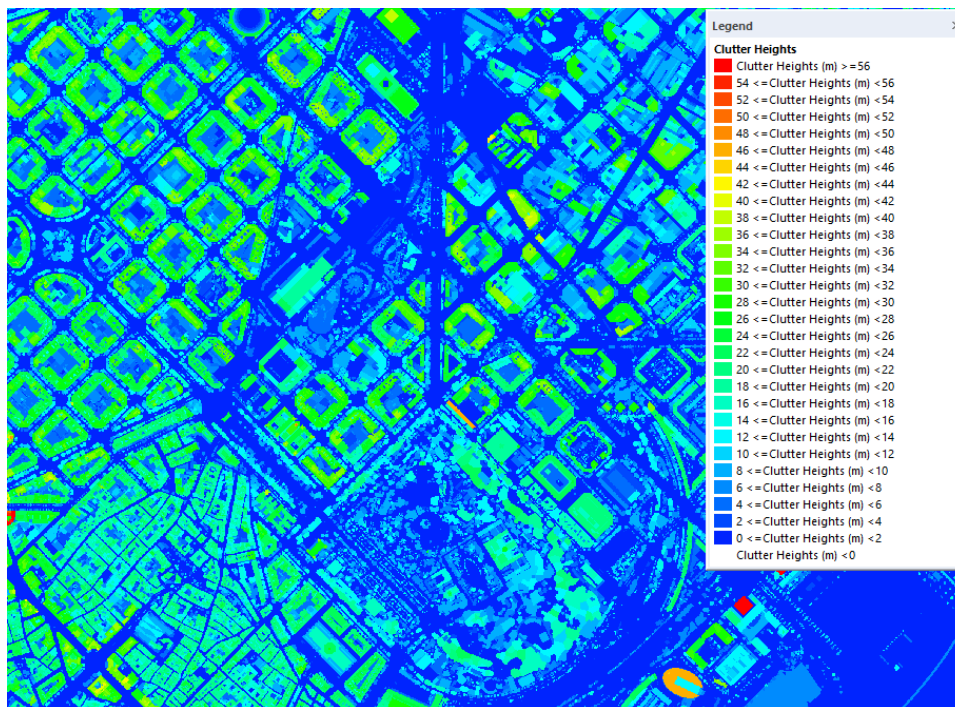


Figure 20. Clutter height

4.1.4. Vector layers

Atoll supports contours, lines, and points to represent polygons such as regions, or lines such as roads or coastlines, or points.

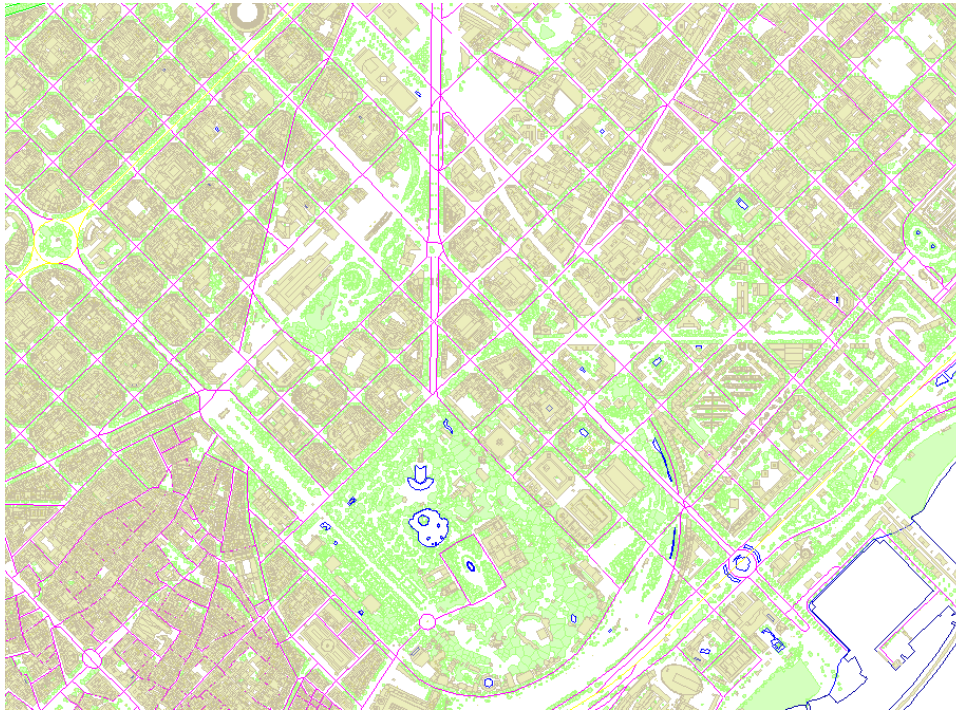










Figure 21. Vector layers

There are defined 8 linear classes in the vector file used:

Table 18. Vector Layers

	Vector Name	Vector Description
	Boundaries	Administrative boundaries of populated places.
	Buildings	Buildings with heights.
	Coastlines	Coastline of ocean and seas.
	Highways	International roads.
	Inland water	Coastline of rivers and lakes. Rivers with less than 10 m width.
	Major roads	Regional roads.
	Streets	Town street axial lines.
	Vegetation	Vegetation with heights.

4.2. Radio propagation modelling

Different radio propagation models were tested in order to understand and compare their path loss response to different type of clutters, different type of cells and different receiver heights.

The propagation models chosen for the study were the Aster Propagation Model and the Standard Propagation Model. The reason to choose these models was because, from all the propagation models available in Atoll, these two are suitable for 5G NR and for the 3.5 GHz frequency band.

4.2.1. Use of clutter information

There are two different types of clutter height information: statistical clutter and deterministic clutter.

Information is statistical when the clutter is roughly defined and without a defined altitude. The Standard Propagation Model (SPM) Propagation Model is a statistical propagation model. For this reason, Atoll recommends defining the losses per clutter class, instead of using the clutter height file to evaluate losses over the transmitter-receiver profile.

The values for losses per clutter class were assigned following the range of values suggested by Atoll. Positive values correspond to denser clutter classes and negative values to less dense clutter classes.

Table 19. Losses per Clutter Class for SPM

Clutter Class	Losses (dB)	Clutter Class	Losses (dB)
Open	-8	Parks in urban	-2
Forest	2.5	Airport	-2
Sea	-10	Open wet area	-10
Inland water	-10	Dense Residential	4
Residential	1	Residential with Trees	3
Urban	3	High Buildings	4
Dense urban	4.5	Low vegetation	0
Block of buildings	4.5	Barren	0
Commercial industrial	-4	Grass	0
Village	2	Agricultural	0
Open in urban	-5		

On the other hand, information is deterministic when there is a clutter height file. The Aster Propagation Model is makes use of deterministic clutter to accurately model the terrain. In this case, there is no need to define losses per class, since losses due to clutter are only taken into account in the calculated diffraction.

The following parameters were used for this section:

- **Frequency band:** n78
- **Transmission losses:** 1.51 dB
- **Antenna height:** 30 m
- **Antenna model:** 70deg 17dBi 3Tilt
- **Carrier:** 50 MHz – NR-ARFCN 621667
- **SSS EPRE:** 15 dBm
- **Shadowing margin:** 8.97 dB
- **Receiver height:** 1.5 m

In order to determine the path loss distribution over area of study, the SS-RSRP ($E_{SS}^{TX_i(ic)}$) was calculated. Then the path loss was obtained using the formula that relates it with the SS-RSRP. The minimum value set for the SS-RSRP was -140 dBm.

$$L_{path} = EPRE_{SS}^{TX_i(ic)} + G_{ANT}^{TX_i} - L^{TX_i} - M_{shadowing} - E_{SS}^{TX_i(ic)}$$

The figure below shows the path loss coverage on the map for the Aster Propagation Model and the Standard Propagation Model. This would also correspond to the SS-RSRP coverage.

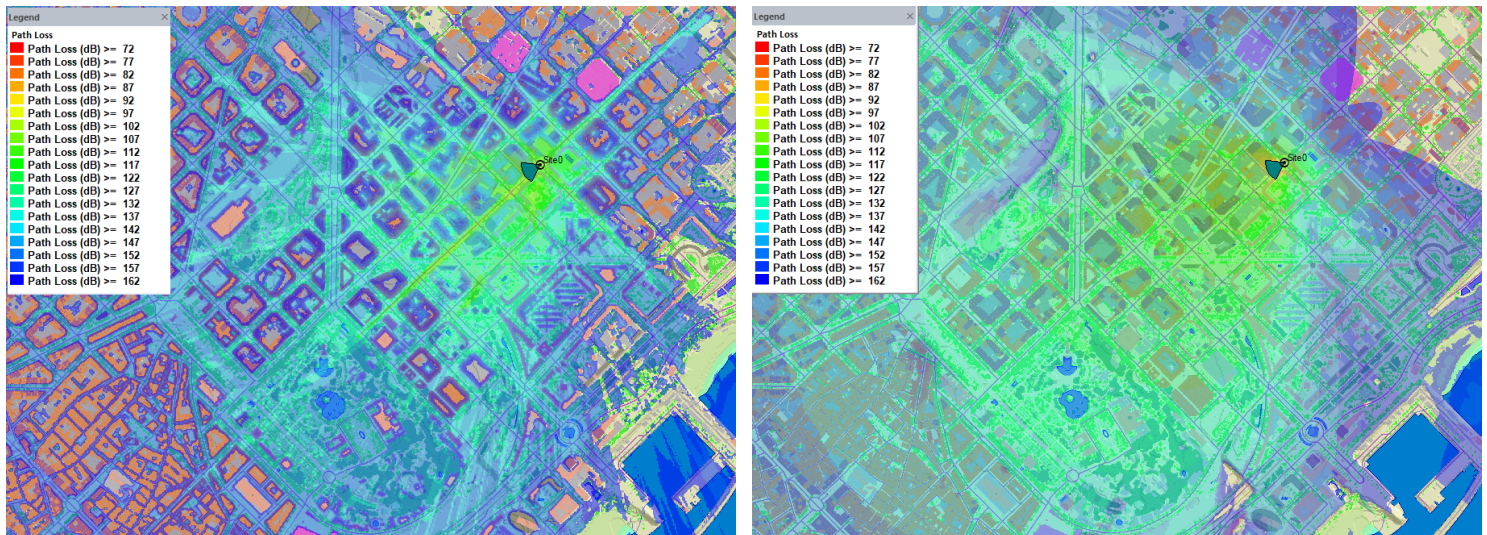


Figure 22. Path loss using the Aster Propagation Model (left) and the Standard Propagation Model (right)

The following figure shows a histogram of the path loss distribution for the Standard Propagation Model, represented by the bars in colors and the Aster Propagation Model, represented by the black lines.

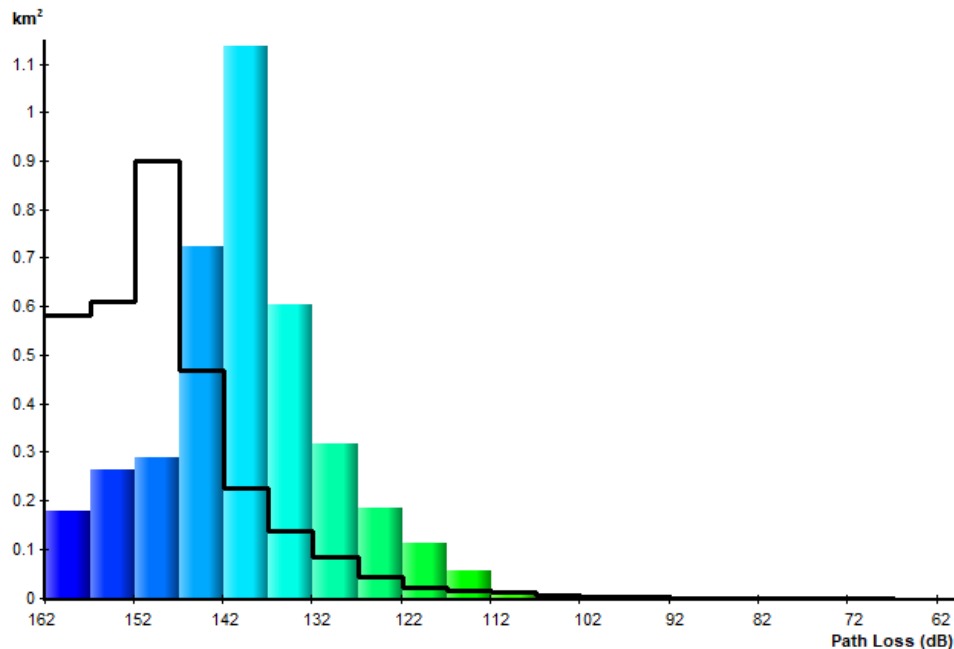


Figure 23. Path loss distribution using the Aster Propagation Model and the Standard Propagation Model

The results showed that the Standard Propagation Model presented a better distribution in terms of SS-RSRP and with more areas covered. This means that more areas received higher SS-RSRP levels compared to the Aster Propagation Model. Therefore, lower path losses were achieved with the Standard Propagation Model.

For example, with the Standard Propagation Model, a total of 3.879 km² received SS-RSRP signal with at least -140 dBm, that is 97% of the area. While with the Aster Propagation Model only 3.1 km² were covered, which represented 77.5%.

From the figure it can be calculated that in the case of the Aster Propagation Model, 25.2% of the area had a path loss between 107 dB and 142 dB and 52.3% is distributed between 142 dB and 162 dB; while for the Standard Propagation Model, these ranges covered 78.8% and 18.2%, respectively.

The reason for having higher values of path loss with the Aster Propagation Model is because of all the parameters taken into account for the path loss calculation.

Some of the parameters considered by the Aster Propagation Model in its path loss calculations are:

- Losses per clutter class.
- Frequency.
- Distance between the antenna and the receiver.
- Penetration losses when the line between the transmitter and the receiver slightly penetrates inside a building.

- The antenna height with respect to the receiver.
- The average height of the profile from the antenna to the receiver.
- The roof to mobile attenuation that depends on the street width and the roof height near the receiver.
- Vertical diffraction loss between the antenna and the last roof before the mobile.

While the parameters considered by the Standard Propagation Model for path loss calculations are:

- Losses per clutter class
- Distance
- Effective height of the transmitting antenna.
- Effective mobile antenna height.
- Diffraction loss due to obstruction in the path.

4.2.2. Impact of the receiver height

The objective of this section is to determine how sensitive the Aster Propagation Model and the Standard Propagation Model are to changes on the receiver height, comparing each model individually for different receiver heights and then comparing both models together for a specific height higher than 2 m.

For this, it is important to know how both models perform calculations depending on the receiver height.

On the one hand, the Aster Propagation Model was configured to consider a user to be inside a building if its height is higher than 2 m. This means that signals are computed outdoor at ground level (receiver height < 2 m) and only indoor in storeys above 2 m.

On the other hand, the Standard Propagation model considers that a user is in the street if the clutter height at that point is lower than the receiver height and that the user is inside a building if the clutter height is higher than the receiver height.

The receiver heights considered for this section were between 2 m and 30 m.

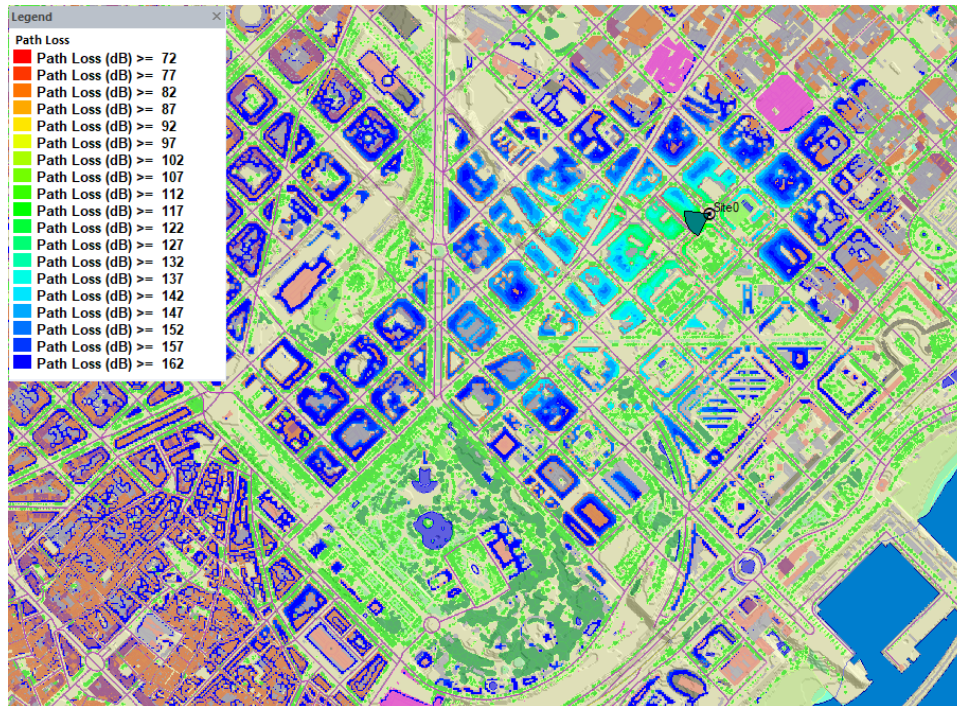


Figure 24. Path loss using the Aster Propagation Model with 5 m receiver height

The figure above shows the path loss coverage for the Aster Propagation Model with receivers located at 5 m from the ground. Here, it is observed how calculations were only performed indoors and not outdoor, since there were no receivers at ground level. This also means that SS-RSRP coverage was reduced only to those users that could actually be inside a building with a height at least 5 m.

The following figure compares the path loss distribution for the Aster Propagation Model with receivers at 1.5 m, 5 m, 10 m, 20 m and 30 m. The bars in colors correspond to the path loss when receiver height 1.5 m and the black lines correspond to the other receiver heights.

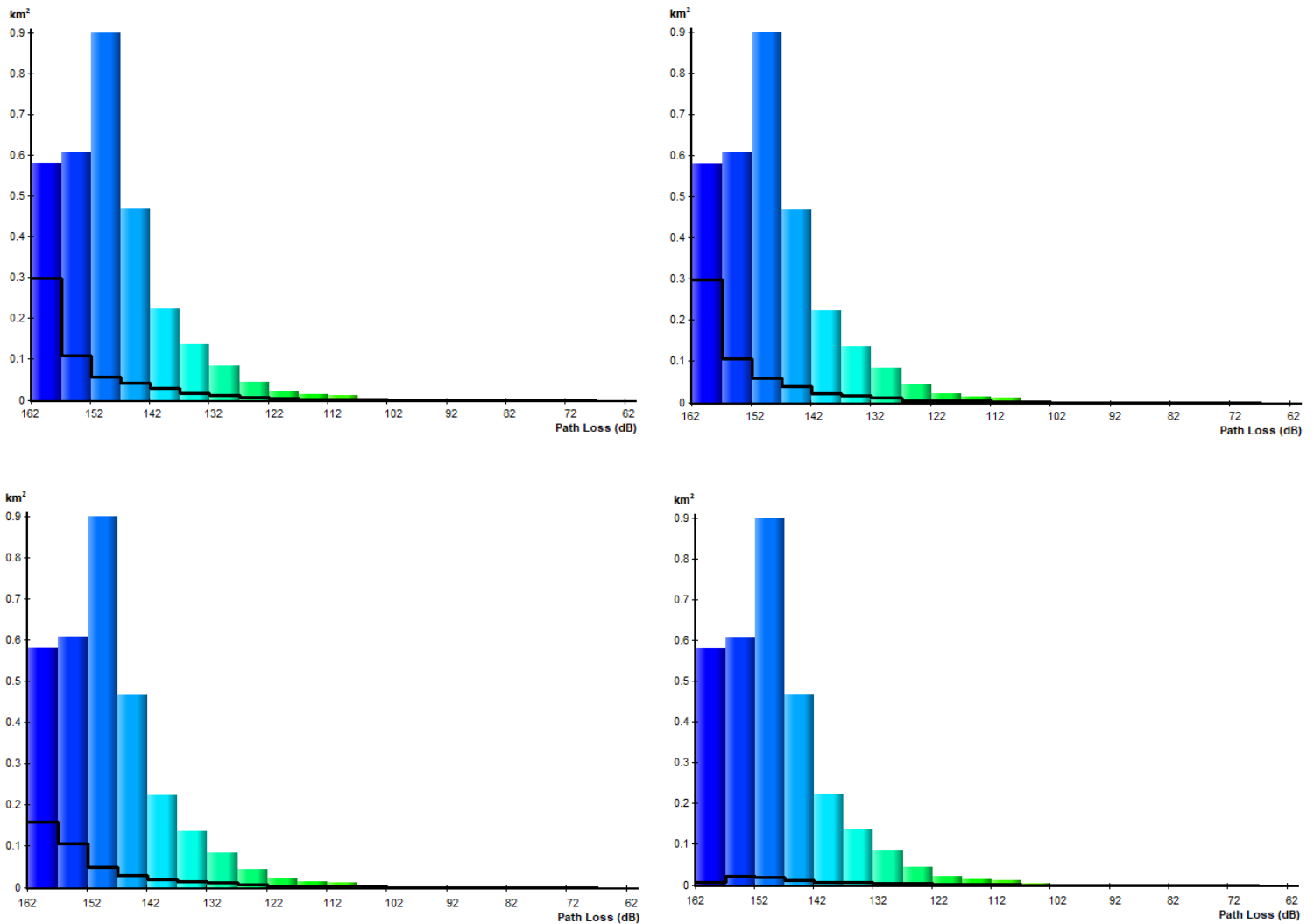


Figure 25. Path loss distribution using the Aster Propagation Model and receiver height at 1.5 m vs receiver height at 5 m (top left), 10 m (top right), 20 m (bottom left) and 30 m (bottom right)

When the receiver height was increased, the coverage on squared kilometers is reduced for those buildings that are at least the same height of the receiver height. This indicates that the Aster Propagation Model is very sensitive to variations on the receiver height. Nevertheless, this sensitivity could be modified by changing the 2 m threshold to higher heights to consider indoor losses.

The same analysis was performed for the Standard Propagation Model. The following figure the path loss coverage for the Standard Propagation Model with receivers located at 5 m from the ground.

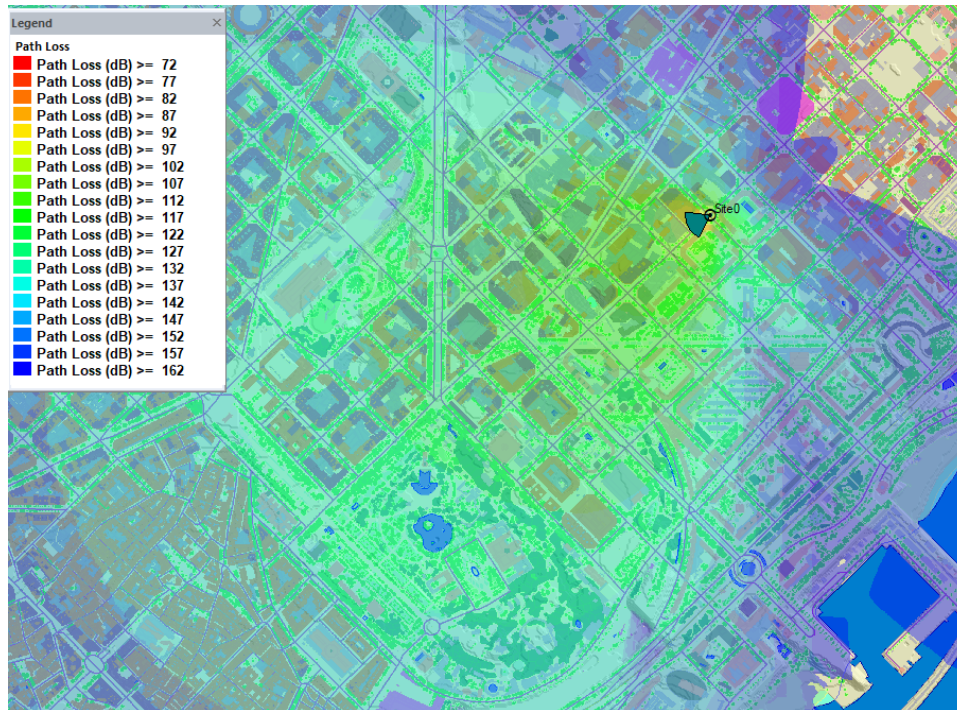


Figure 26. Path loss using the Standard Propagation Model with 5 m receiver height

Different from the Aster Propagation Model, the Standard Propagation Model did not reduce its coverage to buildings with heights at least the same of the receiver height, but calculated the SS-RSRP, therefore the path loss, for all points in the map.

This is because in this model indoor and outdoor calculations do not depend only on the receiver height but also on the clutter height. This means that, for example, at one point of the map, a user with a 5 m height is located indoor, and for another point of the map, a user with the same height is considered to be outdoor. In either cases, signals are computed. This is an advantage compared to the Aster Propagation Model configuration used, since for that model, depending on the receiver height selected, the user could always be indoor or always be outdoor.

The following figure compares the path loss distribution for the Standard Propagation Model with receivers at 1.5 m, 5 m, 10 m, 20 m and 30 m. The bars in colors correspond to the path loss when receiver height was 1.5 m and the black lines correspond to the other receiver heights.

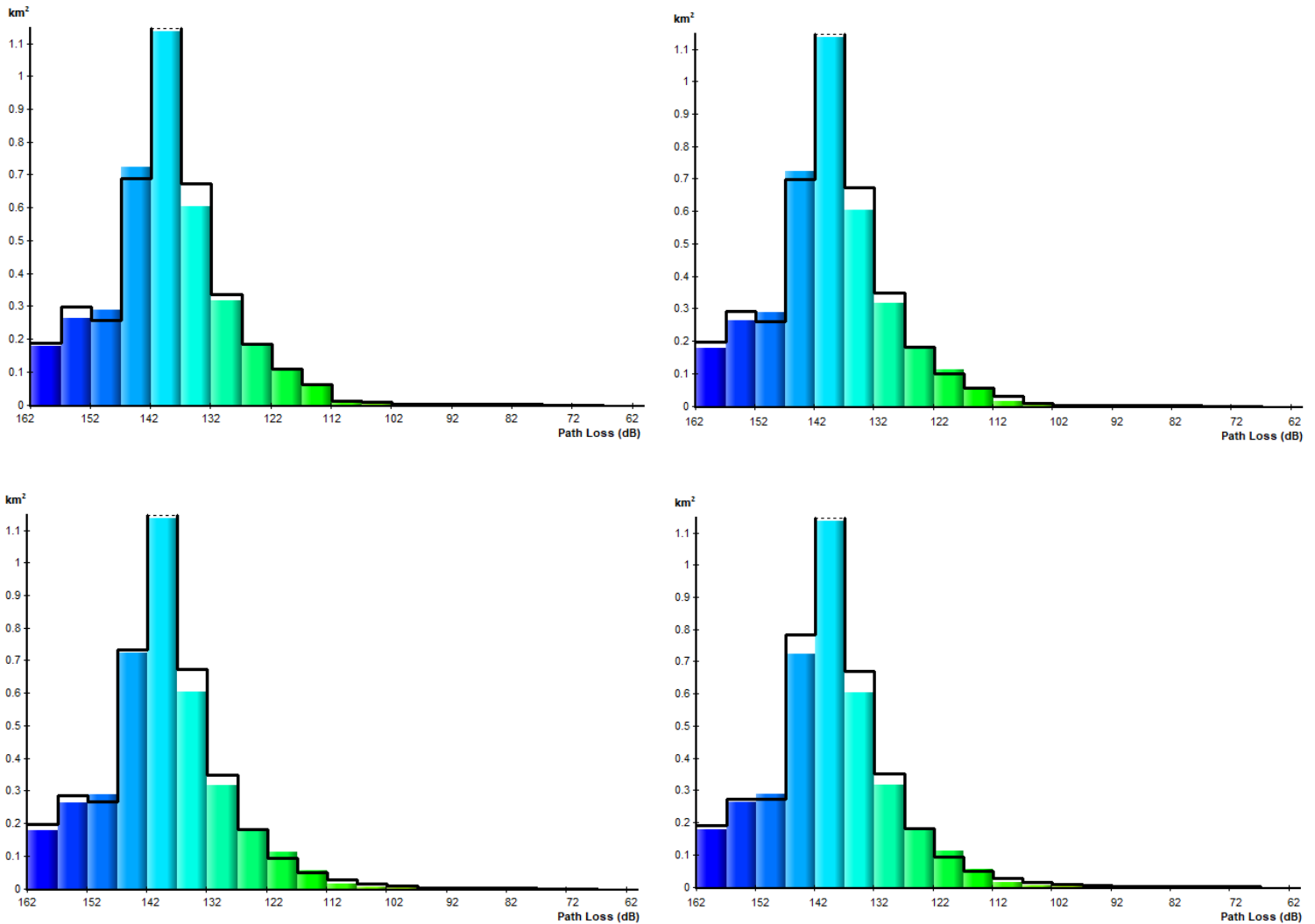


Figure 27. Path loss distribution for the receiver height at 1.5 m vs receiver height at 5 m (top left), 10 m (top right), 20 m (bottom left) and 30 m (bottom right) using the Standard Propagation Model

For the reasons explained before, it can be seen in the figure above that the Standard Propagation Model did not present considerable variations on its coverage and path loss distribution. In this sense, it is not sensitive to variations on the receiver height.

Also, comparing both propagation models at a receiver height of 10 m, it can be observed again, not only the huge difference in coverage, but also that the areas covered by the Aster Propagation Model (black lines) presented lower SS-RSRP levels and therefore, higher path losses. In the case of the Standard Propagation Model (the bars in colors), areas were covered with better SS-RSRP levels and lower path losses.

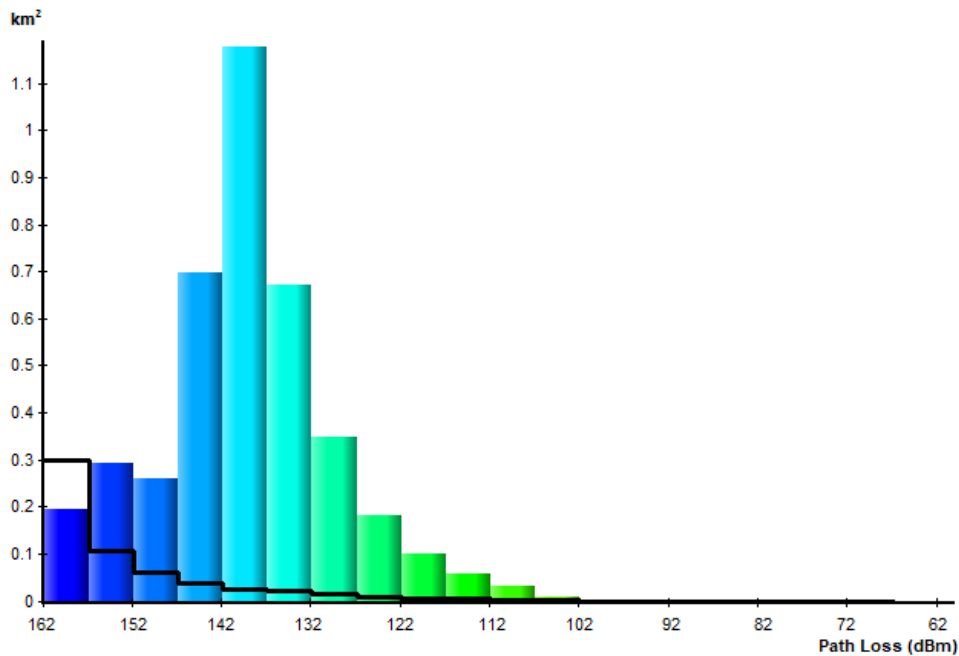


Figure 28. Path loss using the Aster Propagation Model and Standard Propagation Model with 10 m receiver height

4.2.3. Ray tracing on microcells and macrocells

One of the key features of the Aster Propagation Model is the possibility of using ray tracing techniques to add horizontal diffraction and reflection. This feature was not used in previous sections since its use is recommended for micro cells, where the antenna height is below the average building height in the vicinity of the antenna.

In this section, the use of ray tracing is studied by comparing the Aster Propagation Model with ray tracing and without ray tracing for a micro cell with the following specifications:

- **Frequency band:** n78
- **Transmission losses:** 1.51 dB
- **Antenna height:** 7 m
- **Antenna model:** 70deg 17dBi 3Tilt
- **Carrier:** 10 MHz – NR-ARFCN 620333
- **SSS EPRE:** 5 dBm
- **Shadowing margin:** 8.97 dB
- **Receiver height:** 1.5 m

The figure below shows the path loss coverage on the map for the Aster Propagation Model with ray tracing and without ray tracing when a micro cell was deployed.

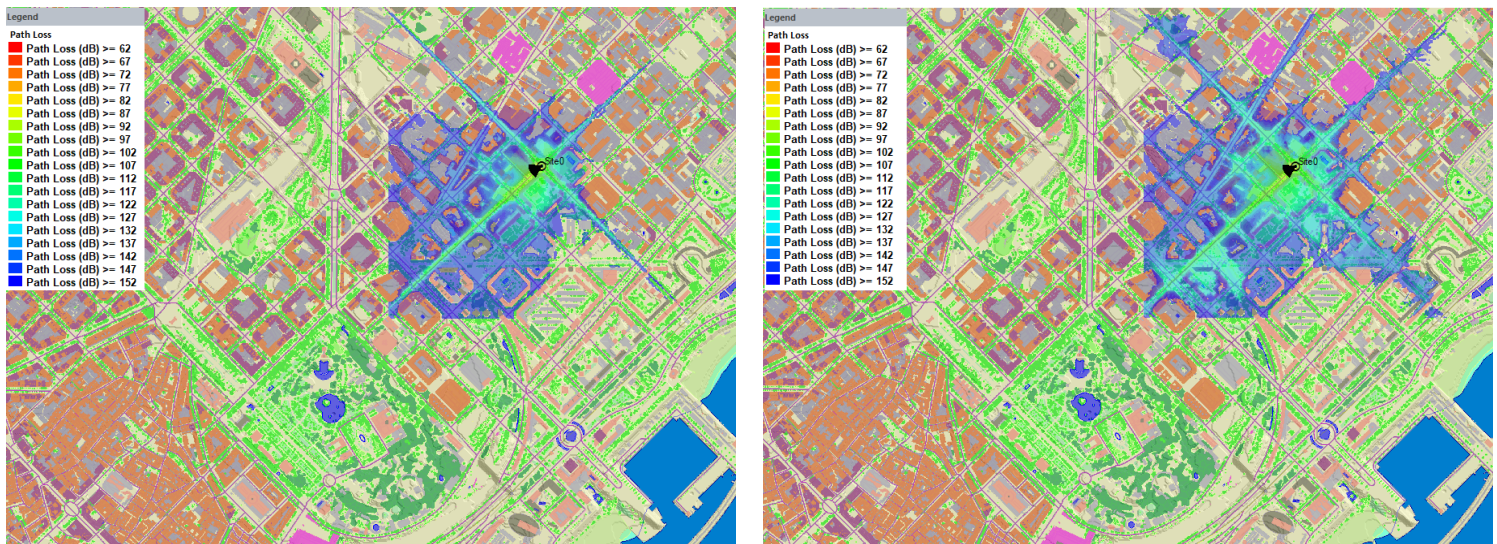


Figure 29. Path loss using the Aster Propagation Model without ray tracing (left) and with ray tracing (right) for a micro cell

The first thing that can be observed is that ray tracing improved the coverage. This is because ray tracing, for this study, had a defined radius of 800 m where horizontal diffractions and reflections were considered and a maximum number of 4 diffraction and reflections during the ray tracing. This allowed signal to reach further. Larger radius and number of reflections could had been set for the study, but no great improvements would had been achieved.

The following figure shows a histogram of the path loss distribution for the Aster Propagation Model with ray tracing represented in colors and without ray tracing, represented by the black lines.

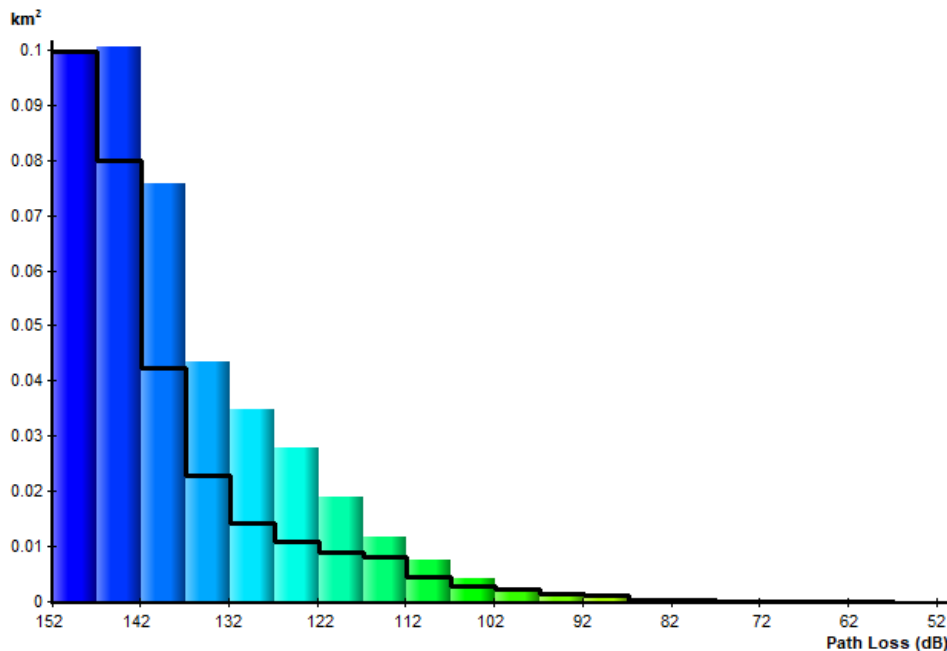


Figure 30. Path loss distribution using the Aster Propagation Model with and without ray tracing for a micro cell

Ray tracing improved the coverage of the SS-RSRP signal, allowing users on 0.43 km² to receive signals at least of -140 dBm, while the scenario without ray tracing coverage was only 0.3 km². This represents an increase of 30%.

It is important to understand that these values are very low since micro cells are not meant to cover a big area, such as the 4 km² are where the study takes place.

Also, a second study was performed in order to compare the contribution of ray tracing. In this case, a macro cell with the following parameters was used:

- **Frequency band:** n78
- **Antenna height:** 30 m
- **Antenna model:** 70deg 17dBi 3Tilt
- **Carrier:** 50 MHz – NR-ARFCN 621667
- **Receiver height:** 1.5 m

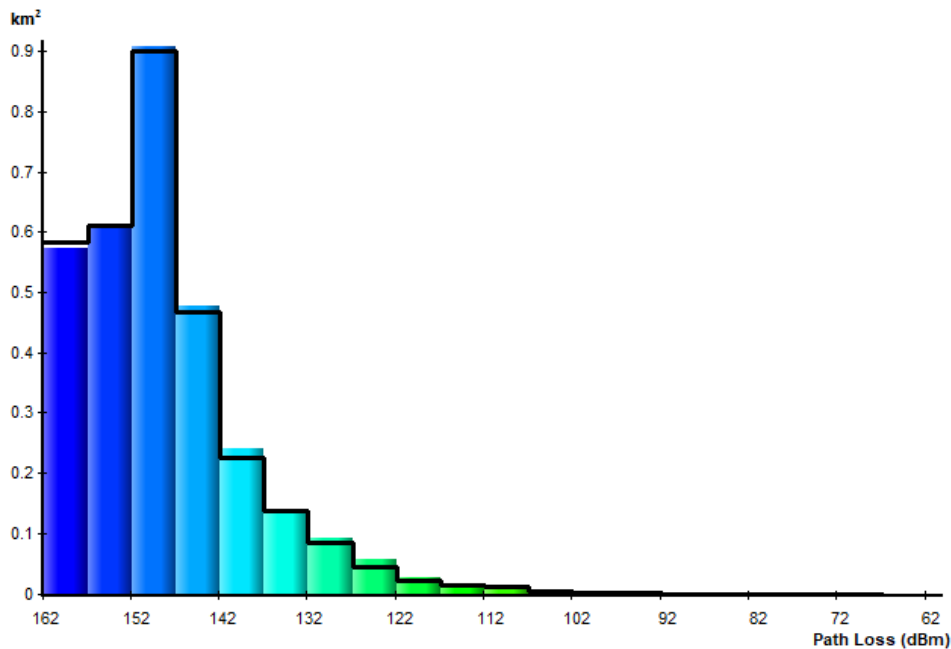


Figure 31. Path loss distribution using the Aster Propagation Model with and without ray tracing for a macro cell

It is observed that ray tracing for a macro cell did not improved coverage nor the path loss distribution. Since the antenna height was higher than most of the buildings, there was almost no horizontal diffraction and therefore, calculations were almost the same as calculation without ray tracing, that only consider vertical diffraction.

4.2.4. Impact of the transmitter height

In this section, the coverage and the path loss are studied for the Aster Propagation Model and the Standard Propagation Model when the transmitter height is changed.

First, a comparison of the Aster Propagation Model behavior for different heights is presented. Then the same is done with the Standard Propagation Model.

The study was performed for transmitter heights of 15 m, 30 m and 45 m. In the case of the Aster Propagation Model, ray tracing was taken into account.

The following parameters for the cell and the receiver were considered:

- **Frequency band:** n78
- **Transmission losses:** 1.51 dB
- **Antenna model:** 70deg 17dBi 3Tilt
- **Carrier:** 50 MHz – NR-ARFCN 621667
- **SSS EPRE:** 15 dBm
- **Shadowing margin:** 8.97 dB
- **Receiver height:** 1.5 m

The following figures compare the path loss distribution for the Aster Propagation Model with the transmitter at 30 m, represented by the bars in colors and with the transmitter at 15 m and 45 m, represented in each histogram by the black lines.

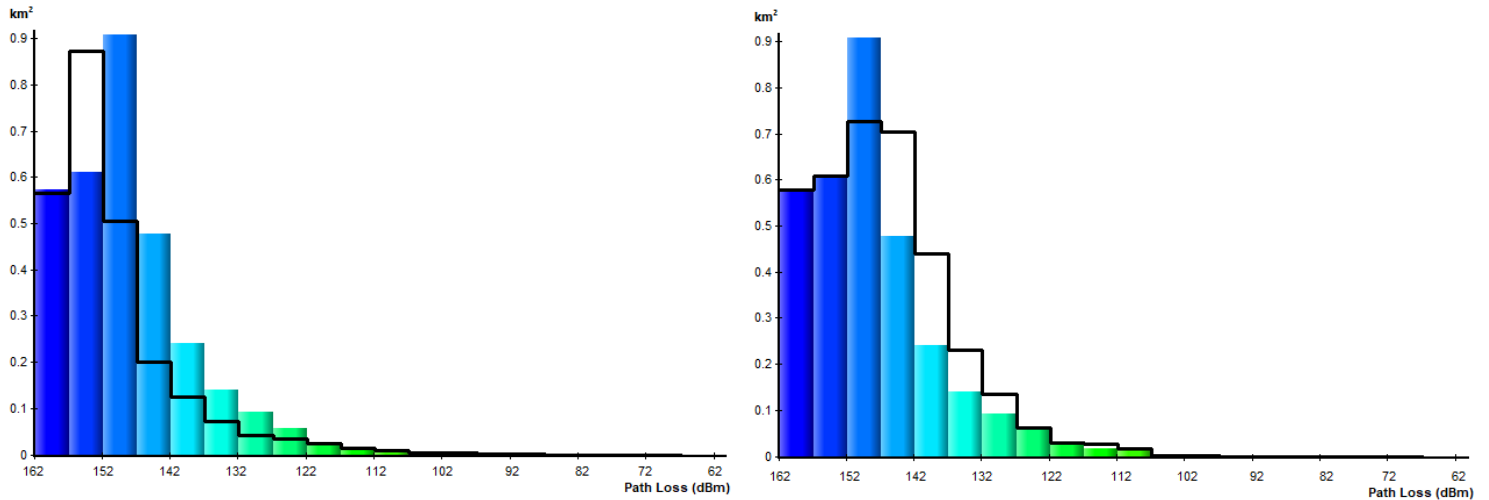


Figure 32. Path loss distribution for the transmitter height at 30 m vs transmitter height at 15 m (left) and at 45 m (right) using the Aster Propagation Model

The covered area was 2.47 km², 3.15 km² and 3.55 km², when the transmitter heights were 15 m, 30 m and 45 m, respectively. In other words, coverage for the 15 m antenna was reduced around 22% and for the 45 m antenna was increased 11%, with respect to the coverage of the 30 m antenna.

It can be observed an improvement in the path loss as the transmitter height was increased. For the case of the 15 m antenna, most areas received signals with path losses between 152 dB and 162 dB; for the case of the 30 m antenna, most areas perceived path losses between 147 dB and 157 dB; and finally for the case of the 45 m antenna, most areas experienced path losses between 142 dB and 152 dB.

On the other hand, for the case of the Standard Propagation Model, similar results were obtained. The following figures compare the path loss distribution for the Standard Propagation Model with the transmitter at 30 m, represented by the bars in colors and with the transmitter at 15 m and 45 m, represented in each histogram by the black lines.

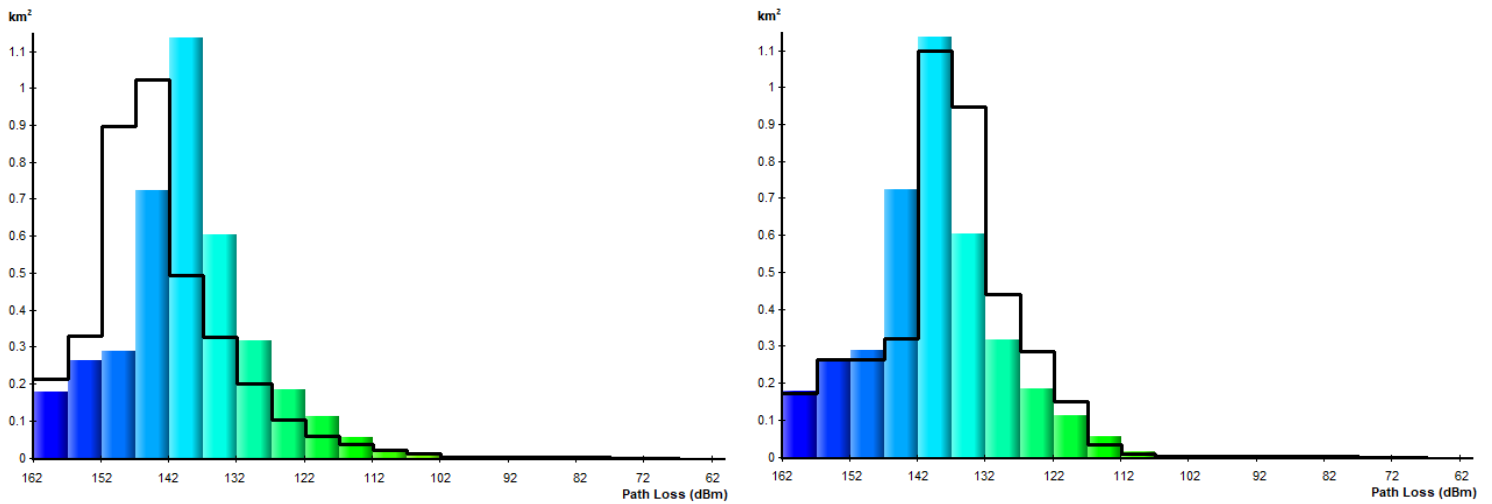


Figure 33. Path loss distribution for the transmitter height at 30 m vs transmitter height at 15 m (left) and at 45 m (right) using the Standard Propagation Model

In this case, covered area was 3.71 km², 3.89 km² and 3.99 km² when the transmitter heights were 15 m, 30 m and 45 m, respectively. This represents a decrease of 4.4% and an increase of 2.7% of the covered area with respected to covered area for the case of the 30 m antenna.

The path loss also presented an improvement for higher antennas. For the case of the 15 m antenna, most areas shown path losses between 142 dB and 152 dB; for the case of the 30 m antenna, most areas shown path losses in the range of the 137 dB and 147 dB; and for the case of the 45 m antenna, most areas shown path losses between 132 dB and 142 dB.

It is demonstrated that the Aster Propagation Model is more sensitive to changes in the transmitter height than the Standard Propagation Model and this is because the Aster Propagation Model takes into account not only the transmitter height but also the average profile height from the transmitter to the receiver.

5. Beamforming features on 5G radio planning

This chapter consists on the analysis of coverage and capacity predictions in the downlink and simulations to determine how beamforming changes the performance of a network.

First, a comparative of a scenario with and without beamforming is shown. Then, different beamforming parameters such as the number of beams and the number of antenna elements are studied in order to understand how beamforming can be improved. Also, different receiver heights are tested to compare how the different beams are used. Finally, some simulations are performed to determine the real impact of beamforming under a certain user distribution.

It is important to mention that in this and the upcoming chapters, the propagation model used is the Aster Propagation Model because of its path loss formula that includes many important factors of the surroundings and its sensitivity to changes on the receiver height.

For the study, four different antennas were used, one without beamforming which is a 70deg 17dBi 3Tilt antenna, and three with different beamforming parameters. All four antennas share the following parameters:

- **Frequency band:** n78
- **Antenna height:** 30 m
- **Carrier:** 50 MHz – NR-ARFCN 621667

The beamforming antennas parameters are shown in the following table:

Table 20. Beamforming Antenna Parameters

Parameters	Default Beamformer	Beamformer 2	Beamformer 3
Columns (N)	8	8	16
Rows (M)	8	8	16
Transmission ports	64	64	64
Reception ports	64	64	64
Number of beams	60	209	60
Azimuth range	-45° to 45°	-45° to 45°	-45° to 45°
Tilt range	-5° to 5°	-5° to 5°	-5° to 5°
Boresight gain (dB)	26.0618	26.0618	32.0824

5.1. Beamforming gain

In this section the default beamformer and a 70deg 17dBi 3Tilt antenna are compared in terms of the SS-RSRP level, the PDSCH level, the PDSCH CINR, the modulation and throughput obtained.

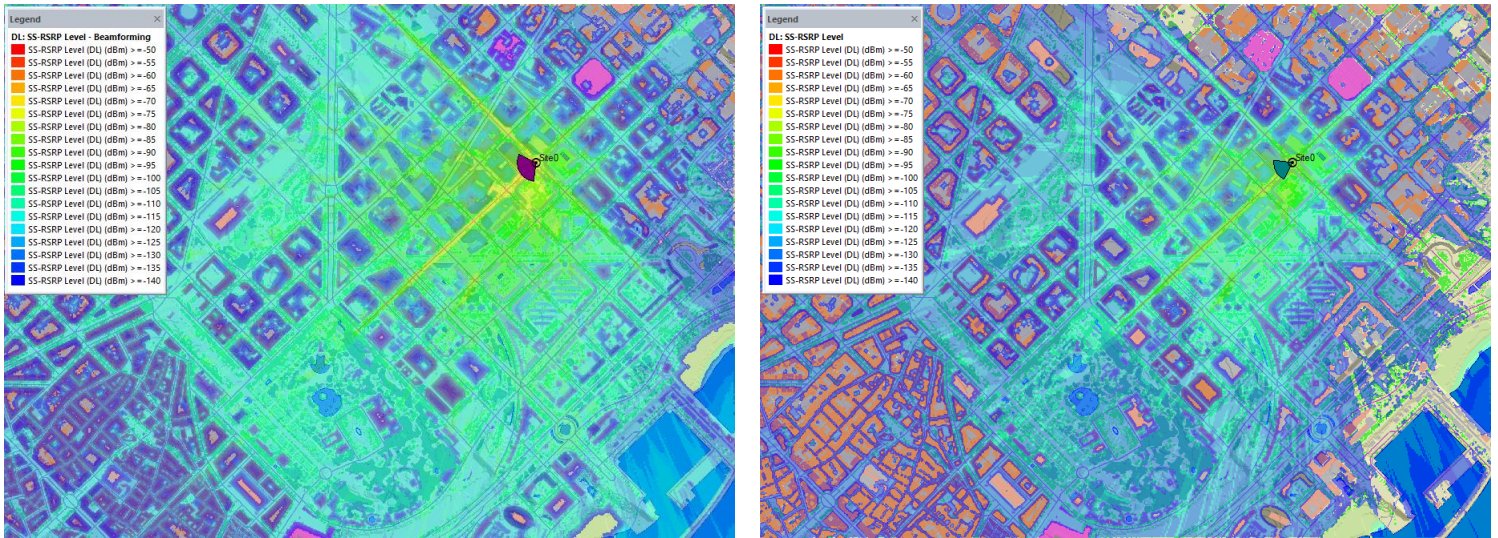


Figure 34. SS-RSRP level with beamforming antenna (left) and without beamforming (right)

In the figure above it is clearly seen that beamforming had a better coverage of the SS-RSRP reference signal. With beamforming all areas received this signal with a level higher than -140 dBm; therefore, users in this covered area could be connected to the cell; while with the 70deg 17dBi 3Tilt antenna some areas are not covered.

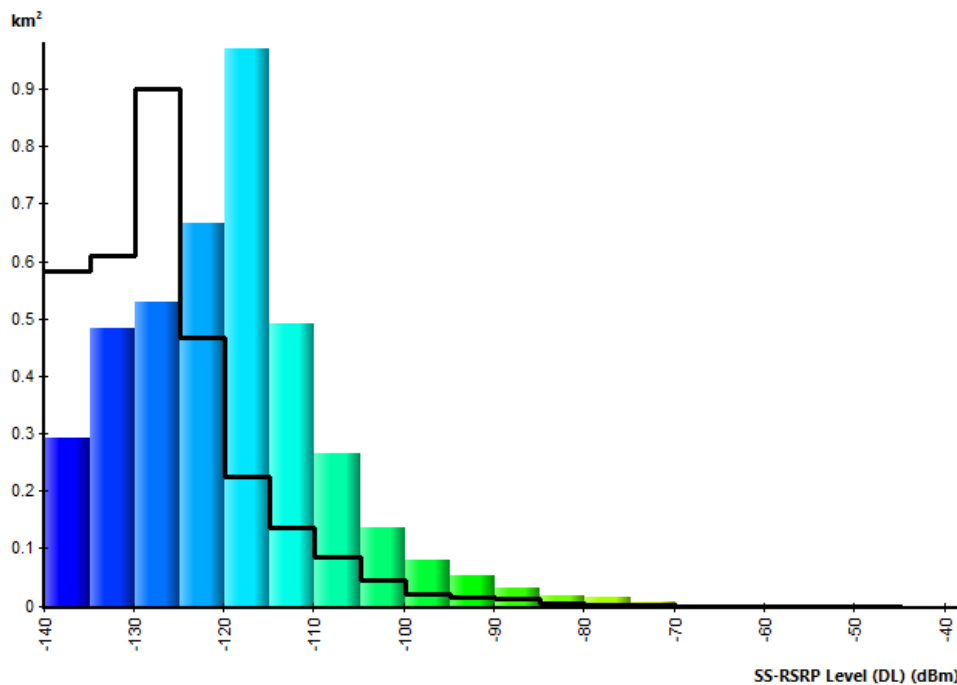


Figure 35. SS-RSRP level distribution with beamforming antenna and without beamforming antenna

The histogram shows the SS-RSRP level distribution for the case with beamforming, represented by the bars in colors, and for the case without beamforming, represented by the black lines.

Beamforming improved coverage 22.5%, allowing reference signals to reach further.

Also, it can be observed that with the 70deg 17dBi 3Tilt antenna, most areas received the reference signal with levels between -135 dBm and -125 dBm; and with beamforming, these levels were improved to -120 dBm to -110 dBm. This is because the beamforming antenna has a higher gain, of 26 dB, than the antenna without beamforming, with a gain of 17 dB.

The same analysis can be performed for the PDSCH signal level, obtaining similar results.

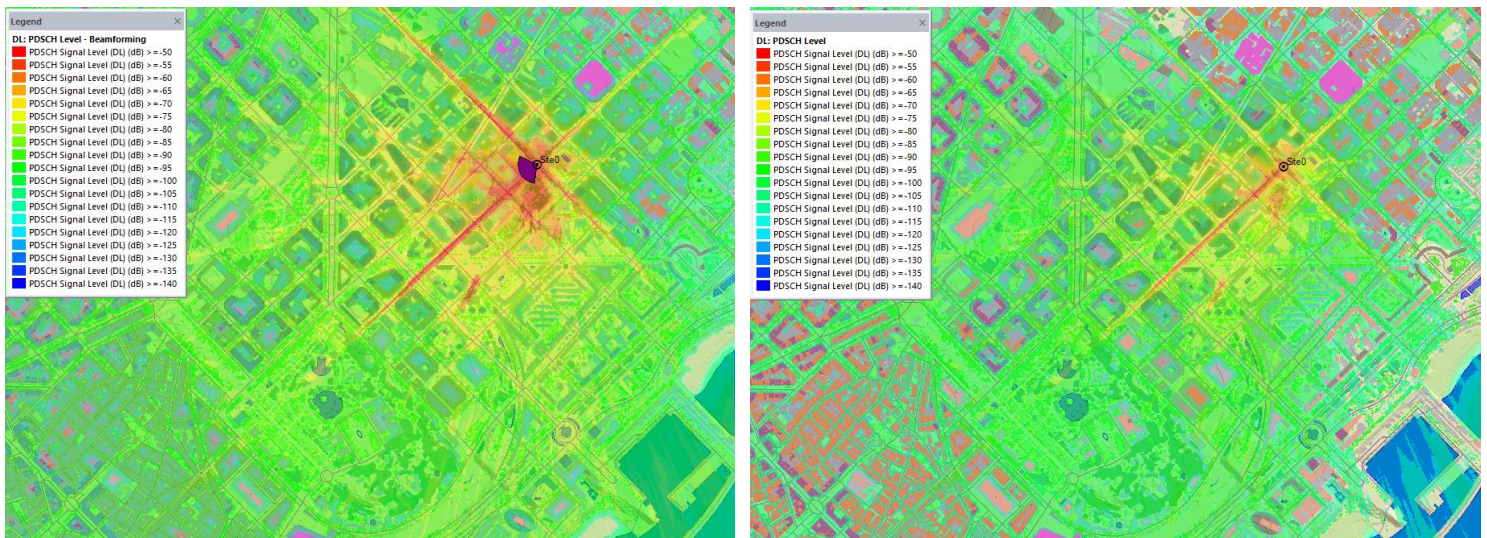


Figure 36. PDSCH level with beamforming antenna (left) and without beamforming (right)

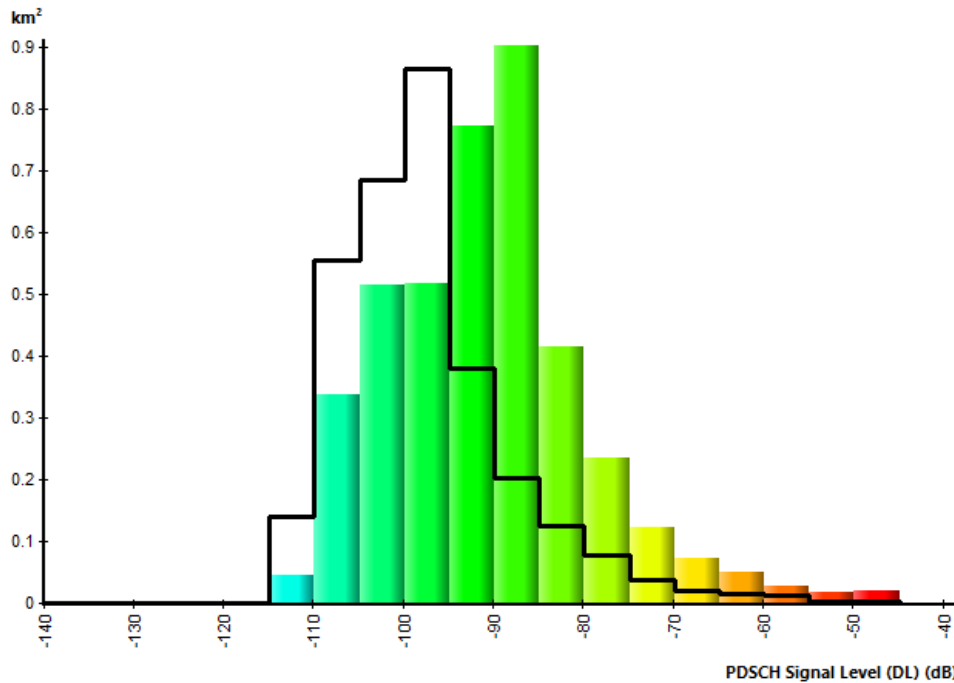


Figure 37. PDSCH level distribution with beamforming antenna and without beamforming antenna

The histogram shows the PDSCH level distribution for the case with beamforming, represented by the bars in colors, and for the case without beamforming, represented by the black lines.

Again, it is seen that beamforming improved the received signal level. Most areas without beamforming received PDSCH signals between -105 dBm and -95 dBm, and with beamforming between -95 dBm and -85 dBm.

The carrier-to-interference-plus-noise ratio (CINR) is another important aspect to be considered, because depending on its value, different bearers, therefore different modulation and coding schemes are assigned for the communication.

In the case of this study, interference was zero, since there was only one cell deployed on the whole area. This means that the CINR only depended on the PDSCH signal level and the noise, which is constant.

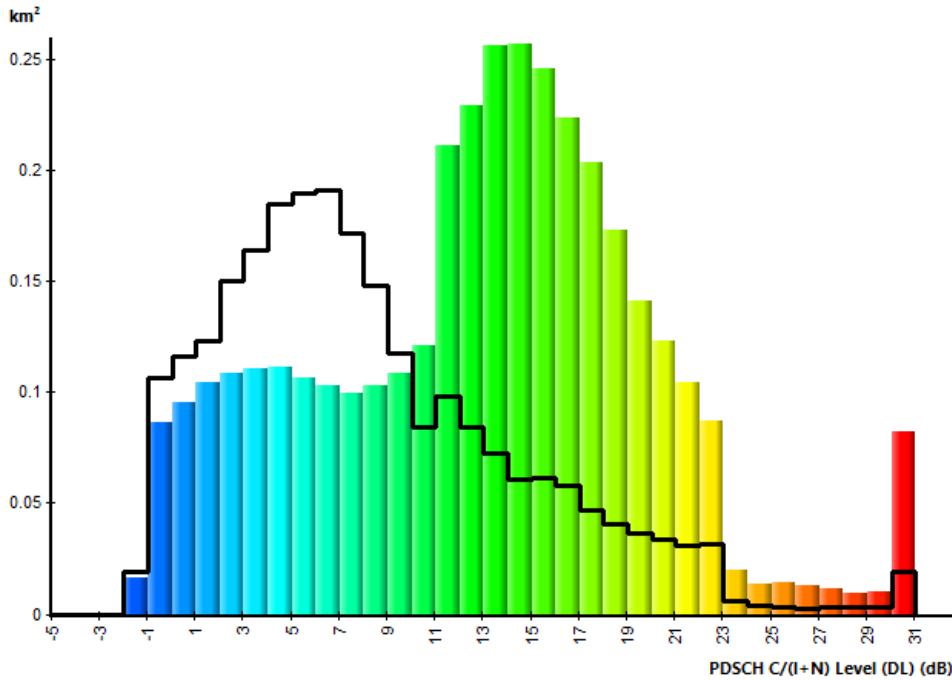


Figure 38. PDSCH CINR distribution with beamforming antenna and without beamforming antenna

The histogram shows the PDSCH CINR distribution for the case with beamforming, represented by the bars in colors, and for the case without beamforming, represented by the black lines.

Improvement on the CIRN was expected since the PDSCH signal level was also improved. Without beamforming most of the areas experienced a CIRN between -1 dBm and 10 dBm, and with beamforming most areas have a better quality, between 10 dBm and 20 dBm.

This improvement in the signal quality impacted directly on the modulation scheme, as it can be seen in the following figures.

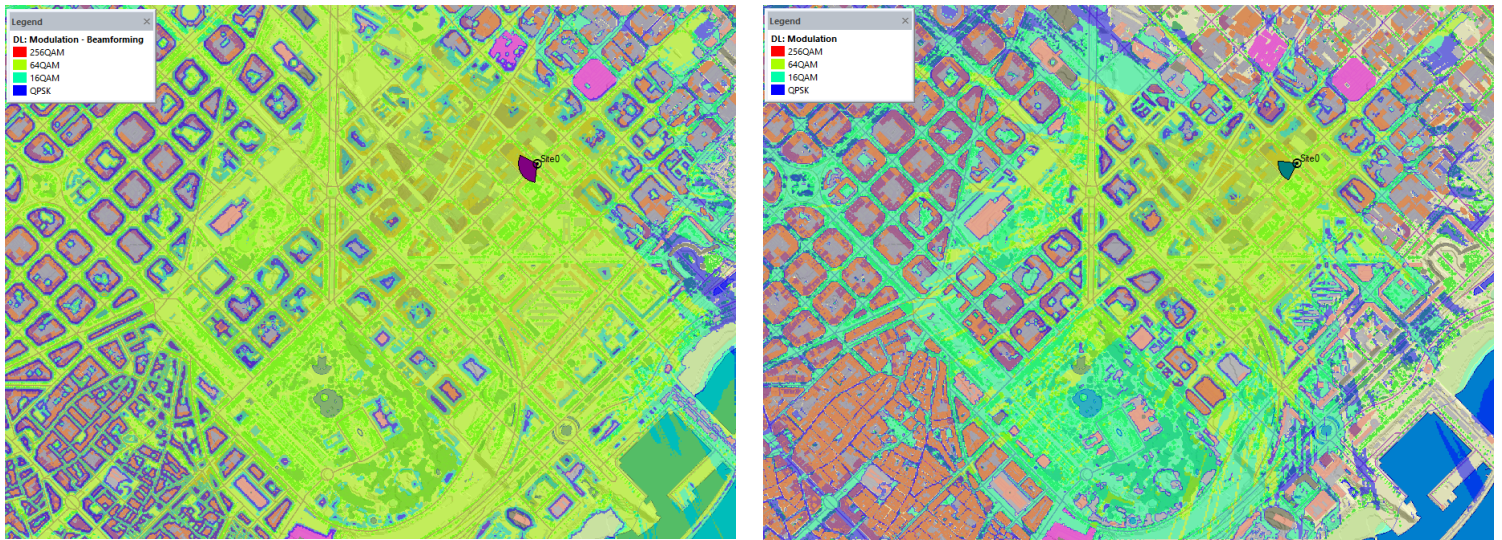


Figure 39. Modulation with beamforming antenna (left) and without beamforming (right)

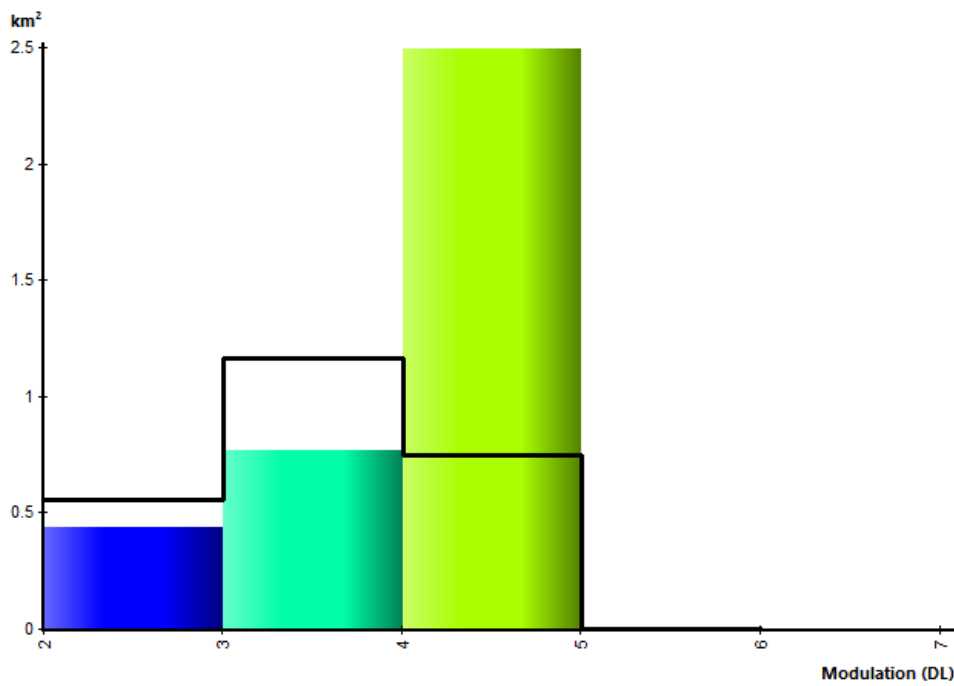


Figure 40. Modulation distribution with beamforming antenna and without beamforming antenna

The histogram shows the modulation distribution for the case with beamforming, represented by the bars in colors, and for the case without beamforming, represented by the black lines.

It is seen a great improvement on 64QAM modulation scheme. Without beamforming, it was only assigned to users on 0.75 km², but with beamforming this value went up to 2.5 km²; this is more than 3 times the covered area.

Nevertheless, even with beamforming there were some areas on the map that were not covered or not assigned a modulation scheme. This is because CINR in those points of the map was too low that did not meet the threshold requirements to assign even the lowest bearer with the lowest modulation scheme.

Finally, as a direct consequence of better signal quality and modulation, more areas experienced better throughput.

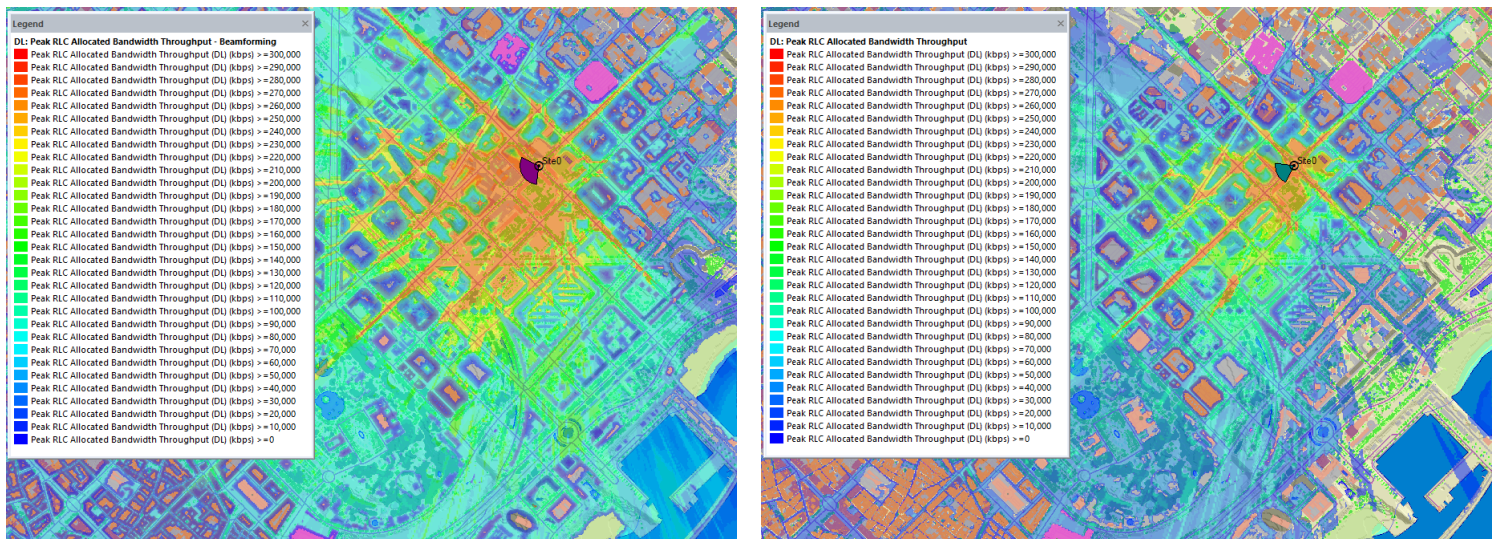


Figure 41. Peak RLC allocated bandwidth throughput with beamforming antenna (left) and without beamforming (right)

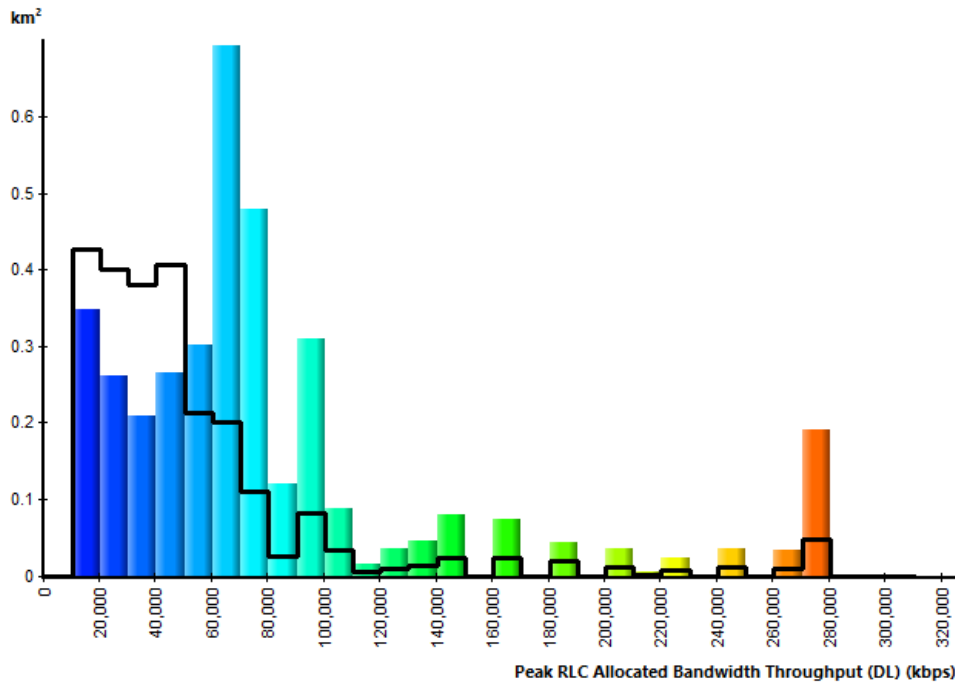


Figure 42. Throughput distribution with beamforming antenna and without beamforming antenna

The histogram shows the throughput distribution for the case with beamforming, represented by the bars in colors, and for the case without beamforming, represented by the black lines.

With beamforming, most areas experienced 60 Mbps throughput, while without beamforming this was less than 10 Mbps. Also, while without beamforming, throughputs higher than 60 Mbps were only found on 16% of the areas, with beamforming those rates were obtained on 58% of the areas.

5.2. Impact of the number of beams

It has been demonstrated that beamforming improves the coverage with higher signal level, the signal quality, the modulation scheme and the throughput, however, better results can be obtained by varying the number of beams.

In this section, the default beamformer, with 60 beams is compared to the beamformer 2, with 209 beams.

The following figure shows the throughput distribution for the case of the beamformer 2, represented by the bars in colors, and for the case of the default beamformer, represented by the black lines.

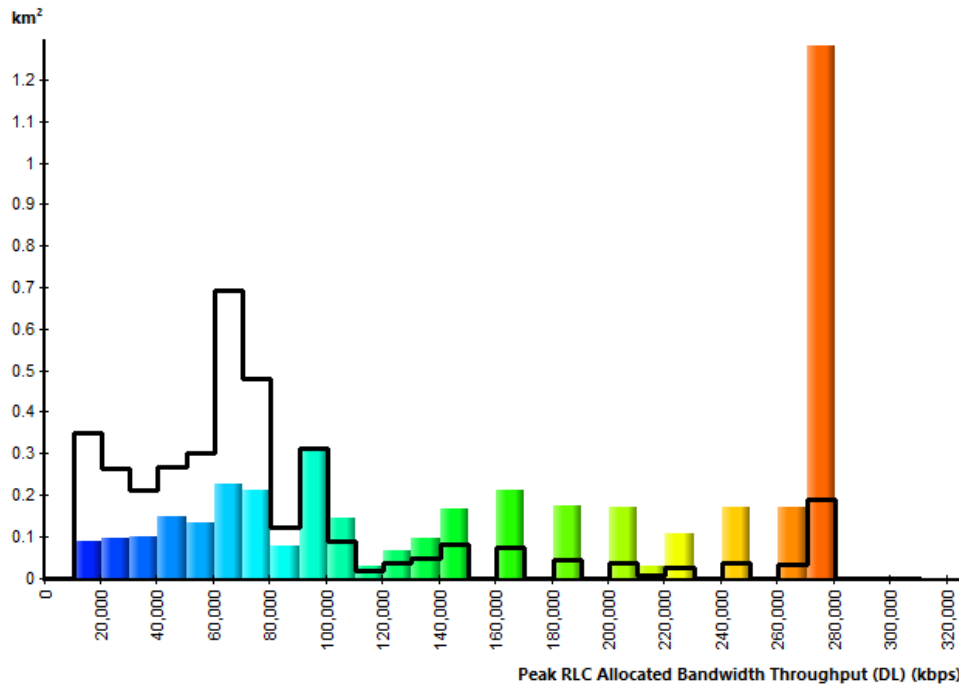


Figure 43. Throughput distribution of beamformer 2 and default beamformer

It can be observed a great improvement on the throughput by increasing the number of beams. Beamformer 2 showed a performance of 270 Mbps on 1.3 km², while this throughput was only achieved on 0.19 km². This represents an increase of almost 7 times the covered area.

5.3. Impact of the number of antennas elements

In this section the beamformer 3, with 16x16 antenna elements and the default beamformer, with 8x8 antenna elements are compared.

The antenna elements of the array are used to produce the different beams of a beamformer. A higher number of antenna elements allow each beam to obtain higher gains. In the case of the beamformer 3, beams have a gain of 32 dB. In fact, increasing by a factor of 2 the number of antenna elements, increases the gain 6 dB. That is, for an array of 8x8, 26 dB are obtained; for an array of 16x16, 32 dB are obtained; for an array of 32x32, 38 dB are obtained and so on.

The following figure shows the throughput distribution for the case of the beamformer 3, represented by the bars in colors, and for the case of the default beamformer, represented by the black lines.

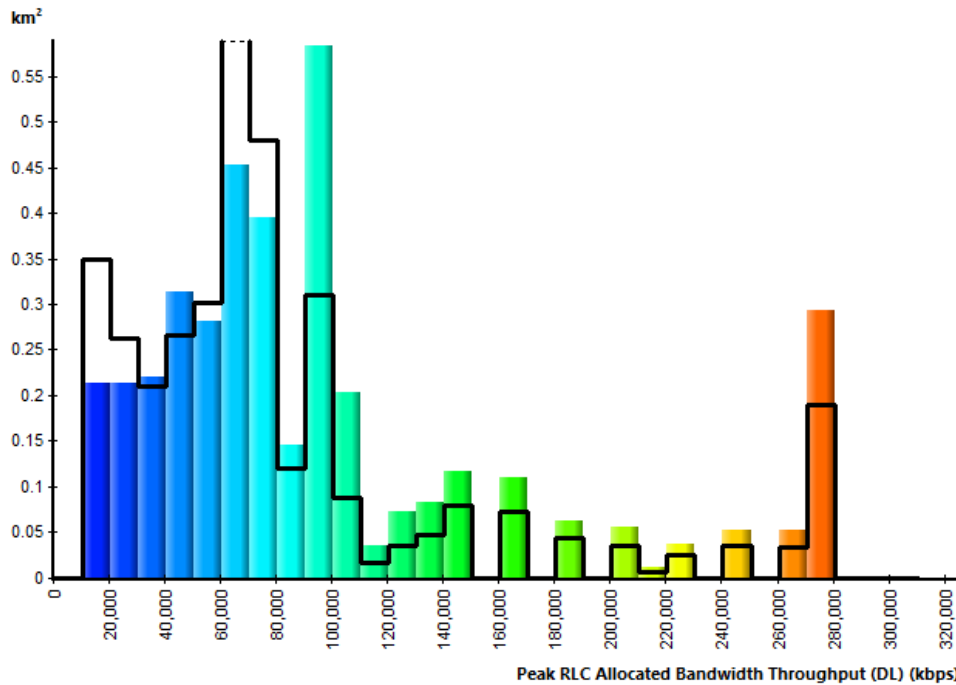


Figure 44. Throughput distribution of beamformer 3 and default beamformer

As a consequence of increasing the gain of the antenna, the throughput increased as well. With beamformer 3, throughputs higher than 90 Mbps covered 1.76 km², which is almost 2 times the coverage obtained for this range of rates with the default beamformer.

5.4. Impact of the receiver height

In this section the performance of the beamformer 2 is tested against different receiver heights and it is compared to the obtained with the 70deg 17dBi 3Tilt antenna.

The study was carried out using 5 m, 10 m, 40 m and 50 m receiver heights.

The following figure shows the distribution of the PDSCH signal level for the different heights. The bars in color correspond to the beamformer 2 and the black lines correspond to the 70deg 17dBi 3Tilt antenna.

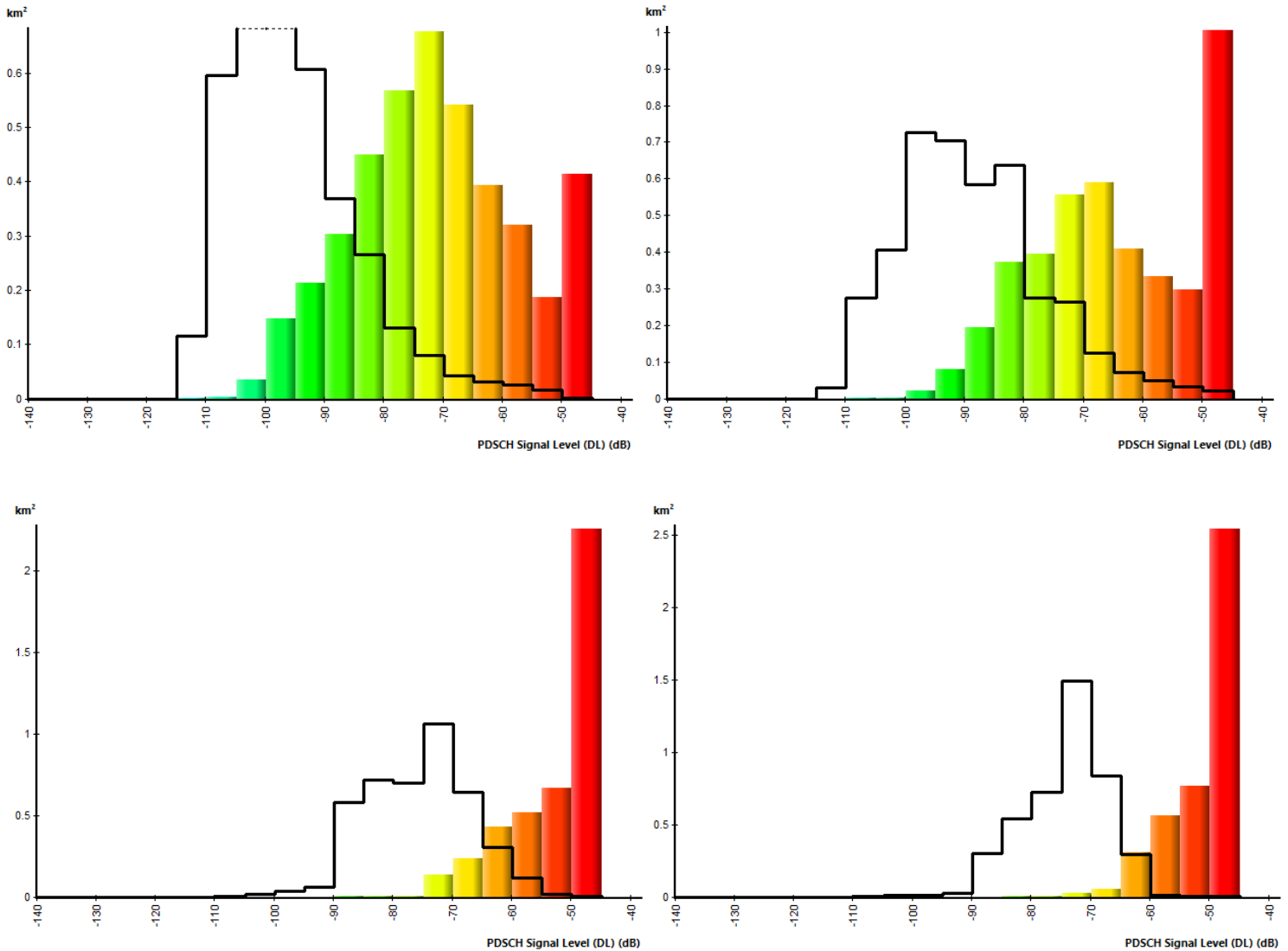


Figure 45. PDSCH signal level distribution for receiver heights at 10 m (top left), 20 m (top right), 40 m (bottom left) and 50 m (bottom right) using beamforming 2 and the 70deg 17dBi 3Tilt antenna

In general, the beamformer 2 presented better PDSCH signal level distribution for all the receiver heights than the 70deg 17dBi 3Tilt antenna, but in order to get more information about these histograms in Figure, the analysis can be divided in two groups, for receiver heights lower than the transmitter height and for receiver heights higher than the transmitter height.

For the first two histograms, corresponding to receiver heights (10 m and 20 m) lower than the transmitter height (30 m), it is observed that as the receiver height increased, the difference on area covered with the same signal level decreased.

For example, let's take the range from -75 dBm to 70 dBm. On the case of 10 m, this range was found on 0.67 km² when the beamformer 2 was used, and on 0.08 km² when the 70deg 17dBi 3Tilt antenna was used. This corresponds to a difference of almost 8.4

times the covered area. While on the case of 20 m, this range covered 0.56 km² and 0.27 km², respectively. This correspond to a difference of 2 times the covered area.

The reason for this is that path loss decreases as the receiver height increases because there are less high buildings to obstruct the signal, and therefore, PDSCH signal distribution moves to better levels for both antennas. While in the example of -75 dBm to -70 dBm, covered area increased for the 70deg 17dBi 3Tilt antenna; for the beamformer 2 covered area decreased, since it moved to higher signal levels.

On the other hand, this is not what occurred when the receiver height was higher than the transmitter height. Taking a look at the other two histograms corresponding to receiver heights of 40 m and 50 m, it is observed that the difference on covered area for the same signal level range is increased when the receiver height increased.

Let's take the range from -60 dBm to -55 dBm. On the case of 40 m, this range covered 0.52 m² when the beamformer 2 was used, and 0.12 when the the 70deg 17dBi 3Tilt antenna was used. This is a 4.4 times the covered area. While on the case of 50 m, the covered areas were 0.561 m² and 0.01 m² respectively. This 56 times the covered area. The same happens with ranges from -55 dBm to 50 dBm, that difference went from 37 times to 254 times.

The reason of this behavior is that when the receiver height is higher than the transmitter height, coverage for the 70deg 17dBi 3Tilt antenna is penalized by the fixed 3° downtilt, while the coverage for the beamformer 2 is not, since it has beams with uptilts from 0° to 5° and therefore it is able to point directly to the receivers.

Also better throughput distribution was obtained for the beamformer 2 compared to the 70deg 17dBi 3Tilt antenna. This can be seen in the following figure, where beamformer 2 is represented by the bars in color and the 70deg 17dBi 3Tilt antenna is represented by the black lines.

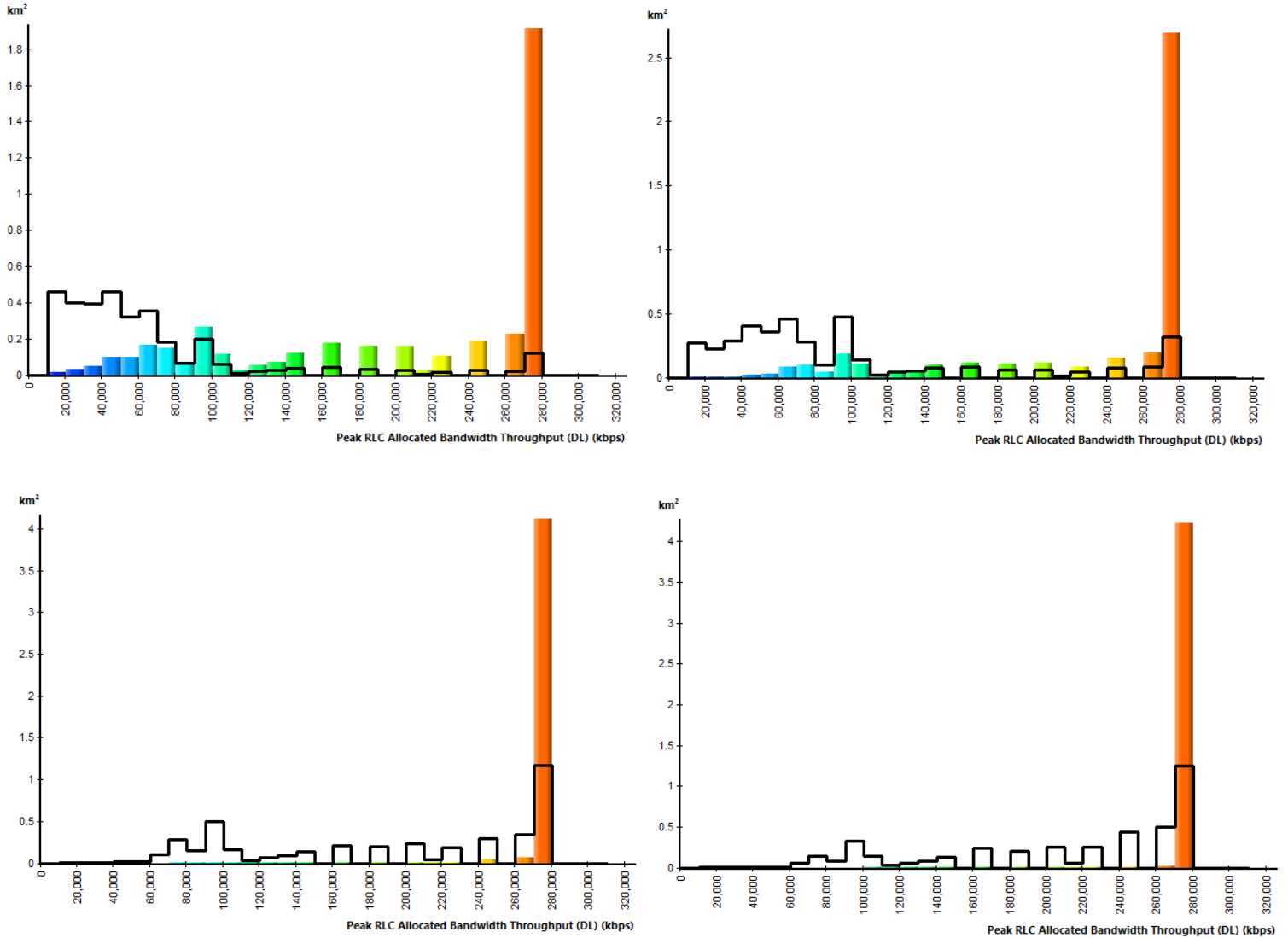


Figure 46. Throughput distribution for receiver heights at 10 m (top left), 20 m (top right), 40 m (bottom left) and 50 m (bottom right) using beamforming 2 and the 70deg 17dBi 3Tilt antenna

5.5. 3D simulation results

In this section, a number of 100 business users located at different heights (between 1.5 m and 20 m) demanding broadband service were distributed over a 1 km² area in order to study a more realistic capacity and coverage of the cell and the average user performance. The study was performed using the beamformer 2 and the 70deg 17dBi 3Tilt antenna.

Also, in this section MIMO capabilities were disabled. Later on section 6.4 some simulations results will be shown, where MIMO and beamforming capabilities were used together.

In total, 10 simulations were performed for each antenna and the following table shows the average results.

Table 21. Average Results for 3D Simulations Using Beamforming

Parameters	Beamformer 2	70deg 17dBi 3Tilt Ant
Users rejected	7.6 (7.6 %)	38.6 (38.6 %)
Active users (DL+UL)	92.4 (92.4 %)	61.4 (61.4 %)
Peak RLC cumulated throughput (DL)	97.60 Mbps	63.07 Mbps
Effective RLC cumulated throughput (DL)	97.52 Mbps	62.9 Mbps
Cumulated application throughput (DL)	92.65 Mbps	59.75 Mbps
Average application user throughput (DL)	1.00 Mbps	0.97 Mbps
Peak RLC cumulated throughput (UL)	111.17 Mbps	104.71 Mbps
Effective RLC cumulated throughput (UL)	110.62 Mbps	104.24 Mbps
Cumulated application throughput (UL)	105.09 Mbps	99.03 Mbps
Average application user throughput (UL)	1.14 Mbps	1.61 Mbps
Traffic load (DL)	100 %	100 %
Traffic load (UL)	99.99 %	99.99 %
Average SS-RSRP	-81.38 dBm	-109.45 dBm
Average PDSCH	-52.46 dBm	-80.53 dBm
Average PDSCH CIRN	36.77 dB	8.70 dBm
Average path loss	120.93 dB	139.94 dB

It is seen that the beamformer 2 achieved better results compared to the 70deg 17dBi 3Tilt antenna.

The first thing that can be observed is that with the beamformer 2, 92.4% of the users were able to connect to the cell, a much higher result if it is compared to the 61.4% of connection success with the 70deg 17dBi 3Tilt antenna.

In terms of cumulated throughput, it is seen that the cell with beamformer 2 handled 1.55 times and 1.1 more traffic compared to what the cell with the 70deg 17dBi 3Tilt antenna handled, in downlink and uplink respectively.

On the other hand, in terms of average user throughput, it is seen that users experienced almost the same data rates.

In terms of the SS-RSRP, on average users received signals almost 28 dB higher when the beamformer 2 was used. This is because the possibility for beamformer 2 to point beams to those users located on heights higher than the transmitter height. Also, the 28 dB difference is seen for the PDSCH signal level. Finally, path loss was almost 19 dB lower for the beamforming case.

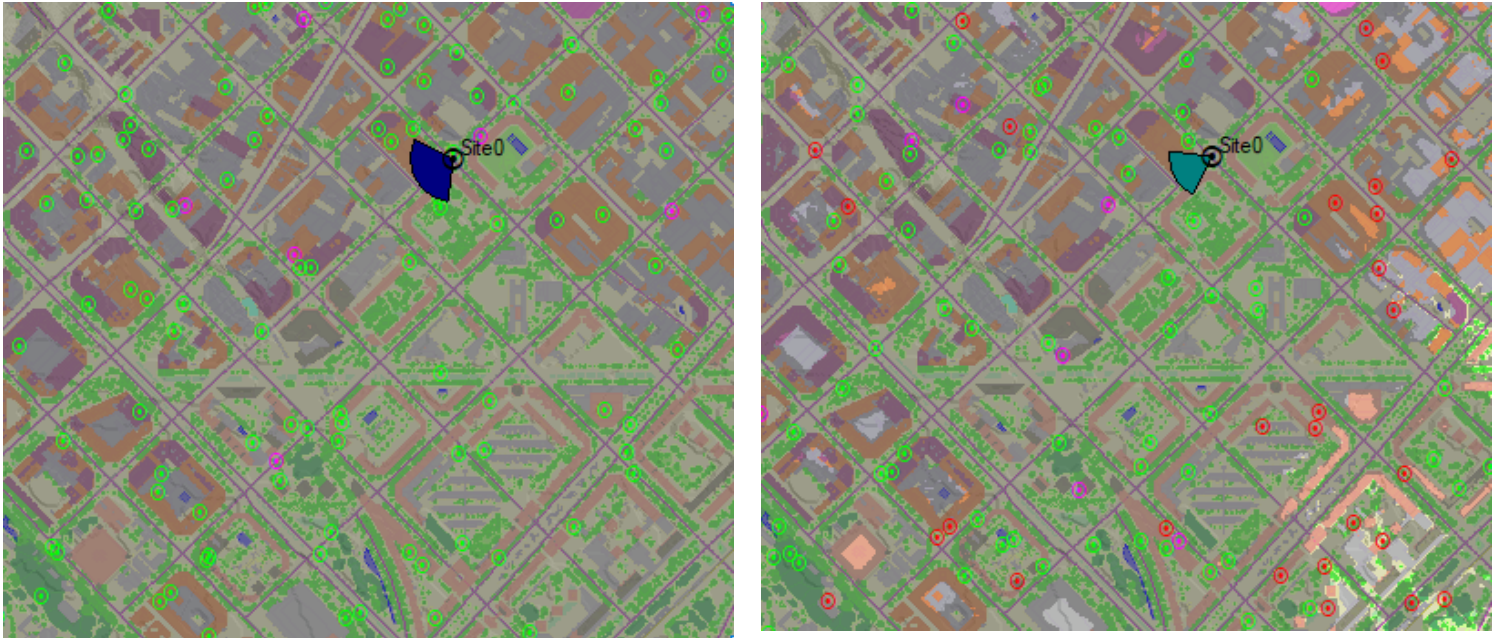


Figure 47. User connection distribution using beamformer 2 (left) and using the 70deg 17dBi 3Tilt antenna (right)

The figure above shows graphically the connection results mentioned before. The green dots represent the users that had allocated resources in the downlink and the uplink and therefore, a successful connection. The red dots represent users with no coverage or no service because mobiles were not able to access a bearer. Finally, the pink dots represent users with resource saturation due to all the cell resources were used before allocation to those mobiles.

6. Massive MIMO features on 5G radio planning

This chapter consists on the analysis of how Atoll models the massive MIMO capabilities of 5G NR and analyze how the use of MIMO improves $C/(I+N)$ and throughput.

On the first section, transmit diversity is studied for different number of transmission and reception antennas. On the second section, single-user MIMO (SU-MIMO) is studied also varying both number of antennas. Finally, on the third section, multi-user MIMO (MU-MIMO) is studied varying the number of antennas and also the number of users. All these studies were performed only for the downlink and they were limited to a 1 km² area.

The transmitter/cell parameters used for this chapter are the following:

- **Frequency band:** n78
- **Antenna height:** 30 m
- **Carrier:** 50 MHz – NR-ARFCN 621667

6.1. Transmit diversity

In this section, the transmit diversity capability of a cell and the how Atoll models it are studied. For this, only transmit diversity mode was configured on the cell.

6.1.1. **Impact of transmission antennas on transmit diversity mode**

The first study consisted on varying the number of transmitting antennas on the base station, while having a fixed number of receiving antennas on the user equipment. The different configurations for transmit diversity tested were: 4x1, 16x1, 64x1 and 128x1.

The following figure shows the results obtained for the PDSCH $C/(I+N)$ predictions, where a SISO configuration, represented by the black line, is compared with the different diversity configurations mentioned above, represented by the blue color.

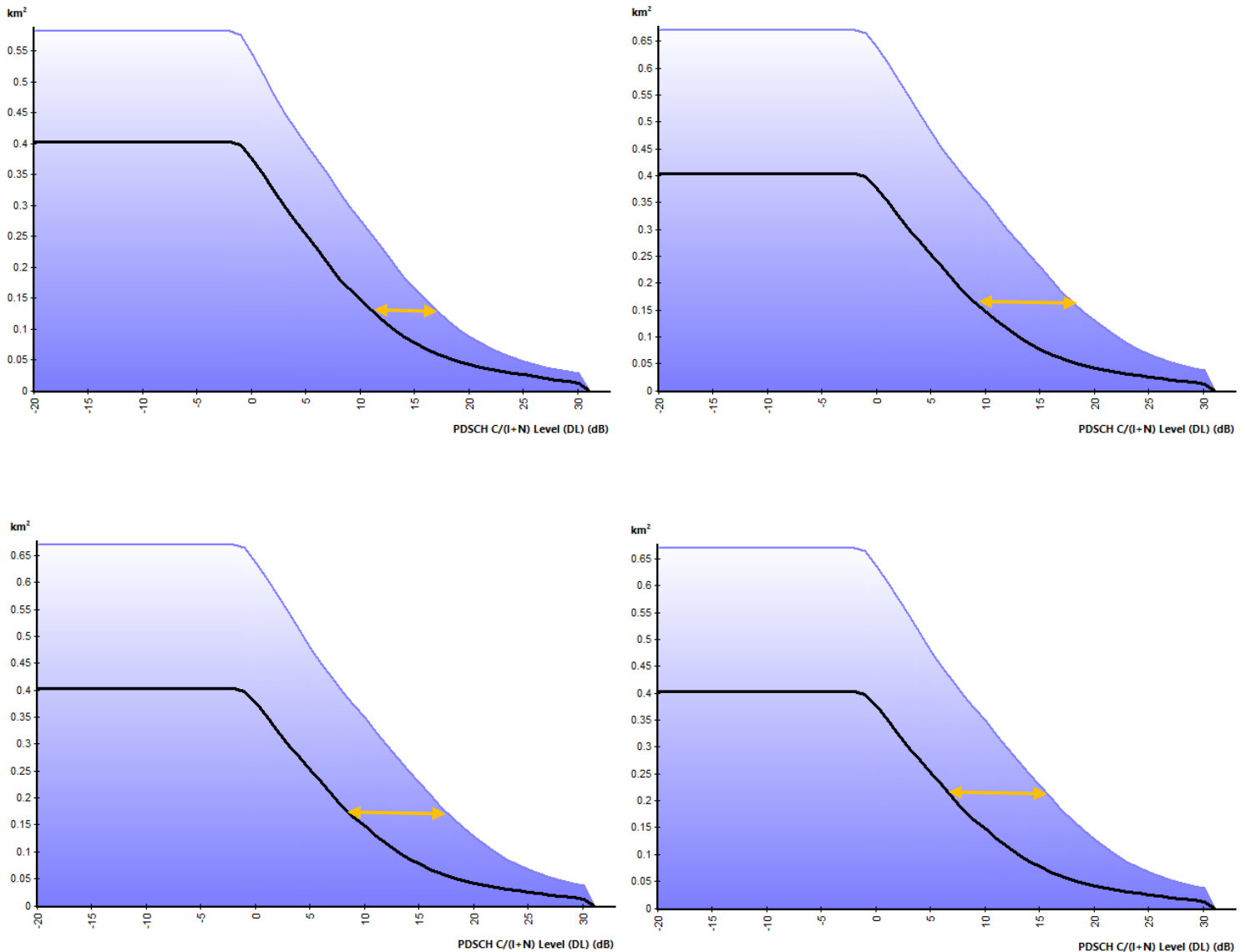


Figure 48. PDSCH C/(I+N) for SISO vs diversity 4x1 (top left), 16x1 (top right), 64x1 (bottom left) and 128x1 (bottom right)

It is observed in the figure above that for the case of diversity 4x1, there was a diversity gain of 6 dB and for the case of diversity 16x1, the diversity gain obtained was 9 dB. Nevertheless, even though that the number of transmission antennas was increased to 64 and 128, for the cases of diversity 64x1 and 128x1, there was no improvement since the diversity gain remained 9 dB. This behavior followed the predefined configuration on Atoll, where improvement by varying the number of transmission antennas is only obtained until a maximum of 16 antennas; after this number, the diversity gain remains constant.

The same behavior seen on the PDSCH C/(I+N) was obtained for the throughput. Since there were no changes on the C/(I+N) level for the cases of 64x1 and 128x1, there was no improvement for the throughput, as it can be seen in the figure below.

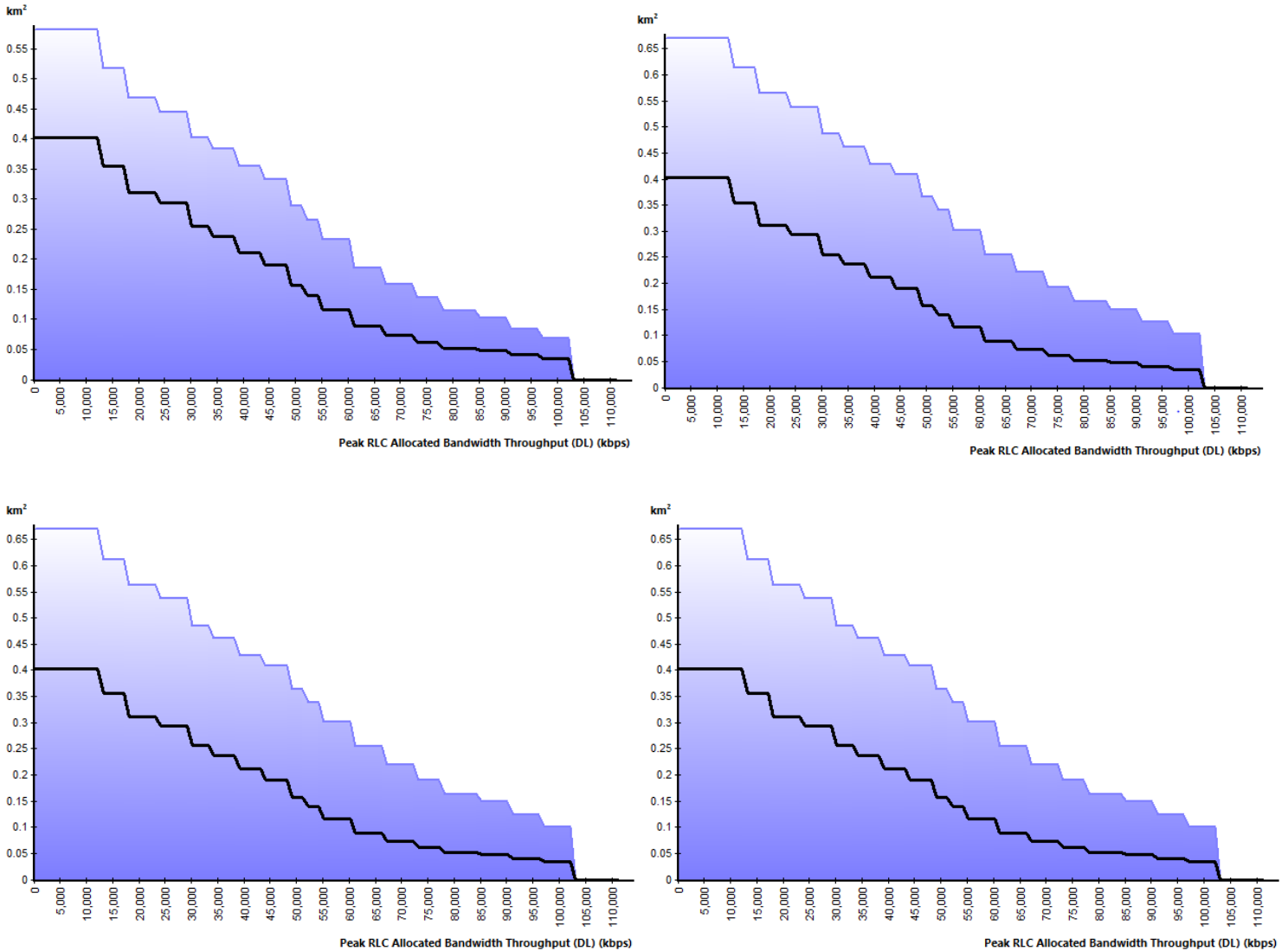


Figure 49. Throughput for SISO vs diversity 4x1 (top left), 16x1 (top right), 64x1 (bottom left) and 128x1 (bottom right)

6.1.2. Impact of receiving antennas on transmit diversity mode

For this study number of receiving antennas on the user equipment were varied, while the number of transmitting antennas on the base station remained fixed and some quality and capacity predictions were performed. The different configurations for transmit diversity tested were: 64x1, 64x2, 64x4 and 64x8.

The following figure shows the results obtained for the PDSCH C/(I+N) predictions, where a SISO configuration (1 transmit antenna and 1 receive antenna), represented by the black line, is compared with the different diversity configurations mentioned above, represented by the blue color.

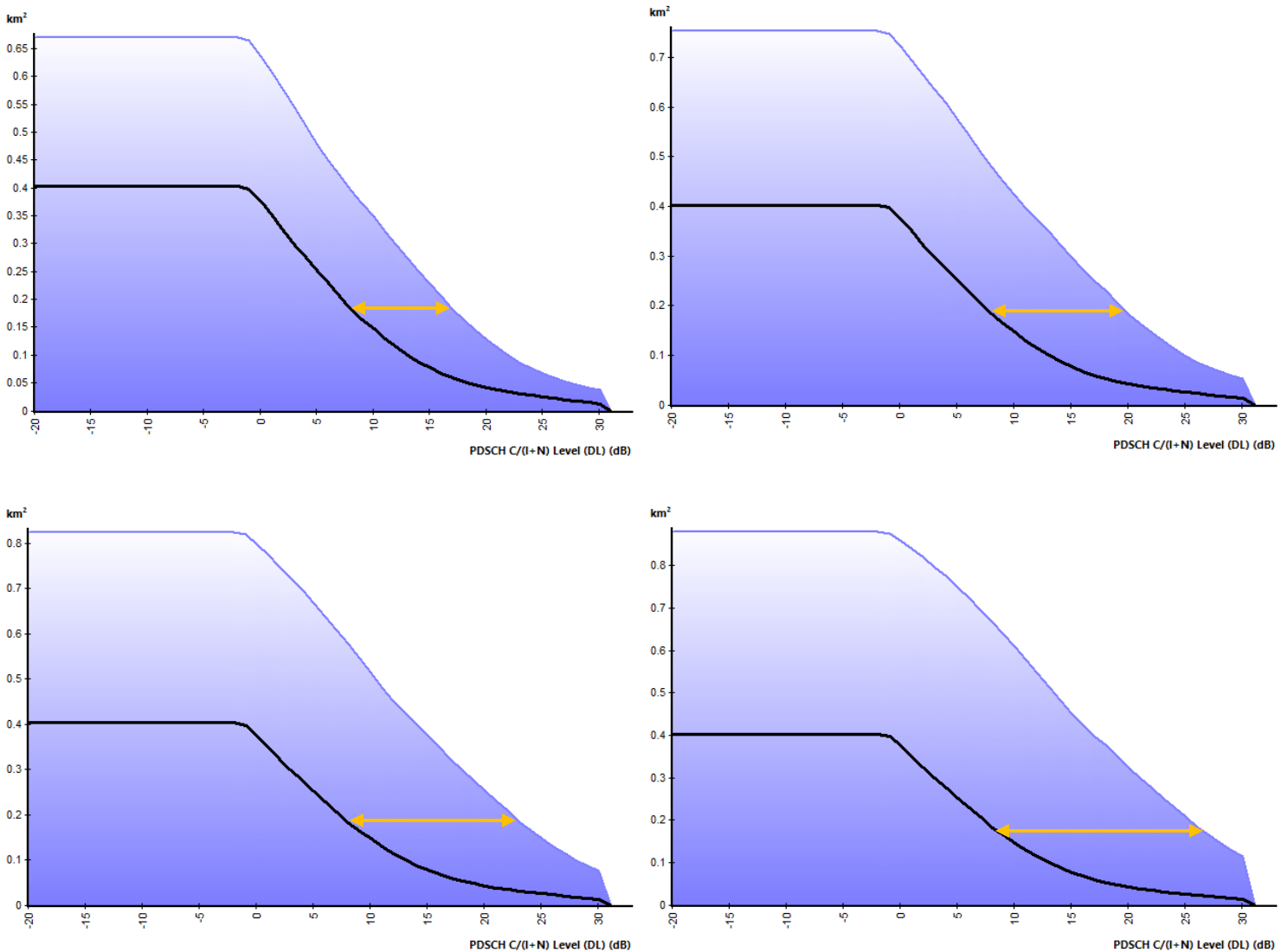


Figure 50. PDSCH C/(I+N) for SISO vs diversity 64x1 (top left), 64x2 (top right), 64x4 (bottom left) and 64x8 (bottom right)

It is seen that the PDSCH C/(I+N) level improved as the number of receiving antennas on the user equipment increased. This improvement was achieved thanks to the receiver diversity gain obtained by these configurations, which is represented by the yellow arrows. It is also observed that the coverage on the PDSCH signal received increased with a higher number of receiving antennas on the user equipment.

Table 22. Diversity Gains and Covered Area for Transmit Diversity

Transmission Antennas	Receiving Antennas	Diversity Gain (dB)	Covered Area (km ²)
64	1	9	0.65
64	2	12	0.75
64	4	15	0.8
64	8	18	0.85

Comparing the results obtained in this section with the results obtained in section 6.1.1 for the 64x1 configuration, it is seen how even though there was a limiting number of transmission antennas to increase the gain, increasing the number of receiving antennas can mitigate this limitation. By doubling the number of receiving antennas, a 3 dB gain improvement is obtained.

In order to study the changes on the throughput, capacity predictions were also performed.

The following figure shows the results obtained for the capacity predictions, where a SISO configuration, represented by the black line, is compared with the different diversity configurations mentioned above, represented by the blue color.

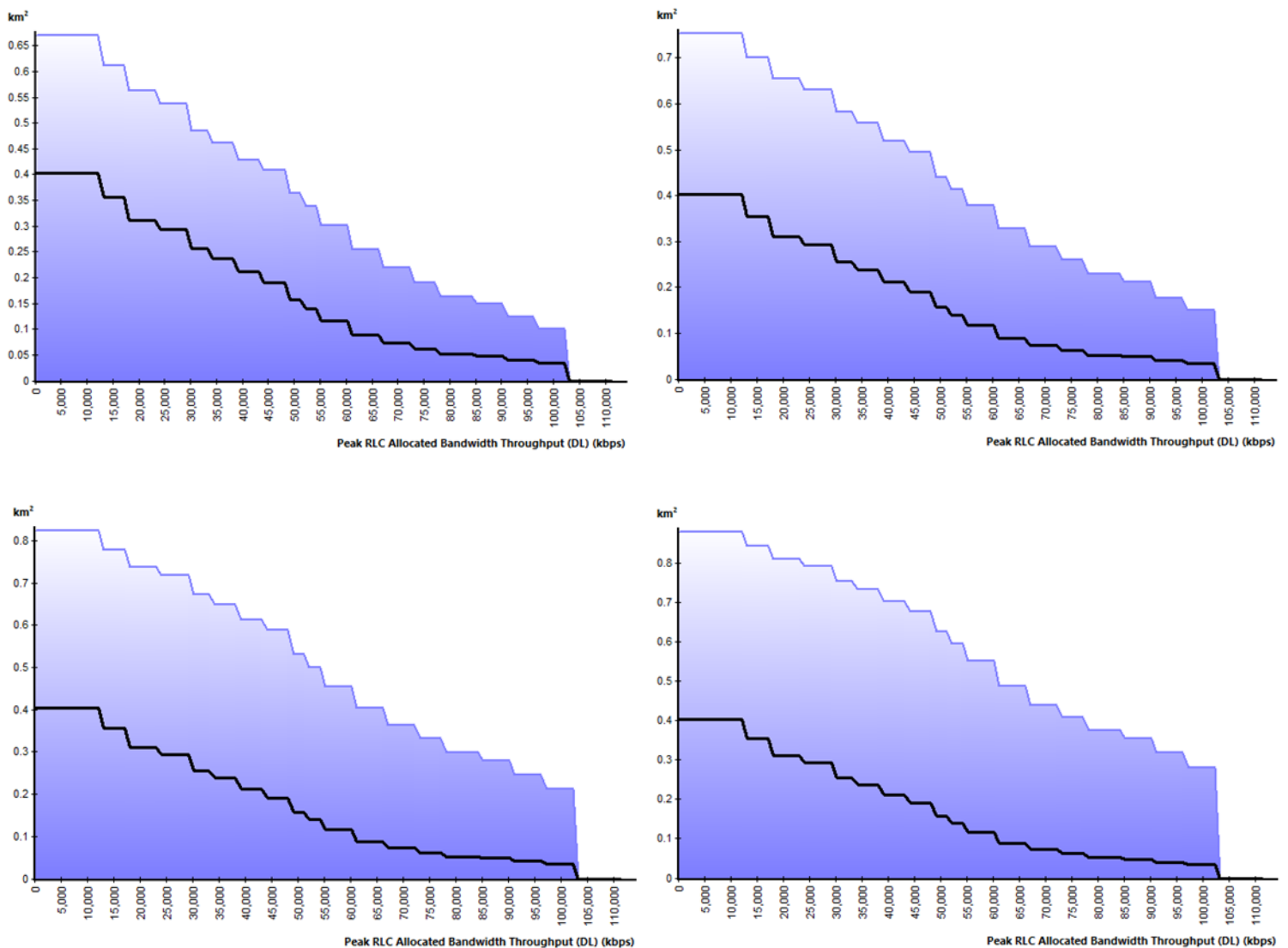


Figure 51. Throughput for SISO vs diversity 64x1 (top left), 64x2 (top right), 64x4 (bottom left) and 64x8 (bottom right)

As it has been said on previous sections, a better C/(I+N) level allows the use of higher bearers, with higher modulation and coding schemes, and therefore throughput also

increases. This can be seen in the figure above, where, as the number of receiving antennas increased and so it did the $C/(I+N)$, more areas experienced better throughputs. For example, for 64x1 only 0.069 km² were covered by 102 Mbps; for 64x2, 0.15 m²; for 64x4 0.212 km² and for 64x8, 0.279 km².

6.2. Single-user MIMO

In this section, the single-user MIMO (SU-MIMO) capability of a cell and how Atoll models it are studied. For this, only SU-MIMO mode was configured on the cell.

6.2.1. Impact of transmission antennas on SU-MIMO

For this section, the number of transmission antennas were varied while the number of receiving antennas remained fixed. The different configurations tested were: 4x4, 16x4, 64x4 and 128x4. The study showed that the PDSCH $C/(I+N)$ level was exactly the same for all SU-MIMO configurations and SISO, because Atoll does not apply any diversity gain to the PDSCH $C/(I+N)$ for SU-MIMO.

Regarding the throughput, there was an improvement in the throughput from SISO to SU-MIMO 4x4, as the receiver can process four different layers of information at the same time. But this is also the case for 16x4, 64x4 and 128x4; therefore, there was no improvement among these configurations.

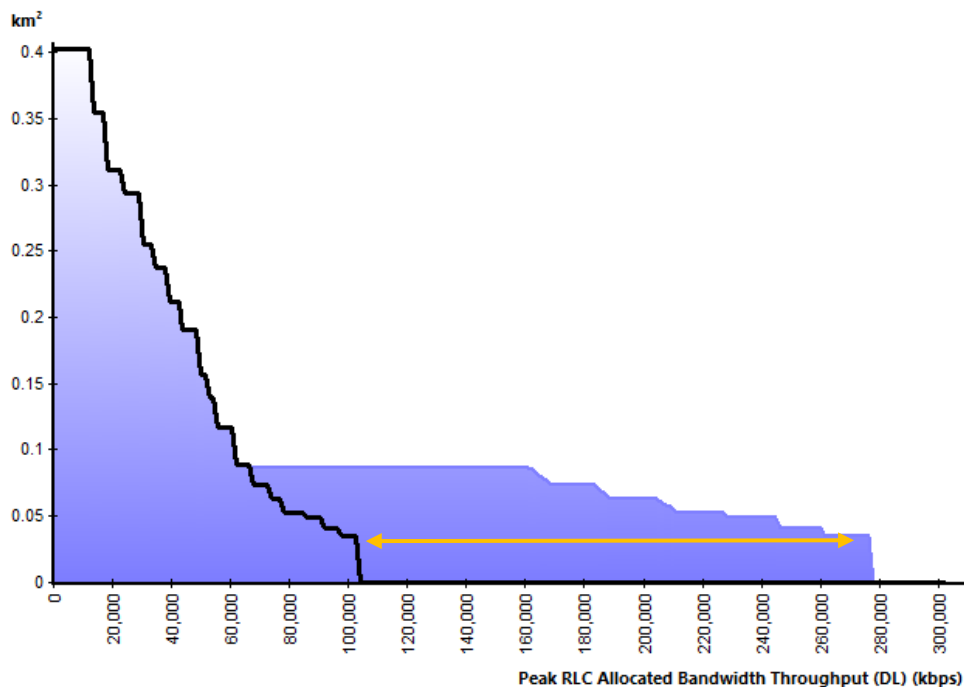


Figure 52. Throughput for SISO vs SU-MIMO 4x4, 16x4, 64x4, 128x4

The following table summarizes the capacity gains obtained and the maximum throughputs achieved.

Table 23. Capacity Gain and Maximum Throughput for SU-MIMO with Different Number of Transmission Antennas

	Capacity Gain	Maximum Throughput (Mbps)
SU-MIMO 4x4	2.7	276.0
SU-MIMO 16x4	2.7	276.0
SU-MIMO 64x4	2.7	276.0
SU-MIMO 128x4	2.7	276.0

6.2.2. Impact of receiving antennas on SU-MIMO

Here, the number of receiving antennas on the user equipment were varied, while the number of transmitting antennas on the base station remained fixed and some quality and capacity predictions were performed. The different configurations for SU-MIMO tested were: 64x1, 64x2, 64x4 and 64x8.

The following figure shows the results obtained for the PDSCH $C/(I+N)$ predictions, where a SISO configuration, represented by the black line, is compared with the different SU-MIMO configurations mentioned above, represented by the blue color.

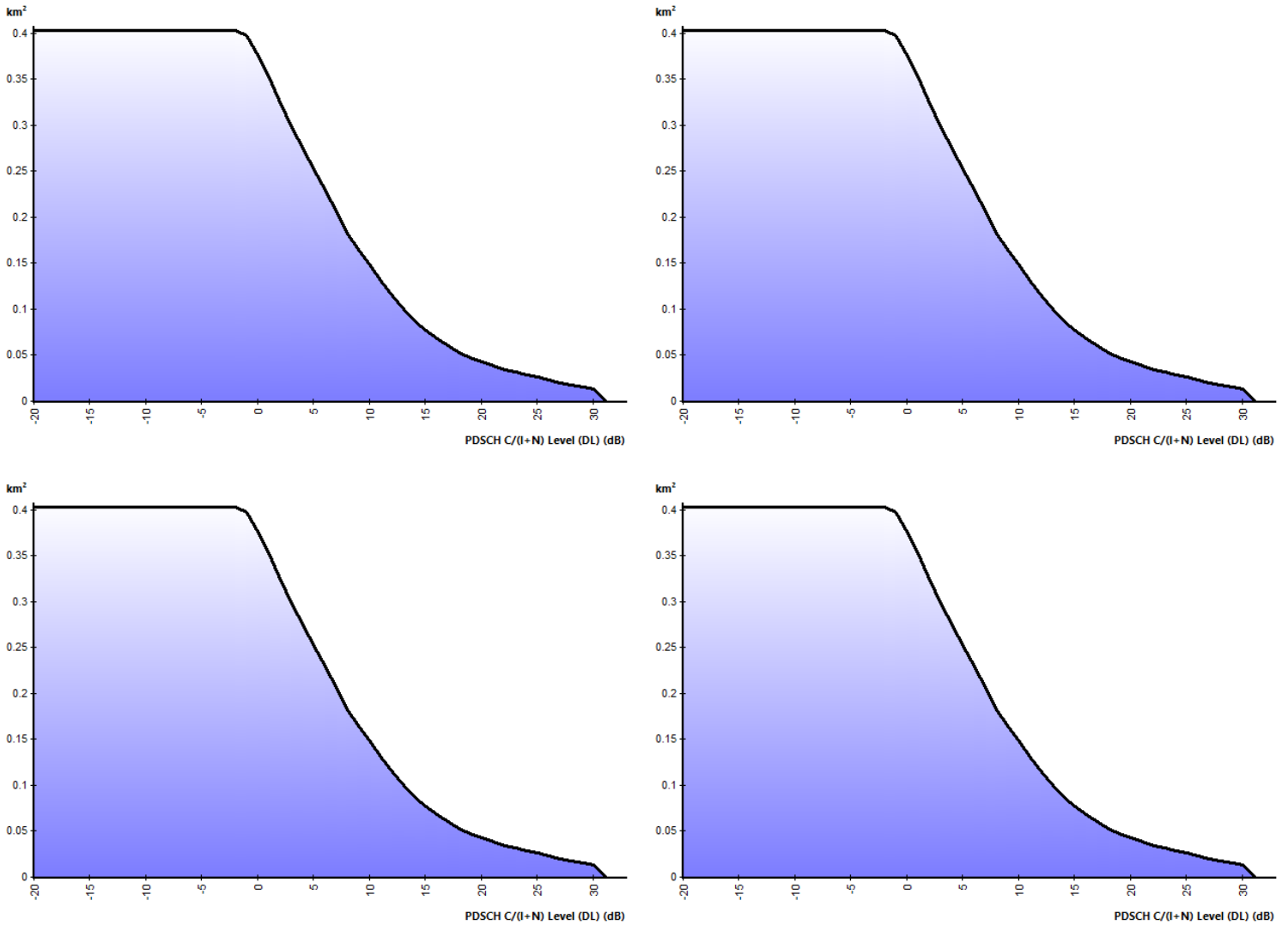


Figure 53. PDSCH C/(I+N) for SISO vs SU-MIMO 64x1 (top left), 64x2 (top right), 64x4 (bottom left) and 64x8 (bottom right)

It is observed that the same PDSCH C/(I+N) levels were obtained for the SISO configuration and for the different SU-MIMO configuration, regardless increasing the number of reception antennas on the user equipment. The reason for this behavior is that, as explained before, Atoll does not apply any gain to increase the C/(I+N).

On the other hand, different results were obtained for the capacity predictions.

The following figure shows the results obtained for the capacity predictions, where a SISO configuration, represented by the black line, is compared with the different SU-MIMO configurations mentioned above, represented by the blue color.

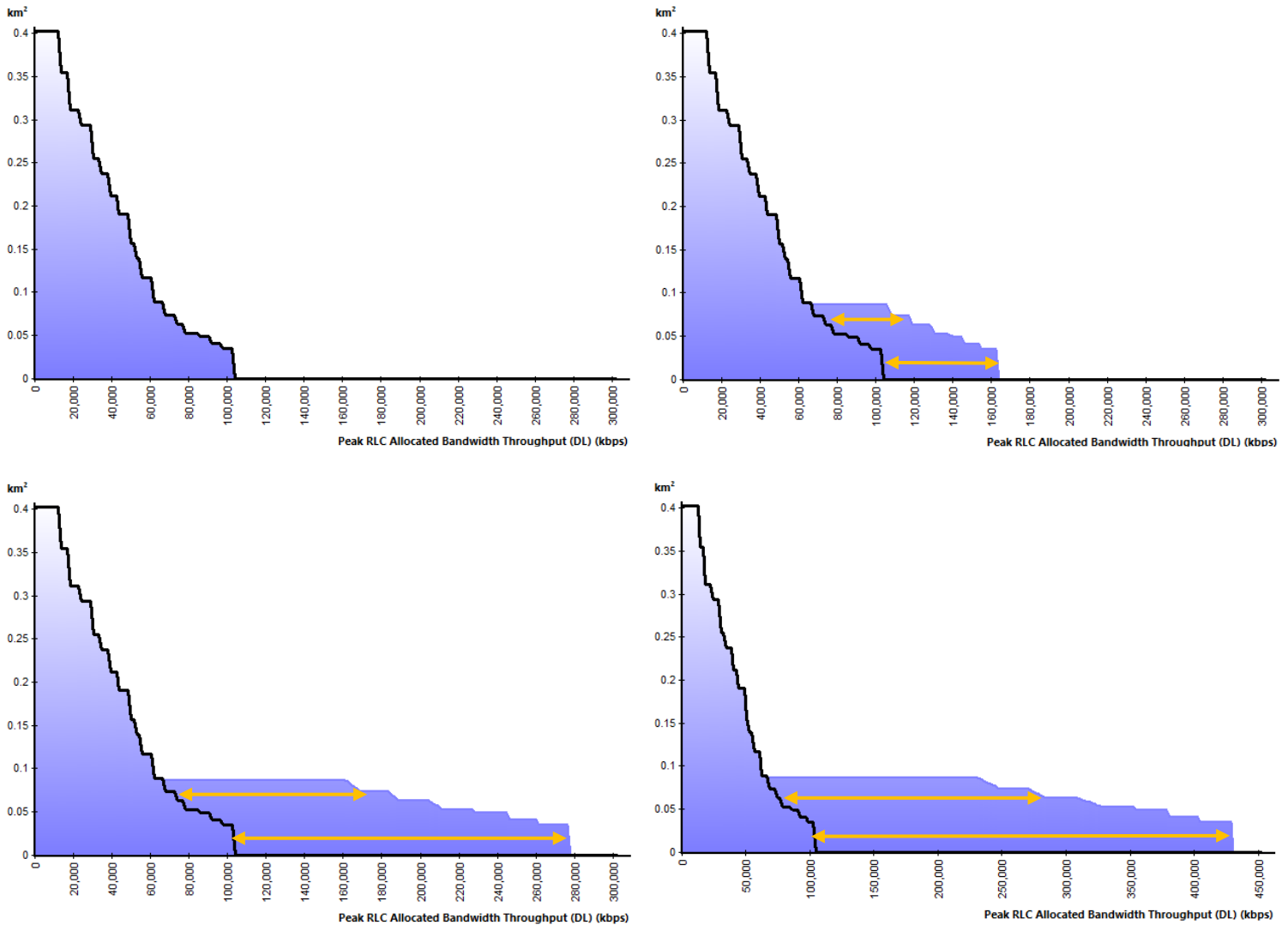


Figure 54. Throughput for SISO vs SU-MIMO 64x1 (top left), 64x2 (top right), 64x4 (bottom left) and 64x8 (bottom right)

Different aspects can be seen from the figure above. The first aspect is that there was no difference between SISO and SU-MIMO 64x1. This is because the SU-MIMO capability and the different layers of information that can be received at the same time is limited to the number of receiving antennas on the user equipment; therefore, even though the base station is capable of transmitting more than one different layer of information, if the user equipment only has one receiving antenna, no capacity gains would be achieved.

The second aspect that can be noticed is that once the number of receiving antennas were increased to more than one, capacity gains and therefore higher throughputs were obtained. For example, with SU-MIMO 64x1 (or SISO) the maximum throughput obtained was 102 Mbps; with SU-MIMO 64x2, 162 Mbps; with SU-MIMO 64x4, 276 Mbps; and finally with SU-MIMO 64x8, it was obtained 428 Mbps.

Nevertheless, it can also be observed that the capacity gains, represented with the yellow arrows, are not constant values. The reason for this is because the capacity gain also depends on the $C/(I+N)$ level. This means that with higher $C/(I+N)$, higher capacity gains are obtained.

Atoll has some predefined values for the capacity gain depending on the $C/(I+N)$ level. Also these values change according to the SU-MIMO configuration, depending on the number of transmission and receiving antennas. For example, the capacity gains depending on the $C/(I+N)$ are not the same for 64x2, 64x4 or 64x8.

As it can be seen from Figure, all SU-MIMO configurations obtained a maximum $C/(I+N)$ of 30 dB and the maximum capacity gain can be calculated from Figure. For 64x2 the capacity gain obtained was 1.6; for 64x4, 2.7 and for 64x8, 4.2.

The following table summarizes the capacity gains obtained and the maximum throughputs achieved.

Table 24. Maximum Capacity Gains and Maximum Throughputs for SU-MIMO with Different Number of Receiving Antennas

	Maximum Capacity Gain	Maximum Throughput (Mbps)
SU-MIMO 64x1	1.0	102.0
SU-MIMO 64x2	1.6	162.0
SU-MIMO 64x4	2.7	276.0
SU-MIMO 64x8	4.2	428.0

6.3. Multi-user MIMO

In this section, the multi-user MIMO (MU-MIMO) capability of a cell and the how Atolls models it are studied. For this, only MU-MIMO mode was configured on the cell.

6.3.1. Impact of receiving antennas on MU-MIMO

The first study consisted on varying the number of receiving antennas on the user equipment while leaving a fixed number of transmitting antennas on the base station and performing some capacity and quality predictions. The different configurations for MU-MIMO tested were: 64x1, 64x2, 64x4 and 64x8. Also, a maximum of 20 MU-MIMO users were supported for the cell.

The following figure shows the results obtained for the PDSCH $C/(I+N)$ predictions, where a SISO configuration, represented by the black line, is compared with the different MU-MIMO configurations mentioned above, represented by the blue color.

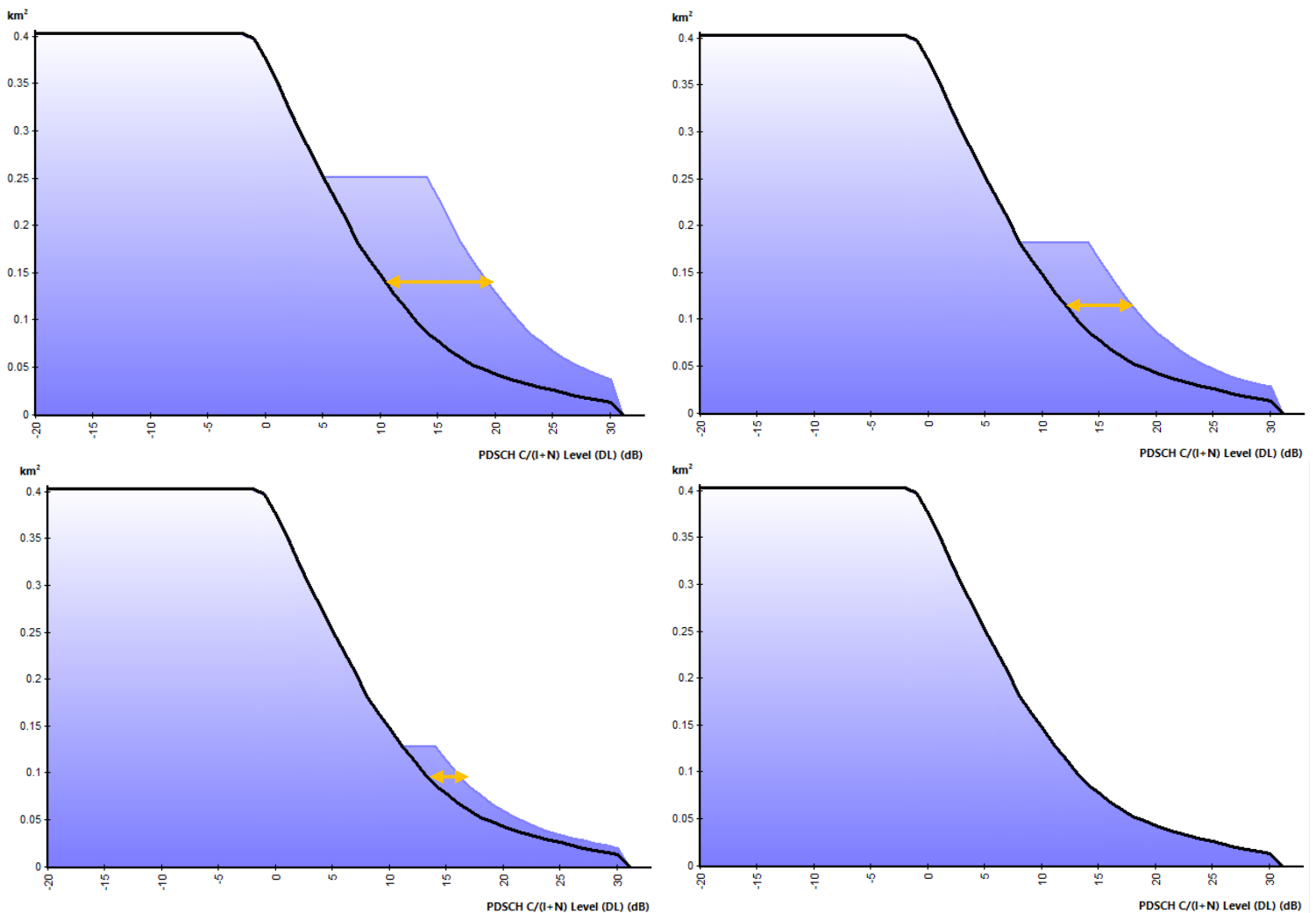


Figure 55. PDSCH C/(I+N) for SISO vs MU-MIMO 64x1 (top left), 64x2 (top right), 64x4 (bottom left) and 64x8 (bottom right)

As it can be seen, the PDSCH C/(I+N) level was reduced as the number of receiving antennas in the user equipment increased. This is because by doubling the number of receiving antennas, the diversity gain, represented by the yellow arrows, reduces 3 dB. For example, for MU-MIMO 64x1 the diversity gain was 9 dB; for MU-MIMO 64x2 the diversity gain was 6 dB; for MU-MIMO 64x4 the diversity gain reduced to 3 dB and finally, for MU-MIMO 64x8 there is no diversity gain at all, and the PDSCH C/(I+N) is the same as in a SISO configuration.

The following figure shows the results obtained for the capacity predictions, where a SISO configuration, represented by the black line, is compared with the different MU-MIMO configurations mentioned above, represented by the blue color.

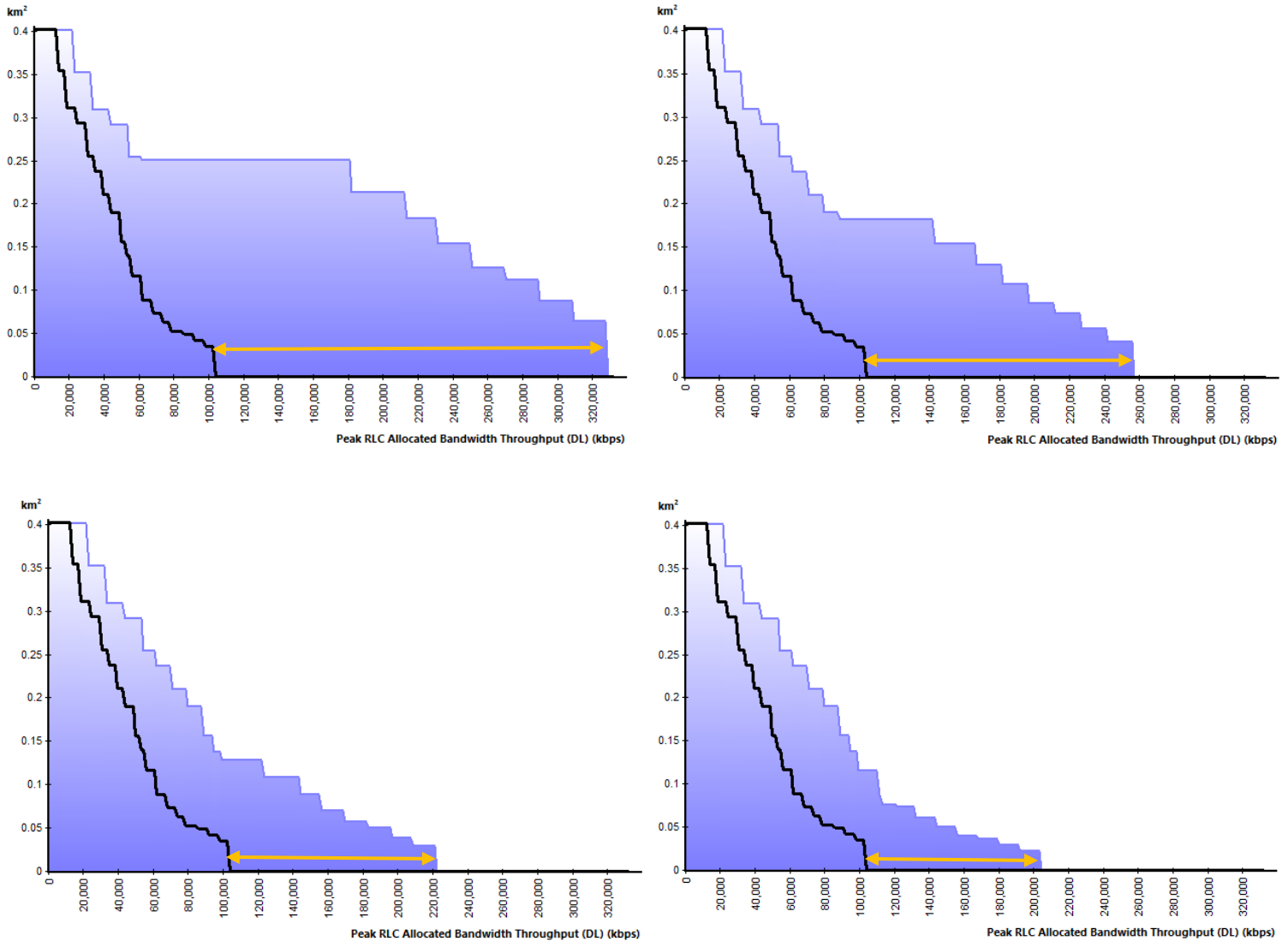


Figure 56. Throughput for SISO vs MU-MIMO 64x1 (top left), 64x2 (top right), 64x4 (bottom left) and 64x8 (bottom right)

In this case, the throughput also reduced as the number of receiving antennas in the user equipment increased. For MU-MIMO 64x1, the maximum throughput obtained was 327 Mbps; for MU-MIMO 64x2, 255 Mbps; for MU-MIMO 64x4, 220.5 Mbps and for MU-MIMO 64x8, 202.5 Mbps.

Another important aspect to be noticed is that the gains obtained (represented by the yellow arrow) respect with SISO were not constant but they varied according to the PDSCH C/(I+N) level, as explained in section 3.4.

The following table shows the minimum gains obtained, when only the MU-MIMO capacity gain was applied; the maximum gains obtained, when the MU-MIMO capacity gain and the multi-user diversity gain was applied, and the maximum throughput achieved.

Table 25. Minimum Gain, Maximum Gain and Maximum Throughput for MU-MIMO with Different Number of Receiving Antennas

	Capacity Gain	Capacity Gain + Multi-user Diversity Gain	Maximum Throughput (Mbps)
MU-MIMO 64x1	1.8	3.2	327.0
MU-MIMO 64x2	1.4	2.5	255.0
MU-MIMO 64x4	1.2	2.2	220.5
MU-MIMO 64x8	1.1	2.0	202.5

6.3.2. Impact of transmission antennas on MU-MIMO

The second study consisted on varying the number of transmission antennas on the base station while having the same number of receiving antennas on the user equipment and performing some capacity and quality predictions. The different configurations for MU-MIMO tested were: 4x4, 16x4, 64x4 and 128x4. Again, a maximum of 20 MU-MIMO users were supported for the cell.

The following figure shows the results obtained for the PDSCH C/(I+N) predictions, where a SISO configuration, represented by the black line, is compared with the different MU-MIMO configurations mentioned above, represented by the blue color.

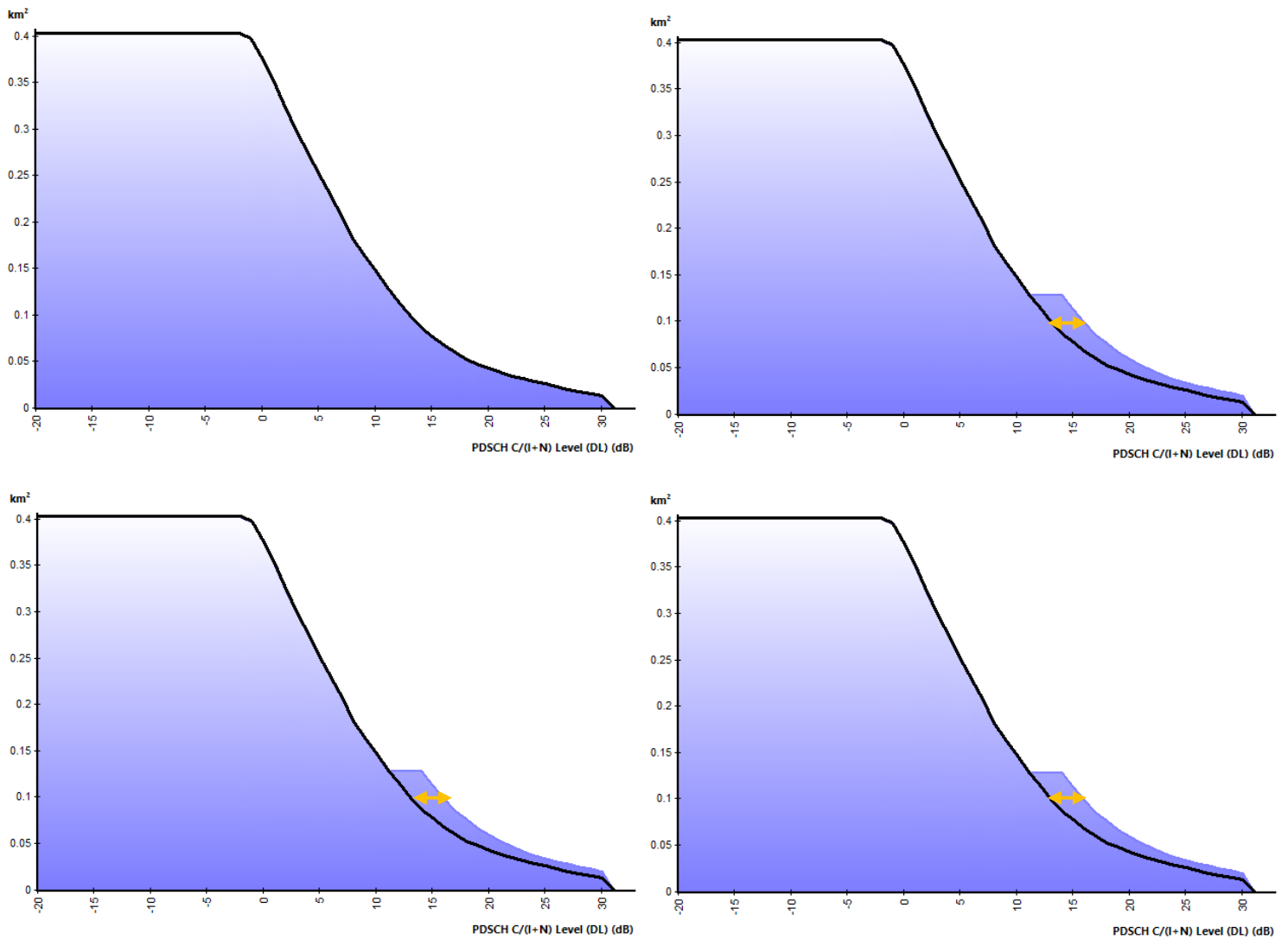


Figure 57. PDSCH C/(I+N) for SISO vs MU-MIMO 4x4 (top left), 16x4 (top right), 64x4 (bottom left) and 128x4 (bottom right)

There was no improvement on the C/(I+N) level when MU-MIMO 4x4 was used, as it is observed in the figure, because Atoll does not apply any gain to configurations with the same numbers of transmitting and receiving antennas. On the other hand, for MU-MIMO 16x4, MU-MIMO 64x4 and MU-MIMO 128x4 results showed an improvement on the capacity gain of 3 dB.

The following figure shows the results obtained for the capacity predictions, where a SISO configuration, represented by the black line, is compared with the different MU-MIMO configurations mentioned above, represented by the blue color.

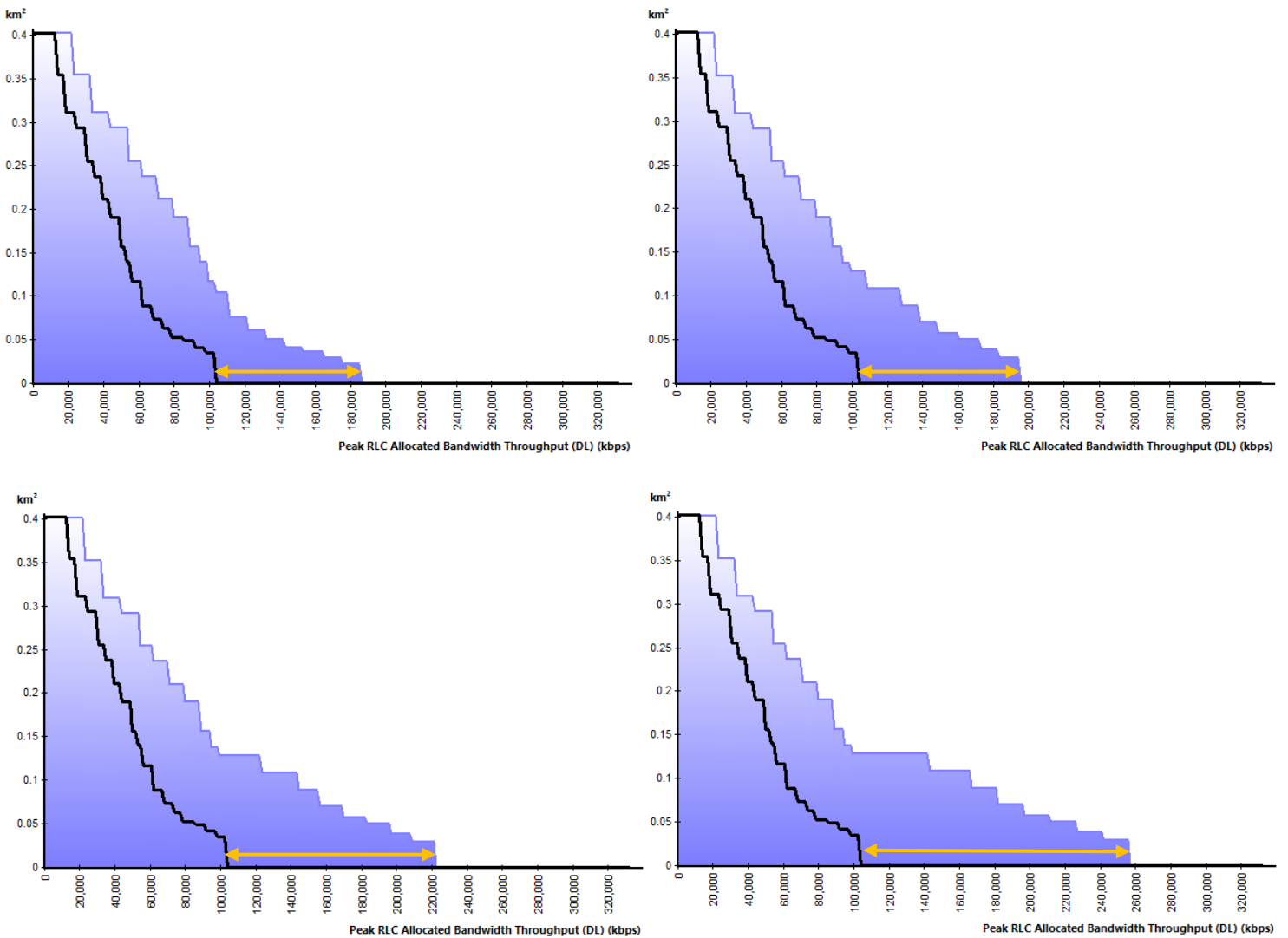


Figure 58. Throughput for SISO vs MU-MIMO 4x4 (top left), 16x4 (top right), 64x4 (bottom left) and 128x4 (bottom right)

It is observed that when the number of transmission antennas was varied, higher throughputs were achieved. For MU-MIMO 4x4 the maximum throughput obtained was 184.5 Mbps; for MU-MIMO 16x4, 193.5 Mbps; for MU-MIMO 64x4, 220.5 Mbps and for MU-MIMO 128x4, 255 Mbps. The reason for this improvement is due the total capacity gains, represented by the yellow arrows, that were applied.

As explained before, the capacity gain is not constant. If the $C/(I+N)$ is between 14 dB and 30 dB, MU-MIMO capacity gain and multiuser diversity gain is applied. The maximum gains obtained were 1.8, 1.9, 2.1 and 2.5, for each of the MU-MIMO configurations.

The following table summarizes the capacity gains obtained and the maximum throughputs achieved.

Table 26. Total Gains and Maximum Throughputs for MU-MIMO with Different Number of Transmission Antennas

	Total Gain	Maximum Throughput (Mbps)
MU-MIMO 4x4	1.8	184.5
MU-MIMO 16x4	1.9	193.5
MU-MIMO 64x4	2.1	220.5
MU-MIMO 128x4	2.5	255.0

6.3.3. Impact of the number of users on MU-MIMO

In this section, the number of simultaneous users was varied in order to study the throughput for a specific MU-MIMO configuration, maintaining a fixed number of transmission and reception antennas.

For the study, MU-MIMO 64x1 was tested for 10, 20, 30 and 40 users.

The following figure shows the results obtained for the capacity predictions, where a SISO configuration, represented by the black line, is compared with the different MU-MIMO configurations mentioned above, represented by the blue color.

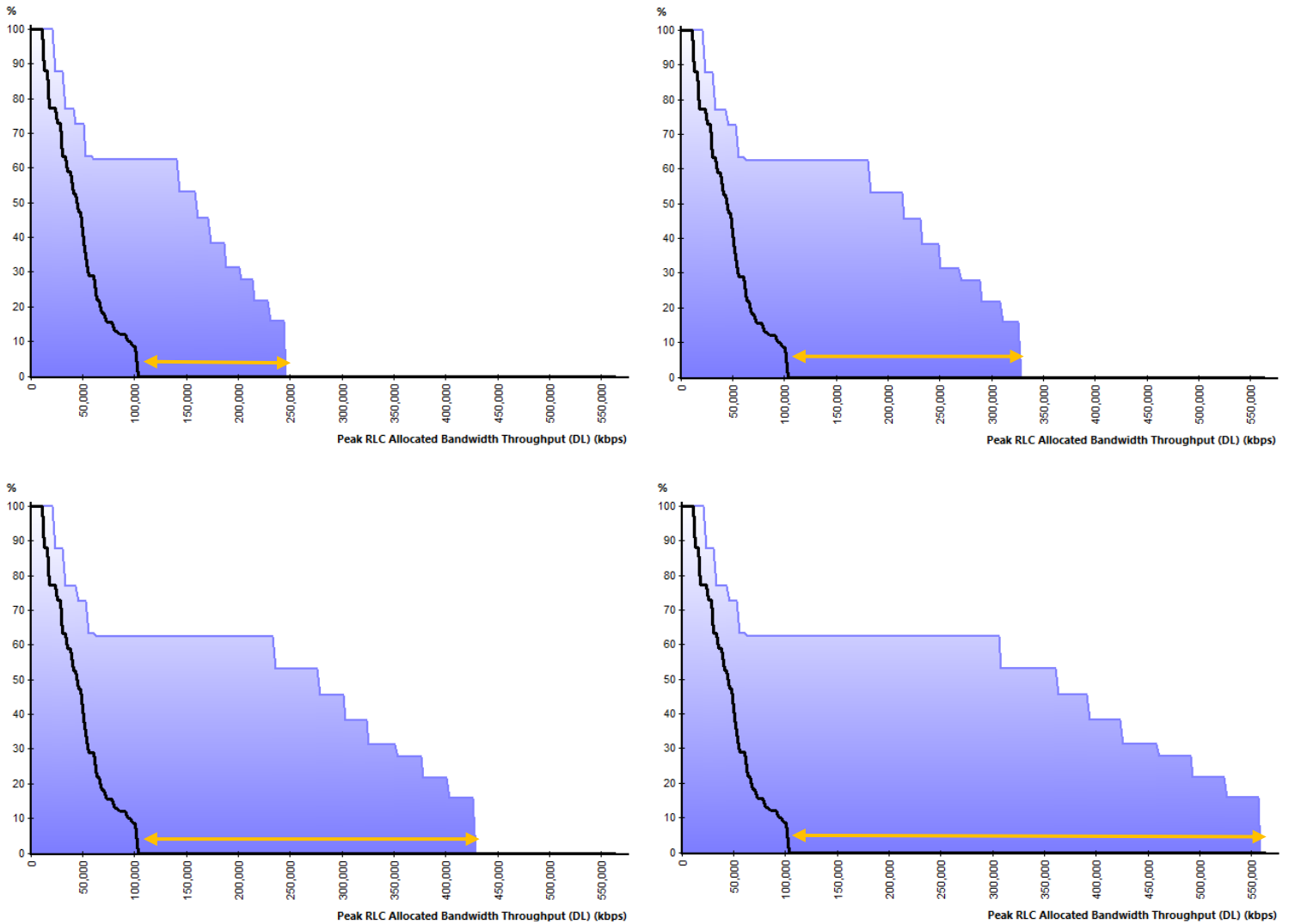


Figure 59. Throughput for SISO vs MU-MIMO 64x1 for 10 users (top left), 20 users (top right), 30 users (bottom left) and 40 users (bottom right)

It is observed that when the number of co-scheduled users sharing the same resources was increased, it also increased the capacity gain and the throughput.

The following table summarizes the maximum gains obtained and the maximum throughput achieved.

Table 27. Maximum Gain and Maximum Throughput for Different MU-MIMO Users

	Maximum Gain	Maximum Throughput (Mbps)
10 users MU-MIMO 64x1	2.4	242.5
20 users MU-MIMO 64x1	3.2	325.0
30 users MU-MIMO 64x1	4.2	425.0
40 users MU-MIMO 64x1	5.4	555.0

6.3.4. 3D simulation results

The purpose of this section is not to compare the different MIMO configurations between them using a realistic user distribution, but to understand how MIMO can improve the results obtained on section 5.5 when it is combined with beamforming.

A number of 100 business users located at different heights (between 1.5 m and 20 m) demanding broadband service were distributed over a 1 km² area in order to study a more realistic capacity and coverage of the cell and the average user performance.

In total, 10 simulations were performed using the beamformer 2 from Chapter 5 and enabling all MIMO capabilities (transmit/receive diversity, SU-MIMO and MU-MIMO). The beamformer 2 has a total of 64 antennas for transmission/reception and the mobile phones used have 4 antennas; therefore, the MIMO 64x4 was used.

Table 28. Average Results for 3D Simulations Using Beamforming and MIMO

Parameters	Beamformer 2 with MIMO 64x4	Beamformer 2	70deg 17dBi 3Tilt Ant
Users rejected	0 (0%)	7.6 (7.6 %)	38.6 (38.6 %)
Active users (DL+UL)	100 (100%)	92.4 (92.4 %)	61.4 (61.4 %)
Peak RLC cumulated throughput (DL)	521.66 Mbps	97.60 Mbps	63.07 Mbps
Effective RLC cumulated throughput (DL)	521.36 Mbps	97.52 Mbps	62.9 Mbps
Cumulated application throughput (DL)	495.29 Mbps	92.65 Mbps	59.75 Mbps
Average application user throughput (DL)	4.95 Mbps	1.00 Mbps	0.97 Mbps
Peak RLC cumulated throughput (UL)	496.34 Mbps	111.17 Mbps	104.71 Mbps
Effective RLC cumulated throughput (UL)	494.32 Mbps	110.62 Mbps	104.24 Mbps
Cumulated application throughput (UL)	469.61 Mbps	105.09 Mbps	99.03 Mbps
Average application user throughput (UL)	4.70 Mbps	1.14 Mbps	1.61 Mbps
Traffic load (DL)	100 %	100 %	100 %
Traffic load (UL)	60.47 %	99.99 %	99.99 %
Average SS-RSRP	-80.98 dBm	-81.38 dBm	-109.45 dBm
Average PDSCH	-52.06 dBm	-52.46 dBm	-80.53 dBm
Average PDSCH CIRN	40.14 dB	36.77 dB	8.70 dBm
Average path loss	120.53 dB	120.93 dB	139.94 dB

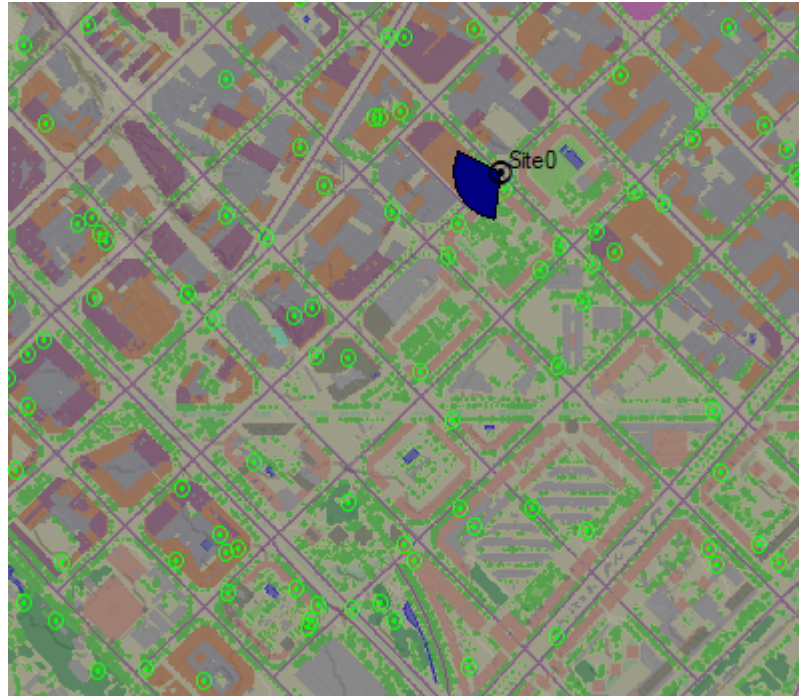


Figure 60. User connection distribution using beamformer 2 together with MIMO

As it was expected, the use of MIMO combined together with beamforming improved not only the coverage, but the signal quality and the throughput.

The first thing that can be observed is that with MIMO, all users were able to connect to the cell.

In terms of cumulated throughput, it is seen that the cell with MIMO capabilities enabled handled 5.35 times more traffic in the downlink and 4.47 times more traffic in the uplink compared to what the cell with no MIMO capabilities handled.

Almost the same proportion was obtained in terms of average user throughput, obtaining 4.95 times more in the downlink and 4.12 times in the uplink. This improvement on the throughput is due to the capacity gains applied when SU-MIMO and MU-MIMO were used.

The traffic load was the same for the downlink, both at 100%. Nevertheless, the cell with MIMO capabilities only had a 60.47% traffic load in the uplink, compared to the 99.99% uplink traffic load obtained for the cell with no MIMO capabilities. This means that with MIMO, more users could have resources allocated for uplink communication.

Also, on average, an improvement of 3.37 dB was obtained on the PDSCH C/(I+N) level. On average, 3 of the 100 users benefited with transmit/receive diversity, which in the case of MIMO 64x4 offers a diversity gain of 15.0515 dB and the other 97 users benefited with MU-MIMO, which offers a MU-MIMO diversity gain of 3.0103 dB. Therefore, the average diversity gain would be $(3/100) \cdot 15.0515 + (97/100) \cdot 3.0103 = 3.37$ dB.

In terms of the SS-RSRP and the PDSCH signal levels, users received signals with the same level on average.

7. Conclusions and future development

For this thesis, Atoll was used to carry out coverage predictions, quality predictions, capacity predictions and realistic simulations in order to study the signal propagation using different propagation models and the benefits of using beamforming and MIMO.

Results showed that the Aster Propagation Model gives higher values of path loss because of its path loss formula, which includes parameters that are not taken into account in the path loss formula of the Standard Propagation Model. Some of these parameters are the penetration losses when the line between the transmitter and the receiver slightly penetrates inside a building, the average height of the profile from the antenna to the receiver and the roof to mobile attenuation that depends on the street width. This means that the Aster Propagation Model can give more realistic values since it takes into account more details of the environment and the surrounding areas to the users.

Also, the Aster Propagation Model improved the coverage calculations on microcells (the antenna height below the surrounding buildings height) compared to the Standard Propagation Model, allowing signals to reach further, due to the use of ray tracing techniques that add horizontal diffraction and reflections.

For the beamforming analysis, results showed that beamforming can improve the coverage, the signal quality and hence the throughput because of its high directivity gain compared to the no beam-based antenna. Two ways of increasing the throughput were found. The first one is by increasing the number of beams, which means that more users could benefit from a dedicate beam; and the second one by increasing the number of antenna elements, which increase directivity and hence the gain of the beam. Also, beamforming antennas showed a huge difference compared to the no beam-based antenna when users were distributed vertically at different heights. The reason was because beamforming antennas can have beams covering different height by changing the electrical tilt.

Regarding the MIMO capabilities available in Atoll, three different transmission diversity techniques were tested: transmit diversity, single-user MIMO (SU-MIMO) and multi-user MIMO (MU-MIMO).

For transmit diversity, results showed that the PDSCH $C/(I+N)$ can be improved up to a 9 dB more by increasing the number of transmission antennas and up to 18 dB more by increasing the number of antennas in reception. This impacts directly on the throughput, which it is increased due to higher modulation and coding schemes selected according to the $C/(I+N)$ level. This MIMO technique is useful for users are located on regions of a cell with bad quality conditions.

For SU-MIMO, gains were applied to the throughput only when the number of receiving antennas was increased. These capacity gains were not constant since they depend on the $C/(I+N)$ experienced by the user. The number of transmission antennas has no impact on the capacity gains on SU-MIMO.

For MU-MIMO, gains were applied to the $C/(I+N)$ and to the throughput. Nevertheless, increasing the number of receiving antennas reduced the gains applied, which penalized the signal quality and the throughput. On the other hand, when the number of transmission antennas was increased, the gains applied to the $C/(I+N)$ remained the same, but the capacity gains applied and hence the throughput, increased. Another important factor considered was the number of co-scheduled users handled by the cell. It was observed that by increasing the number of co-scheduled users, higher throughputs can be obtained.

Finally, by means of simulations using a distribution of 100 users, it was demonstrated that by combining beamforming with MIMO, a single cell can increase its capacity by almost 5 times in the downlink compared to a cell with beamforming but without MIMO capabilities and more than 8 times compared to a cell with no beamforming and no MIMO.

As for future work, it can be considered the study of millimeter waves and how the use of beamforming and MIMO can help to counter the well-known path loss and blocking issues. Also, the deployment of more than one cell and the planning of a 5G network that meets certain throughput and user requirements can be analysed.

Since Atoll is a software that allows to consider many parameters related to propagation models, the traffic and user conditions and the radio access technology, further modifications could be tested in order to improve the results obtained.

Bibliography

- [1] 5G Americas, "5G Services and Use Cases," 2017.
- [2] ITU-R, "Minimum requirements related to technical performance for IMT-2020 radio interface(s)," 2017.
- [3] 3GPP, "Release 15 Description," 2018.
- [4] E. Dahlman and S. Parkvall, "NR - The new 5G radio-access technology," 2017.
- [5] J. L. X. Lin, R. Baldemair, T. Cheng, S. Parkvall, D. Larsson, H. Koorapaty, M. Frenne, S. Falahati and A. G. a. K. Werner, "5G New Radio: Unveiling the Essentials of the Next Generation Wireless Access Technology," 2018.
- [6] E. Dahlman, S. Parkvall and J. Skold, 5G NR The Next Generation Wireless Access Technology, 2018.
- [7] 3GPP, "TS 38.211 NR Physical channels and modulation," 2018.
- [8] A. Zaidi, F. Athley, J. Medbo, U. Gustavsson, G. Durisi and X. Chen, "5G Physical Layer: Principles, Models and Technology Components," 2018.
- [9] 3GPP, "TS 38.215 5G NR Physical layer measurements," 2018.
- [10] Analog Devices, "Phased Array Beamforming ICs Simplify," 2019.
- [11] Keysight Technologies, "White Paper "3 Key Challenges Implementing and Testing MIMO and Beamforming in 5G Base Stations and Components",," 2019.
- [12] L. Liu, R. Chen, S. Geirhofer, K. Sayana, Z. Shi and Y. Zhou, "Downlink MIMO in LTE-Advanced," 2012.
- [13] M. Pappa, C. Ramesh and M. N. Kumar, "Performance Comparison of Massive MIMO and Conventional MIMO Using Channel Parameters," 2017.
- [14] Qualcomm, "White Paper: Exploring the Potential of mmWave for 5G Mobile Access," 2016.
- [15] Y. Niu, Y. Li, D. Jin, L. Su and A. V. Vasilakos, "A Survey of Millimeter Wave (mmWave) Communications for 5G: Opportunities and Challenges," 2015.
- [16] Lu, J. S., D. Steinbach, P. Cabrol and P. Pietraski, "Modeling Human Blockers in Millimeter Wave Radio Link," 2012.
- [17] Y. Bandy, G. M. Rather and G. R. Begh, "Effect of atmospheric absorption on millimeter wave frequencies for 5G cellular networks," 2018.
- [18] F. Al-Ogaili and R. M. Shubair, "Millimeter-Wave Mobile Communications for 5G: Challenges and Opportunities," 2016.
- [19] Forsk, "Atoll 3.4.0: User Manual for Radio Networks," 2019.
- [20] Forsk, "Atoll 3.4.0: Technical Reference Guide for Radio Networks," 2018.
- [21] Forsk, "Aster 2.7.1: User Manual," 2019.
- [22] Forsk, "Aster 2.7.1: Technical Reference Guide," 2019.
- [23] Visicom, "Visicom," 2018. [Online]. Available: <https://visicomdata.com/samples?lang=en>.

Abbreviations and acronyms

3GPP	3rd Generation Partnership Project
5G	Fifth Generation
ARFCN	Absolute Radio-Frequency Channel Number
BPSK	Binary Phase Shift Keying
CDMA	Code Division Multiple Access
CINR	Carrier to Interference and Noise Ratio
CP	Cyclic Prefix
CSI-RS	Channel State Information Reference Signal
DL	Downlink
DM-RS	Demodulation Reference Signal
DTM	Digital Terrain Model
eMBB	Enhanced Mobile Broadband
EPRE	Energy Per Resource Element
FDD	Frequency Division Duplex
GSM	Global System for Mobile communications
IMT-2020	International Mobile Telecommunications 2020
ITU	International Telecommunications Union
ITU-R	International Telecommunications Union-Radio Communications Sector
LTE	Long-Term Evolution
MAC	Medium Access Control
MIMO	Multiple-Input Multiple-Output
mMTC	Massive Machine Type Communication
MU-MIMO	Multi-User MIMO
NB-IoT	Narrow-Band Internet-of-Things
NR	New Radio
OFDM	Orthogonal Frequency-Division Multiplexing
PBCH	Physical Broadcast Channel
PDCCH	Physical Downlink Control Channel
PDCP	Packet Data Convergence Protocol
PDSCH	Physical Downlink Shared Channel
PHY	Physical Layer
PRACH	Physical Random-Access Channel
PSS	Primary Synchronization Signal
PT-RS	Phase Tracking Reference Signal
PUCCH	Physical Uplink Control Channel
PUSCH	Physical Uplink Shared Channel
QAM	Quadrature Amplitude Modulation
QPSK	Quadrature Phase Shift Keying
RB	Resource Block
RLC	Radio Link Control
SDAP	Service Data Adaptation Protocol
SISO	Single-Input Single-Output
SNR	Signal to Noise Ratio
SPM	Standard Propagation Model
SRS	Sounding Reference Signal
SS	Synchronization Signal
SS-RSRP	SS Reference Signal Received Power
SSS	Secondary Synchronization Signal



SU-MIMO	Single-User MIMO
TDD	Time Division Duplex
UE	User Equipment
UL	Uplink
UMTS	Universal Mobile Telecommunication System
URLLC	Ultra-Reliable Low-Latency Communication